Technische Universität München

Max Planck-Institute für Biochemie

Abteilung für Molekulare Strukturbiologie

"Structural and functional studies of 19S regulatory particle subunits of the 26S proteasome"

Ganesh Ramnath Pathare

Vollständiger Abdruck der von der Fakultät für Chemie der Technischen Universität München zur Erlangung des akademischen Grades eines Doktors der Naturwissenschften genehmighten Dissertation.

Vorsitzender: Univ.-Prof. Dr. J. Buchner

Prüfer der Dissertation:

1. Hon.-Prof. Dr. W. Baumeister
2. Univ.-Prof. Dr. S. Weinkauf

Diese Dissertation wurde am **25-06-2014** bie der Technischen Universität München eingereicht und durch die Fakultät für Chemie am **20-10-2014** angenommen.

Dedicated to my family members who spent sleepless and painful nights for getting me educated.

Preface

This thesis describes the work I performed in Prof. Dr. Wolfgang Baumeister's lab (MPI of Biochemistry, Department of Molecular Structural Biology), during the last three and a half years. I have worked on two distinct but related projects. Thus, the "Results" are divided into two sections. The first chapter was published as a research article in Proceedings of National Academy of Sciences America with the title: *"The proteasomal subunit Rpn6 is a molecular clamp holding the core and regulatory subcomplexes together"* and describes the structure of Rpn6 and its role in the 26S proteasome. The results in the second chapter were also published as a research article in Proceedings of National Academy of Sciences America titled as *"Crystal structure of the proteasomal deubiquitylation module Rpn8-Rpn11"*. This chapter describes the structure of the Rpn8-Rpn11 heterodimer, based on which we propose the mechanism of substrate recognition and substrate deubiquitylation. As both papers are comprehensive with regard to results and analysis, these are inserted "as they are" into the thesis, after a detailed introduction to the field. An extended discussion section follows the "Results" part, which presents those implications that are not part of the manuscript and the scope for further research.

Summary

The ubiquitin-proteasome pathway (UPP) is responsible for degradation of a large amount of cellular proteins. In the UPP misfolded, otherwise damaged and obsolete proteins are labeled with ubiquitin chains that are recognized by the 26S proteasome, which then deubiquitylates and degrade these proteins. The UPP contributes to maintain protein homeostasis of eukaryotic cells and plays a major role in many cellular processes, including cell cycle regulation, apoptosis, DNA damage repair, antigen processing. The involvement of proteasome in many important biochemical processes makes it an important target for structural and functional studies.

The 26S proteasome consists of two subcomplexes, the 20S core particle (CP) and one or two 19S regulatory particles (RPs). The CP, which executes the degradation of target proteins into short peptides, has been studied in great detail. The availability of high-resolution structural data has provided the detailed mechanism of proteolytic cleavage, which has been exploited for the design of specific inhibitors. In contrast, the molecular mechanism of substrate recognition, deubiquitylation and substrate translocation, which take place in the 19S regulatory particle, have remained largely elusive so far due to the sparse structural information on this subcomplex.

My project was focused on obtaining information on the structure of the 19S regulatory particle using X-ray crystallography in combination with single particle cryo-electron microscopy. For crystal structure determination, single subunits from the RP were cloned, expressed, purified and crystallized. This resulted in the crystal structure of Rpn6 from *D. melanogaster*, a proteasome, COP9 signalosome and eukaryotic translation initiation factor (eIF3) complex (PCI) domain subunit, solved at 2.4 Å resolution. Fitting of the Rpn6 crystal structure into a 9 Å resolution EM map of the 26S proteasome allowed the localization of this subunit revealing its role in the assembly of the 26S holocomplex.

In our structural analysis of Rpn6 with respect to the 26S proteasome, Rpn6 contacts at least four subunits from the three independently assembled modules of the proteasome, the lid, the ATPase, and the core particle. Thus, Rpn6 is reinforcing the association of lid and base and that of the regulatory particle and core particle. Because of the symmetry mismatch between the heptameric alpha ring of the core particle and the hexameric AAA-ATPase from

the base of regulatory particle, their contacts appear rather sparse and weak, thus enabling relative motions. Thus, Rpn6 appears to have a pivotal role in holding the holocomplex together by acting as a clamp between RP and CP. It also provided clues for the arrangement of other PCI domain proteins in the complex. Based on the crystal contacts observed in Rpn6 crystals, mutagenesis, chemical crosslinking and computational modeling the positions of most RP subunits could be identified.

Considering the important role of catalytic subunits the project was further focused on getting structural insights into deubiquitination. The crystal structure of the MPR1, PAD1 N-terminal (MPN) domain heterodimer (Rpn8-Rpn11) was solved at 1.9 Å resolution providing detailed insights into ubiquitin recognition, deubiquitination and substrate translocation. The structure of Rpn8-Rpn11 heterodimer reveals the presence of two insertion loops (Ins-1 and Ins-2) in both Rpn8 and Rpn11, which are functionally important in regulating the activity of these subunits. Ins-1 of Rpn11 also plays a role in preventing premature substrate deubiquitination by aligning itself around the active site in respect to substrate-accepting and substrate-engaged confirmations of the 26S complex. The high-resolution studies helped us deciphering the mechanistic and functional details.

Rpn11 was localized in a high resolution EM map (7 Å). It sits above the AAA ATPase positioning the active site of Rpn11 directly over the pore of AAA ATPase's during the substrate-engaged state. The active site of Rpn11 is a composite active site regulated by its positioning with respect to the ATPase pore in the substrate-engaged state and substrate-accepting states, respectively. In the substrate-accepting state of the proteasome the active site of Rpn11 is distorted breaking the hydrogen bond network supporting the active site Zn ion. In the substrate-engaged state the active site geometry of Rpn11 is properly established along with reliable hydrogen bond network holding the Zn ion and a water molecule in place providing efficient cleavage isopeptide bond.

Contents

Chapter 1: Introduction

Proteins of living organisms participate in various cellular activities and their timely synthesis and degradation plays a major role in proper functioning of the organism (1). Controlled cellular protein degradation is executed by various protein degradation systems. In eukaryotes, the major part of this function is carried out by the ubiquitin-proteasome pathway (UPP) (1-3). Substrate proteins (misfolded, obsolete and/or damaged) are targeted for degradation by the attachment of a signal tag, ubiquitin, to lysine residues (4).

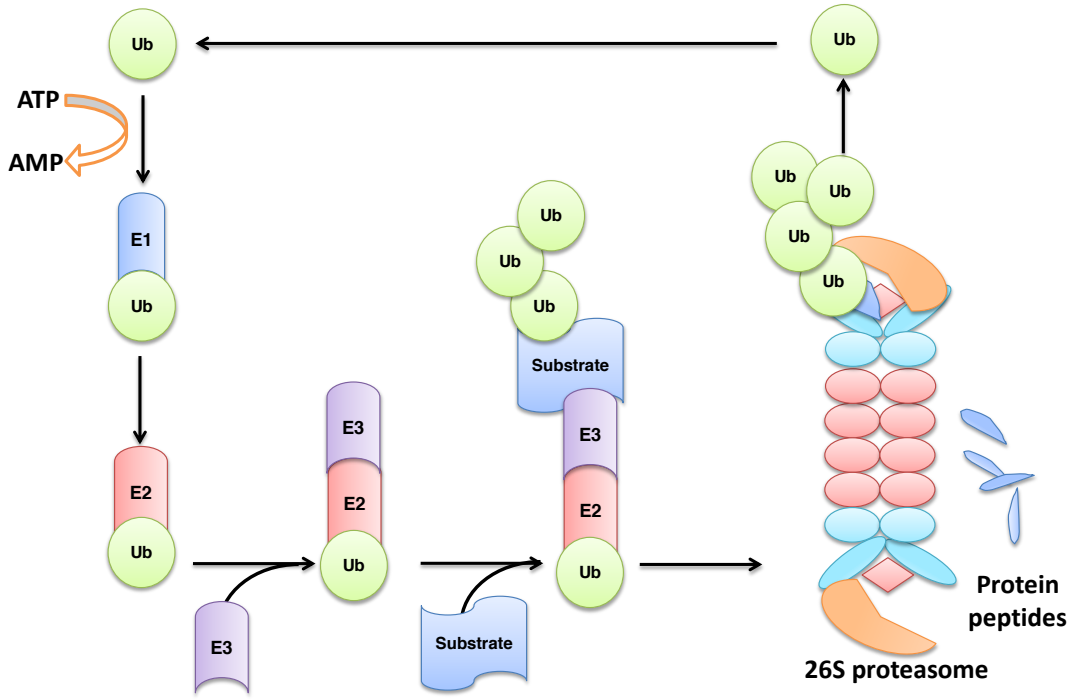

Fig 1. The Ubiquitin Proteasome Pathway.

Principal steps of the UPP. Ubiquitin is activated by the ubiquitin-activating enzyme (E1) with the help of ATP. Thereafter the activated ubiquitin is transferred to a ubiquitin-conjugating enzyme (E2). E2 transfers the activated ubiquitin moieties to the target protein substrate that is bound to ubiquitin ligase (E3). Conjugation of more ubiquitin forming a polyubiquitin chain serves as a targeting signal for the 26S proteasome. The protein substrate is degraded into short peptides, and free ubiquitin can be reused for another cycle.

A cascade of E1, E2 and E3 enzymes executes the ligation of ubiquitin to target proteins. In the first step the E1 enzyme (the ubiquitin activating enzyme) adenylates ubiquitin at the expense of one ATP molecule (Fig. 1) (5). An E2 enzyme subsequently conjugates the adenylated ubiquitin molecule to one of many E3 ligase enzymes, which transfers the ubiquitin tag to substrate proteins (6). Thereafter this substrate protein attached to a mono-ubiquitin signals other ligases to attach additional ubiquitin molecules resulting polyubiquitin chain. This serves as a signal that allows for recognition and degradation of the substrate by the 26S proteasome (7).

In eukaryotes the proteasome is present in both, nucleus and cytosol, and performs diverse cell- and tissue-specific degradation functions (8). It was also reported that the different regulatory complexes and subcomplexes of proteasomes have different distributions in mammalian cells depending on the cell type (9). Depending on tissue types, specialized inducible forms of the proteasome are found in vertebrates. The immunoproteasome for instance is optimized to process antigens and it directs the differentiation of T helper (Th) cells. Furthermore, the immunoproteasome has also been shown to be a more efficient degradation machine than the constitutively expressed proteasome, and may thus alleviate proteotoxic stress more efficiently (10).

Proteasomes have multiple catalytic sites in the beta subunits of the CP and the deubiquitylation site. Both are targets for drug development. A number of structurally diverse proteasome inhibitors have been identified and tested as chemical tools. Some of them have been used to study intracellular functions of the proteasome as well as its substrate specificity. Two drugs, Velcade and Kyprolis, have made their way to pharmacological use (11). Bortezomib (the active ingredient of Velcade) is the first clinically approved proteasome inhibitor for the first-line treatment of multiple myeloma. It is also effective against mantle cell lymphoma and acute allograft rejection. Five other drugs have entered clinical trials and some more are at earlier stages (12).

This introduction covers the structure of core and regulatory particles of the 26S proteasome. We focus on the 19S regulatory particle and an extended discussion, which describes the characterization, localization and mechanistic details of different subunits of 19S RP, is given.

Chapter 2: The 26S proteasome

The 26S proteasome is a molecular machine of 2.5 MDa comprising two sub-complexes, the cylinder-shaped 20S core particle (CP) (4) and one or two 19S regulatory particles (RPs), (Fig. 2) which associate with the ends of the CP (4, 13, 14). The recognition and recruitment of polyubiquitinated substrates, their ATP-dependent unfolding, deubiquitination and translocation into the core particle take place in the RP. The structurally and mechanistically well-characterized CP houses the proteolytically active sites and sequesters them from the cellular environment, thereby avoiding collateral damage (15). The proteasome complex is altogether composed of 33 different canonical subunits and some additional subunits present in sub-stoichiometric amounts (15). The dimensions of the core particle are 15 nm height by 11.5 nm width. The 19S RP complex has dimensions of 20 nm height by 17 nm width (16, 17). The inner chamber of the CP is 5.3 nm wide with the entry channel of 1.3 nm diameter suggesting the need for substrate unfolding prior to degradation (18).

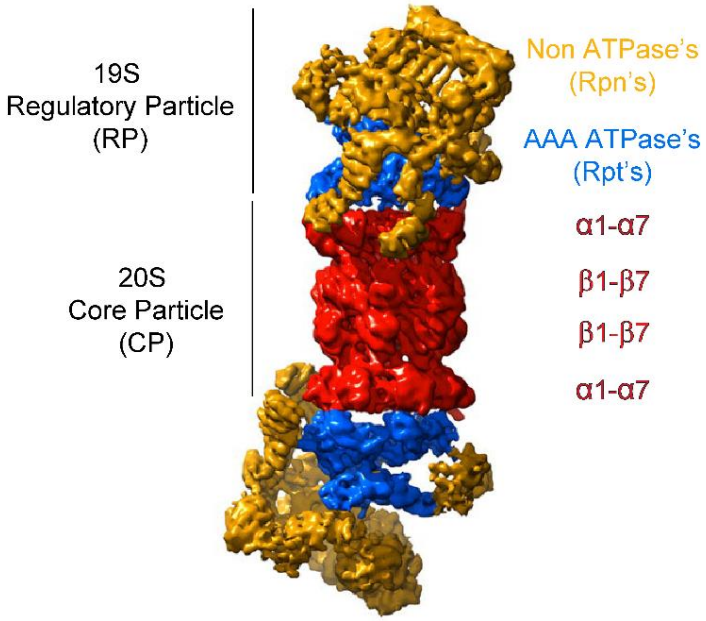

Fig. 2. The 26S Proteasome.

EM map of 26S proteasome from S. cerevisiae. The 20S core particle is the central proteolytic chamber composed of rings of alpha and beta subunits depicted in red where protein degradation takes place. The AAA ATPase translocates the substrate by binding on both sides above the alpha rings of the 20S CP is represented in blue. The non-ATPase subunits colored in gold have a scaffolding role.

Structural and functional studies on the 20S proteasome revealed its fundamental catalytic mechanisms. Unlike other proteases, the 20S proteasome degrades its protein substrates in a linear processive fashion. It cleaves them into smaller peptides without requiring cofactors or ATP, whereas pre-degradation processes like substrate tagging and deubiquitination, unfolding, and translocation are coupled with ATP hydrolysis. Elucidation of this ATP-dependent mode of action of the 19S RP can help us to better understand the mechanisms and functions of the proteasome.

The 20S Core Particle

The 20S proteasome, also known as the core particle (CP), was initially called “cylindrin” when it was first found in human erythrocytes lysate in 1968 (4, 15). In the 1980s the complex was isolated from bovine pituitary glands and functionally characterized, identifying different proteolytic activities. Initially it was believed to be present only in eukaryotes, until in the early 1990s high molecular weight complexes structurally very similar to eukaryotic 20S proteasomes with chymotrypsin-like proteolytic activity were found both in archaea (*Thermoplasma acidophilum*) (19) and actinomycetes *(Rhodococcus erythropolis*) (20).

The 20S proteasome of both, prokaryotes and eukaryotes is composed of 28 subunits (Fig. 3) (19). The prokaryotic 20S complex is composed of four homoheptameric rings with [(α_7)-(β_7)-(β_7)-(α_7)] architecture, while the eukaryotic 20S is composed of heteroheptameric rings with [(α_1-α_7)-(β_1-β_7) -(β_1-β_7)-(α_1-α_7)] subunit architecture (20) (Fig. 3A, D, E). The two β-rings are arranged back-to-back and each β-ring contacts one α-ring, resulting in a structure resembling a barrel-shaped cylinder with an α-β-β-α topology and D7 symmetry in archaea and actinomycetes and C2 symmetry in eukaryotes (15, 19). The central chamber formed by β rings contains the catalytic sites, which degrade the substrates into smaller peptides of 6-14 amino acids in length (15). Two additional cavities are formed at the interface of α and β-rings. These so-called antechambers have been shown to create a microenvironment that keeps substrate proteins in an unfolded state prior to degradation. The gate of the CP is formed from seven alpha subunits. Peptide degradation takes place in the presence of RP docked to the CP. Even though the eukaryotic 20S CP harbor the active sites it becomes fully

activated only after association with the regulatory complexes as gate opening is coupled to interactions with the ATPase subunits (21).

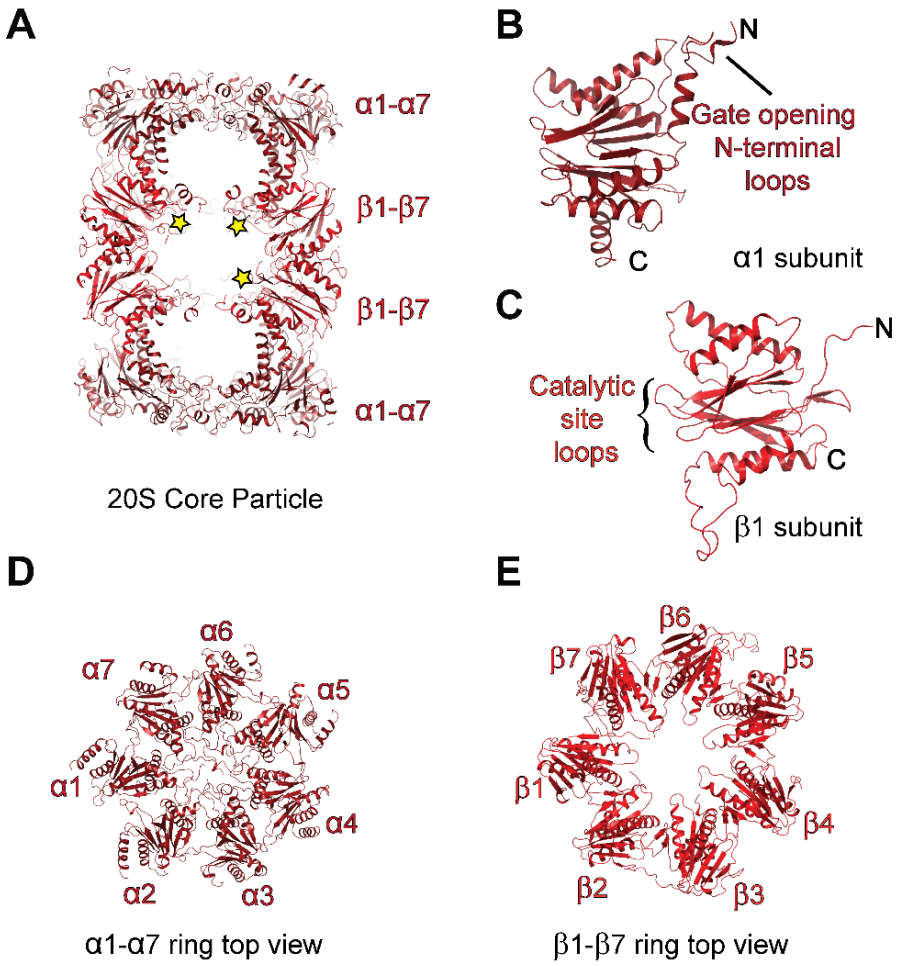

Fig 3: Crystal structure of the 20S core particle:

(A) Clipped view of a crystal structure (1RYP) (22) from yeast 20S proteasome. The alpha and beta subunits are represented in shades of red colour. The catalytic sites are indicated by yellow stars.

(B) Alpha-1 subunit, where the N-terminus is responsible for gate opening and closing.

(C) Beta-1 subunit, where the catalytic loops protruding into the antechamber are responsible for substrate degradation.

(D) Top view of the alpha ring showing a closed conformation, which blocks substrate entry.

(E) Top view of the beta ring which forms the proteolytic chamber.

The alpha subunits

The alpha subunits are catalytically inactive, and they oligomerize to a ring of seven subunits with a pore in the center, serving as the entry point for the substrate. The alpha subunits present in each ring retain a similar architecture in all structures solved (4). The fold is characterized by a sandwich of two five-stranded antiparallel beta-sheets flanked by three helices on both sides of the sandwich (15, 19-21). The N-terminal residues of each alpha subunit form a short helix (H0) and conjointly form a gate on the outer face of the particle, allowing for the regulation of substrate entry (Fig 3B). In the open gate confirmational state, N-terminal extensions of ~35 residues in the α-type subunits fold into α-helix (H0) and fill a cleft in the β-strand sandwich (15) (Fig 3A-E). This process is believed to require binding of regulatory complexes to the alpha rings. Besides the eukaryotic 19S RP, which will be discussed in detail in this thesis, regulators of simpler architectures like homohexameric ATPases have also been characterized (9, 23, 24).

The beta subunits

The beta subunits form two seven-membered rings stacked on top of each other forming a catalytic chamber where they degrade the substrate. Seven-membered alpha rings on each side sandwich two beta rings. The active sites of beta subunits are unique among proteases with N-terminal threonine as catalytic nucleophile (20) (Fig 3C). The catalytically active beta subunits of prokaryotes have chymotrypsin-like substrate selectivity (4, 19). In eukaryotes only three subunits (β1, β2, and β5) are catalytically active having caspase-like, trypsin-like and chymotrypsin-like activities respectively (22). In addition, vertebrates have inducible paralogous beta subunits that can replace the catalytic subunits to form the immunoproteasome (25-28). Such modified CPs contain β1i, β2i, and β5i (or β5t in the case of thymoproteasome) (28) in place of their constitutive paralogs and are expressed to orchestrate the immune response and deal better with proteotoxic stresses (29).

Beta subunits exhibit high structural and sequence similarity to each other and also to alpha subunits. They adopt a fold comprising a sandwich of two five-stranded antiparallel β-sheets flanked by three helices. Each of the beta subunits occupies a specific position within the respective rings. The catalytic site residues of β1, β2, and β5 subunits are located in the cleft

between the loops of beta strands S1 and S8 and are involved in the cleavage of peptide bonds of substrates (4).

The beta subunits in both prokaryotes and eukaryotes are expressed as an inactive precursor containing an N-terminal propeptide to prevent uncontrolled protein degradation (15). During CP maturation, two half-proteasomes form a holo-proteasome and the pro-peptides are subject to self-cleavage where the catalytic Thr1 residues become exposed to the catalytic chamber. Pro-peptides have double functions: one is to prevent premature activation and the other is to help CP assembly by acting as an intrinsic chaperone (4, 15).

Catalytic β-subunits are targets for various drugs. Inhibitors like epoxymicin and MG132, have been used to inhibit the proteasomal activity to study cellular processes. Considering the active sites as drug targets, many small molecule inhibitors have also been designed to inhibit the proteolytic activity of the proteasome.

The 19S Regulatory particle (RP)

ATP-dependent protein degradation was first observed in reticulocyte lysates by Goldberg et,al. in 1977 (30). Later Ciechanover (31) and Hershko (32) found that ATP-dependent protein degradation can be connected to protein substrates labeled with a small heat-inducible protein which, due to its ubiquitous presence was termed ubiquitin. In 1993 the formation of the 26S species by association of 20S proteasome with one or two subcomplexes, then termed ball complexes, but later called 19S regulatory particles (RPs), was confirmed (17, 24). These ATPases were shown to hydrolyze ATP, GTP, CTP and UTP in recombinant protein preparations of some archaeal proteasomes and hence were called proteasome-activating nucleotidases (PAN) (17). In *Rhodococcus erythropolis* AAA-ATPases related to the 19S ATPases exist as a hexameric complex and are called ATPases forming ring-shaped complexes (ARC) (33, 34). In most of the organisms the ATPases not only function in unfolding and substrate translocation but also recognize substrate proteins destined for degradation (4, 21, 35).

The 19S regulatory particle is composed of six Rpt (*Regulatory Particle ATPase*) subunits (Rpt1-6) and 13 Rpn (*Regulatory Particle Non-ATPase*) subunits (Rpn1, 2, 3, 5, 6, 7, 8, 9, 10, 11, 12, 13, 15) and can be subdivided into two subcomplexes that assemble independently, referred to as the base and the lid (21, 36). The base contains the hetero-hexameric AAA-ATPase ring, which drives the conformational changes in 19S RP needed for substrate processing, including their unfolding and translocation into the adjacent CP (37). Moreover, the base also contains the largest RP non-ATPase subunits Rpn1 and Rpn2 and the ubiquitin receptor Rpn13 (38). The second resident ubiquitin receptor Rpn10 (38-40) is neither part of the base nor the lid; it binds only to the assembled 26S proteasome and is positioned close to the ATPase module (41). Most of the RP subunits have structurally distinct domains known as PCI domains which are common in complexes like COP9 signalosome, eukaryotic translation initiation factor (eIF3) (42, 43). In the following section we will discuss RP subunits based on their domain organization and describe their structural characteristics in more detail.

AAA ATPase subunits of the 26S proteasome

The AAA ATPase (*ATPases* Associated with diverse cellular Activities) module of the RP is a molecular motor, which is responsible for unfolding and translocation of substrate proteins into the CP at the expense of ATP hydrolysis. The crystal structures of domains of the archaeal regulatory particle PAN (Proteasome Activating Nucleotidase) (44) are the only structures of AAA ATPase homologues available hitherto (45). The proteasomal AAA ATPase's is thought to have evolved from the PAN-like evolutionary precursor, with the introduction of ubiquitination signals for degradation along with the addition of non-ATPase subunits. However, the striking similarity between PAN and Rpt proteins revealed by previous studies suggests similar architectural features.

The AAA ATPase of the RP is composed of six structurally similar but distinct subunits, Rpt1, Rpt2, Rpt3, Rpt4, Rpt5 and Rpt6 (Fig 4C). EM studies along with biochemical data localized the hexameric ATPase ring directly on top of the hetero-heptameric alpha ring of the 20S CP (46, 47).

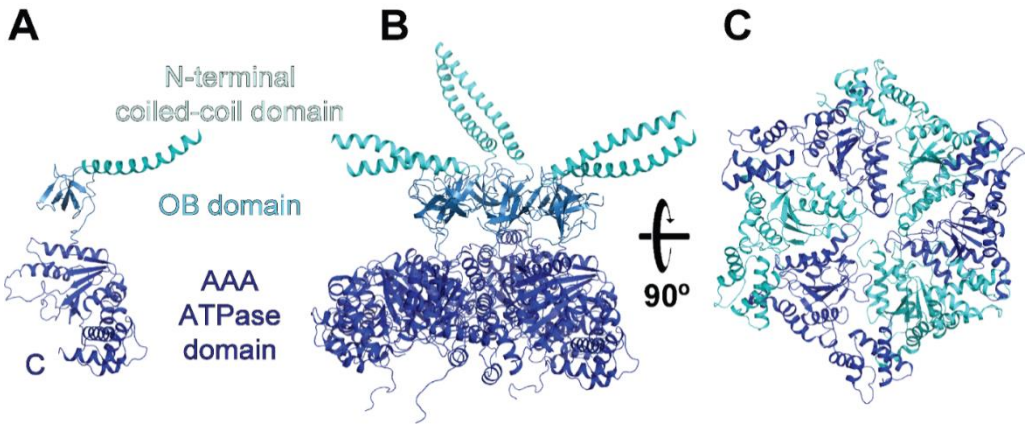

Fig 4. Proteasomal AAA ATPases *(PDB: 2WG5)(44).*.

(A) A single subunit of the proteasomal AAA ATPase ring. The N-terminal coiled-coil domain, the OB domain and the C-terminal ATPase domain are represented in cyan, sky blue and dark blue, respectively.

(B) The AAA ATPase's forming a ring, which sits on the 20S core particle.

(C) Bottom view of the AAA ATPase's where the adjacent subunits are shown in cyan and dark blue color for clarity.

Each ATPase subunit is composed of three domains: an *N*-terminal coiled-coil domain an oligosaccharide/oligonucleotide binding domain (OB) (48) and a *C*-terminal AAA ATPase domain *(ATPases Associated with diverse cellular Activities)* (44) (Fig 4A). The N-terminal domain, which is formed of one single helix from each subunit, is involved in substrate binding and in interactions with the degradation tag or with subunits of the RP. The crystal structure of the OB domain suggests that it has a N-terminal helix followed by a five-beta stranded domain that assembles to form a six-subunit ring structure with an inner surface diameter of 13 Å. The coiled-coil N-terminus of the OB domain possesses energy-independent chaperone activity which can be enhanced and modulated when coupled with ATP hydrolysis occurring in the nucleotidase domain (44) (Fig 4A). The ADP is bound between a hinge region of the alpha/beta fold domain and the helical domain and is coordinated by residues from both domains. This domain contains another characteristic feature, an Arginine finger (also known as pore 1 loop) which lies in the central pore and defines the constriction points (45) (Fig 4A).

The C-terminus tail of the ATPase domain possess an HbYX (hydrophobic-tyrosine-any amino acid-C-terminus) motif which penetrates into the binding pockets of the alpha ring subunits of the CP, thereby stabilizing the open gate confirmations of their N-terminal ends (46, 49) (Fig 4B). The binding of ATP or a non-hydrolysable ATP analog to PAN associates C-termini on the 20S alpha ring and triggers gate opening. The HbYX mechanism is conserved in the Rpt2, Rpt3 and Rpt5 subunits of eukaryotic proteasome (47). ATP hydrolysis is believed to cause conformational changes in the ATPase arrangement, exerting a mechanical force which pulls the substrate thereby unfolding and the protein translocating it into the CP cavity (44, 50),(51).

PCI domain proteins

A common domain architecture is shared by Proteasome, COP9 signalosome and eukaryotic translation Initiation Factor (eIF3) is called PCI (43, 52). PCI-domain proteins have been thought to play architectural roles within the three complexes. However, despite extensive work done on these complexes, very little is known about their interactions with each other. The PCI domain proteins were originally defined based on bioinformatics analysis of primary sequence. Interestingly, the N-terminal sequences of the PCI-domain containing proteins present in the RP are not conserved and do not show homology to each other but are predicted to have similar helical-repeat units (42). Previous studies suggested that PCI motifs mediate and stabilize protein-protein interactions within large complexes (53) and these were thought to have a scaffolding role with no direct involvement in catalytic functions of the proteasome. Despite of bioinformatics analysis and genetic studies conducted on the PCI domain subunits, have thus far defied rigorous biochemical characterization.

A crystal structure of Csn7 (a paralog of Rpn9), a PCI domain protein from the COP9 signalosome complex (CSN), was solved revealing the structural characteristics of the PCI domain family. The C-terminal domain of the proteins form a winged-helix subdomain with N-terminal residues forming a helical bundle with HEAT/ARM-like repeats (52). There are few more structures of PCI domain proteins registered in the protein database, but they have barely provided any further information on functional roles of these proteins. Several

mutational studies on the PCI domain proteins suggest assembly defects in the holo-complexes but they don't provide any specific information about the functions.

There are six PCI domain proteins, Rpn9, Rpn5, Rpn6, Rpn7, Rpn3 and Rpn12, in the lid (50) (52). These subunits contribute to structural flexibility and may thus destabilize the complex. Three-dimensional interaction maps of the lid suggested that Rpn7, Rpn3 and Rpn12 loosely associate with the RP complex whereas multiple interactions were found with Rpn9, Rpn5, Rpn6, Rpn8 and Rpn11. Mutations in these subunits lead to proteasomal assembly defects (54). Interestingly, PCI dimers of protein Rpn7 and Rpn3 often bind an additional 8 kDa component, Sem1 (Rpn15), a multi-tasking organizer of PCI/MPN complexes (55-58).

MPN-domain containing subunits

Most of the (MPR1, PAD1 N-terminal) MPN domain proteins fall into a specific class of DUBs, which remove the conjugated ubiquitin from substrates to regulate various cellular processes. It was found by Verma et.al., and Yao et.al., that the proteasomal subunit Rpn11 is an MPN domain-containing protein which is responsible for the removal of polyubiquitin tags (35, 59). It was also reported that the MPN domain of this protein contains a JAMM motif present in the active site and responsible for the catalytic activity (35, 59). Later on efforts by the same group to crystallize the JAMM motif (Jab1/MPN domain-associated metalloisopeptidase) containing proteins provided with the structure of a protein from a prokaryote thermophile, *Archaeoglobus fulgidus (59)*. After determining the structure of the JAMM motif containing protein (called AfJAMM), Deshaies and colleagues discovered that AfJAMM is a deubiquitinating enzyme (60). Later on it was also found that the set of amino acids that binds the zinc ion at the active site resembles thermolysin, a metalloprotease. Mutations in the JAMM motif of Csn5, an MPN domain containing protein found in CSN, suggested the importance of the JAMM motif as a novel metalloprotease (60).

Metalloproteases having an MPN domain are constituents of complexes like proteasome and COP9 signalosome, but some of the independently existing forms, like AMSH-LP and AfJAMM are also common. (59-61). The crystal structure of AMSH-LP, an MPN domain-containing protein reveals the cleavage mechanism of Lys-63 linked polyubiquintin. This

protein subunit has a highly conserved JAMM motif, EX_nHS/THX_nSXXD, that is characteristic for metalloproteases with zinc ions in their active sites. AMSH-LP has two zinc-binding sites where one of them, the JAMM motif, is responsible for isopeptide cleavage whereas the other zinc-coordinating site is responsible for recognition of the proximal ubiquitin (62, 63).

The 26S proteasome contains two MPN domain-containing subunits in the RP: Rpn8 and Rpn11. Rpn11 have been shown to be critical for deubiquitylation (35, 59). This metalloprotease has been shown to be the proteasome-resident deubiquitylase, which cleaves the isopeptide bond of the polyubiquitin chain proximal to the substrate prior to degradation of the substrate. It was also reported that Rpn11, along with other subunits in the 19S regulatory particle, might mediate transcriptional regulation and DNA repair independent of their roles in proteolysis (60, 64, 65). More recently, assembly pathway studies, cryo-EM structures and pull-down analyses of subcomplexes demonstrated that Rpn8 and Rpn11 form a heterodimer (50). Furthermore, the crystal structures of AfJAMM (*Archaeoglobus fulgidus* JAB1/MPN/Mov34 metalloenzyme), MOV34 (Rpn8 homologue in human) and AMSH-LP (associated molecule with the SH3 domain of STAM- like protein) provided the basis for functional characterization of MPN domain proteases (60, 61, 63, 65).

A sequence alignment of the different MPN domains of AMSH, AMSH-LP and Rpn11 reveals high sequence similarity of the active sites of ubiquitin cleavage. The catalytically inactive Rpn8 subunit contains an MPN domain but lacks the JAMM motif, which is essential for proteolytic activity (35, 59). Except for providing scaffold for Rpn11 the exact functions of Rpn8 subunit within the RP have not been understood completely till today.

More detailed knowledge on the Rpn11 active site architecture in context with the 26S proteasome is expected to pave the way for structure-based approaches to develop proteasome inhibitors for therapeutic purposes (60) and structural characterization of Rpn11 and Rpn8 would provide insights into the mechanism of substrate deubiquitylation and processing.

PC subunits

Rpn1 and Rpn2 are the two largest subunits of the RP consisting of nine repeats each (21, 38). They have a toroid-like architecture – continuous superhelical structural repeats adopting elongated curved structures resembling bi-helical LRR's (leucine rich repeats). These subunits are common in proteasome and cyclosome complexes (PC), (66, 67), and each subunit contains distinct repeats of 34-40 residues.

Biochemical experiments together with EM studies have been undertaken to localize and structuraly characterize Rpn1 and Rpn2. However they provided only limited insights into the localization of Rpn1 (50). The variability in this region of the EM maps may be due to Rpn1's function of recruiting shuttling proteins. Rpn1 provides binding sites for proteasome-interacting proteins (PIPs) like Rad23, Ubp6, Dsk2 and chaperones (68). Rpn2 harbors the binding site for one of the ubiquitin receptor proteins Rpn13 on its N-terminal helices (38).

Ubiquitin Receptors

Proteasomal subunits involved in recognizing specific protein substrates tagged with ubiquitin are called ubiquitin receptors. Rpn10 and Rpn13 are considered to be the two major ubiquitin receptors in the 26S proteasome complex. Deletion mutations of both of these subunits are stress-sensitive but have no structural defects, suggesting the presence of additional ubiquitin-binding receptors present within the yeast 26S proteasome (21, 38, 40).

Rpn10 has a von Willebrand factor type A domain (vWA) on its N-terminus whereas the flexible C-terminal domain is a single helix (in *S. cerevisiae*) with a ubiquitin-interacting motif (UIM) serving as a binding site for tetra-ubiquitinated substrates (69-72) (Fig 5A). Rpn13 is the other ubiquitin receptor subunit, which is located on Rpn2 and binds ubiquitin through a conserved amino-terminal region called Pleckstrin-like receptor for ubiquitin (Pru) domain (73-76) (Fig 5B). . This domain binds K48-linked diubiquitin chains (76). Rpn13 is also the proteasomal receptor for the deubiquitinating enzyme Uch37 (73).

Ubiquitin

Ubiquitin is one of the smallest proteins like the Sem1P protein (8.5 kDa) of the UPS. It is a key regulator of many important processes in the eukaryotic cells (5, 6, 77, 78). Ubiquitination is a post-translational modification where ubiquitin is ligated to proteins (5). Ubiquitin attachment to a protein determines its fate. It can promote protein interactions, it can signal for sub-cellular localization or it serves as a signal for protein degradation via the proteasome. A series of reactions involving enzymes E1-E3 attaches a lysine residue of the target protein to the C-terminal glycine of a ubiquitin molecule (proximal ubiquitin) forming an isopeptide bond (3). Repeated addition of ubiquitin moieties to the preceding ubiquitin results in poly-ubiquitin chains attached to substrates. The poly-ubiquitin chain can be recognized by different ubiquitin receptor proteins of the proteasome cleaved off during substrate processing, and recycled for signaling reactions (5). In addition to higher eukaryotes ubiquitin-like modifier proteins are also present in most archaea (79, 80).

The ubiquitin molecule is a highly-conserved 76 amino acid-long polypeptide composed of four antiparallel beta strands and two helices. Ubiquitin contains lysine residues at positions 6, 11, 27, 29, 33, 48 and 63, which allows for seven different types of ubiquitin linkages (81) (Fig 5C) . These differences in the linkages provide a vast array of signals for different processes in the cell. To date Lys48 and Lys63 have been extensively studied in the context of protein degradation.

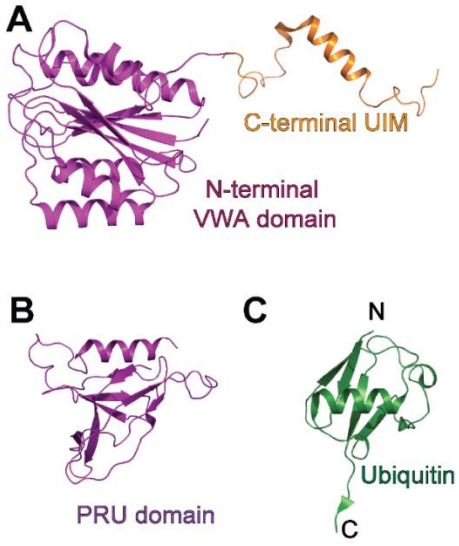

Fig 5. The Ubiquitin receptors

(A) Crystal structure of the vWA domain of Rpn10 (purple) with C-terminal ubiquitin interacting motif (orange) modeled on to it (PDB: 2X5N) (40).

(B) Crystal structure of PRU domain of Rpn13 domain (purple) (PDB: 2R2Y) is other ubiquitin receptor (38).

(C) Ubiquitin protein molecule which is usually conjugates to the substrate proteins serving as a degradation signal (PDB: 2ZNR)(63).

Chapter 3: Aim of the project

Structure and function of the core particle have been studied extensively whereas much less is known about the 19S regulatory particle. The knowledge of its subunit architecture is of great importance for understanding its mechanisms, and it could guide the development of pharmaceuticals targeting this complex. High-resolution structural information would enable interpretation of molecular functions of RP subunits in conjugation with the proteasome holoenzyme complex. Many trials have been carried out to crystallize the 26S holoenzyme complex, but it failed due to its compositional and conformational heterogeneity. Therefore, the primary aim of this project was to obtain crystal structures of regulatory particle subunits that could be positioned in the context of the holocomplex. This information would further be combined with the available cryo-EM reconstructions of the 26S proteasome complex and auxillary data.

Until recently, structural studies of the RP as a holocomplex had not yielded high resolution structures, however, recent progress in sample preparation of the 26S particle as well as novel computational methods allowed for reconstruction of densities approaching sub-nanometer resolution. While it was possible to localize the AAA ATPase module due to its distinct shape and pseudo six-fold symmetry, no information on interactions between other RP subunits and on their location in the complex was available.

Furthermore, in the beginning of this study a neither recombinant 19S RP complex nor the individual recombinant proteins were available. The approaches involving deletion or engineering of proteasomal proteins mostly led to lethal phenotypes or proteasomal assembly defects, hampering further studies. As the entire 26S assembly has remained recalcitrant to crystallization for many years, the approach relying on combining the crystal structures of individual subunits with cryo-EM data of the entire complex appeared as a promising option.

In the course of this project we attempted to clone, express, purify and crystallize all RP subunits. We attempted to obtain subcomplexes of the RP recombinantly and characterized them structurally. Structural information obtained was used as a basis for interpretation of the cryo-EM data, and served further hypothesis-driven studies of proteasome function.

Chapter 4: Results

Part 1:

The proteasomal subunit Rpn6 is a molecular clamp holding the core and regulatory subcomplexes together

The proteasomal subunit Rpn6 is a molecular clamp holding the core and regulatory subcomplexes together

Ganesh Ramnath Pathare[a], István Nagy[a], Stefan Bohn[a], Pia Unverdorben[a], Agnes Hubert[a], Roman Körner[b], Stephan Nickell[a], Keren Lasker[c,d], Andrej Sali[c], Tomohiro Tamura[e,f], Taiki Nishioka[f], Friedrich Förster[a], Wolfgang Baumeister[a,1], and Andreas Bracher[b,1]

[a]Department of Molecular Structural Biology, Max-Planck-Institute of Biochemistry, Am Klopferspitz 18, 82152 Martinsried, Germany; [b]Department of Cellular Biochemistry, Max-Planck-Institute of Biochemistry, Am Klopferspitz 18, 82152 Martinsried, Germany; [f]Laboratory of Molecular Environmental Microbiology, Graduate School of Agriculture, Hokkaido University, Kita-9, Nishi-9, Kita-ku, Sapporo 060-8589, Japan; [c]Department of Bioengineering and Therapeutic Sciences, Department of Pharmaceutical Chemistry, and California Institute of Quantitative Biosciences, 1700 4th Street, University of California, San Francisco, CA 94158; [d]Blavatnik School of Computer Science, Raymond and Beverly Sackler Faculty of Exact Sciences, Tel Aviv University, Tel Aviv 69978, Israel; and [e]Bioproduction Research Institute, National Institute of Advanced Industrial Science and Technology (AIST), 2-17-2-1, Tsukisamu-Higashi, Toyohira-ku, Sapporo 062-8517, Japan

Contributed by Wolfgang Baumeister, October 26, 2011 (sent for review August 4, 2011)

Proteasomes execute the degradation of most cellular proteins. Although the 20S core particle (CP) has been studied in great detail, the structure of the 19S regulatory particle (RP), which prepares ubiquitylated substrates for degradation, has remained elusive. Here, we report the crystal structure of one of the RP subunits, Rpn6, and we describe its integration into the cryo-EM density map of the 26S holocomplex at 9.1 Å resolution. Rpn6 consists of an α-solenoid-like fold and a proteasome COP9/signalosome eIF3 (PCI) module in a right-handed suprahelical configuration. Highly conserved surface areas of Rpn6 interact with the conserved surfaces of the Pre8 (alpha2) and Rpt6 subunits from the alpha and ATPase rings, respectively. The structure suggests that Rpn6 has a pivotal role in stabilizing the otherwise weak interaction between the CP and the RP.

26S proteasome | cryoelectron microscopy | PSMD11 | S9 | PCI domain

Protein degradation is of vital importance for the maintenance of protein homeostasis, for the removal of misfolded proteins, and for the control of numerous regulatory processes (1, 2). In eukaryotic cells, the main pathway for protein degradation is the ubiquitin-proteasome system (3). It has the capability of degrading almost any protein, and yet it acts with exquisite specificity. The ubiquitin system selects proteins and marks them for destruction, whereas the 26S proteasome is the executioner of proteolysis. Malfunctions of the system have been implicated in a variety of diseases (2).

The 26S proteasome is a molecular machine of approximately 2.5 MDa built from two copies each of 34 canonical subunits and several proteasome interacting proteins, which are present in substochiometric amounts (4–6). The 26S holocomplex comprises two subcomplexes: The barrel-shaped core particle (CP) that harbors the proteolytically active sites and sequesters them from the cellular environment, and the regulatory particles (RPs) that bind to one or both ends of the CP. Their role is to prepare substrates for degradation; this preparation includes the recognition of polyubiquitylated proteins, their deubiquitylation and unfolding and, eventually, assistance in their translocation into the CP through the gate in the α-ring of the CP.

The CP, which is a stack of four seven-membered rings (α1–7; β1–7; β1–7; α1–7), is structurally well characterized; it is highly conserved from archaea to mammals, and crystal structures are available for CPs from several species (7–9). In contrast to the CP, the structure of the RP is only dimly understood. So far, all attempts to crystallize the RP alone or in association with the CP have been unsuccessful. Recently, EM single particle analysis has provided a map of the 26S holocomplex at medium resolution (9.1 Å), which provides a platform for the integration of high-resolution structures of the constituent subunits (10).

The RP is composed of a core of 19 different subunits, which can dissociate into a "base" and a "lid" subcomplex (11). The base is thought to form the proximal part of the RP, which associates with the α-rings of the CP, whereas the lid forms the distal end. The base comprises a heterohexameric AAA-ATPase module (Rpt1–Rpt6) and the non-ATPase subunits Rpn1 and Rpn2 (11). The often substoichiometric subunits Rpn10 and Rpn13 are also commonly assigned to the base subcomplex (5). The lid part of the RP is composed of the Rpn3, Rpn5–Rpn9, and Rpn11–Rpn12 subunits (11). The lid subunits can be classified into two groups according to their predicted domain structure: Rpn3, Rpn5, Rpn6, Rpn7, Rpn9, and Rpn12 are predicted to share a C-terminal module present in proteasome, COP9/signalosome, and eIF3 subunits (PCI module), whereas Rpn8 and Rpn11 subunits have an MPN (Mpr1, Pad1 N-terminal) domain in common (12). Functionally, Rpn10 and Rpn13 serve as polyubiquitin receptors, whereas Rpn11 has deubiquitylation activity (4, 5). The PCI module was proposed to have a structural role and is composed of an N-terminal helix bundle and a winged-helix subdomain (13–15).

The PCI subunit Rpn6 was found to be an essential component of the 26S proteasome in *Saccharomyces cerevisiae* (16), *Trypanosoma brucei* (17), *Plasmodium falciparium* (18), and *Drosophila melanogaster* (19). Upon conditional knock-out in *S. cerevisiae*, only partially assembled complexes lacking all the lid subunits were found, and the cells were arrested in G2/M phase (20). Similarly, a temperature-sensitive Rpn6 mutant strain of *S. cerevisiae* yielded only partially assembled complexes at the restrictive temperature, suggesting a critical role of Rpn6 for assembly (21).

Here, we present the crystal structure of Rpn6 from *D. melanogaster*. The distinctive shape of this subunit and the prevalence of α-helices allowed us to fit the structure into the 9.1 Å cryo-EM map of the 26S proteasome of *Schizosaccharomyces pombe* with high confidence. The hybrid structure reveals highly conserved

Author contributions: A.S., F.F., W.B., and A.B. designed research; G.R.P., I.N., S.B., A.H., R.K., T.T., T.N., and A.B. performed research; G.R.P., P.U., S.N., K.L., F.F., and A.B. analyzed data; and G.R.P., A.S., F.F., W.B., and A.B. wrote the paper.

The authors declare no conflict of interest.

Freely available online through the PNAS open access option.

Data deposition: The coordinates and structure factors have been deposited in the Protein Data Bank, www.pdb.org (PDB ID codes 3TXM and 3TXN).

[1]To whom correspondence may be addressed. E-mail: bracher@biochem.mpg.de or baumeist@biochem.mpg.de.

This article contains supporting information online at www.pnas.org/lookup/suppl/doi:10.1073/pnas.1117648108/-/DCSupplemental.

contact interfaces between Rpn6 and subunits of both the CP and RP.

Results and Discussion

Crystallization and Structure Solution. Rpn6 of *D. melanogaster* was expressed as a soluble 6xHis-tag fusion protein in *Rhodococcus erythropolis* (22). The 6xHis-tag was cleaved for biochemical analysis. Size-exclusion chromatography suggested that Rpn6 is monomeric in physiological buffer. Crystals from the 422-residue full-length protein showed only weak diffraction to approximately 9 Å resolution. To find a better construct for crystallization, we performed a limited proteolysis experiment using Proteinase-K. Mass spectrometry analysis of the most prominent SDS-PAGE fragment bands showed that the N-terminal region up to residue 29 is most sensitive to protease cleavage, indicating that it is flexibly linked. At higher protease concentrations, the protein is furthermore nicked at position 337, which maps to the PCI module (Fig. 1*A*). The Rpn6 construct comprising residues 30–422 yielded hexagonal crystals diffracting to 2.5 Å resolution. The crystal structure was solved by Gd-MAD at 3.0 Å resolution (Table S1). The model comprises residues 38–390 (Fig. 1*B*); the remaining residues were not resolved in the electron density and are presumably disordered.

Structure Overview. The crystal structure of Rpn6 consists of an α-helical solenoid followed by the PCI module (Fig. 1*B*). The overall shape is that of a right-handed suprahelical turn with approximate dimensions of 100 Å × 45 Å (height × width). The solenoid contains a slightly elongated N-terminal capping helix and five double-helix repeats with structural similarity to tetratricopeptide repeats (TPR). However, the helices are approximately one turn longer than in canonical TPR units; i.e., each repeat contains approximately 40 residues compared to 34 for TPRs. A conserved sequence signature for the Rpn6 repeats could not be detected. The hydrophobic final helix of the solenoid, α11, forms the central hub of a helix bundle, contacting helices α12, α14, and α16 of the PCI module (Fig. 1*C*). This interaction enables additional contacts between α9 and α16 that reinforce the solenoid-PCI module interface, strongly suggesting that the orientation of the two domains is rigidly fixed to form the right-handed suprahelical configuration. Thus, there is no discrete N-terminal boundary of the PCI module, which supports the conclusion of prior bioinformatic analyses of PCI-protein sequences (14). The winged-helix subdomain of Rpn6 has an elongated first helix, α16, which is markedly kinked in the center. Its N-terminal segment forms part of the helix bundle (Fig. 1*C*). The three-stranded antiparallel β-sheet of the PCI module is located at the tip of the suprahelical structure. α18, the so-called recognition helix in canonical winged-helix transcription factors, is arranged perpendicular to the long axis of the protein. In DNA complex structures, this helix is placed into the major groove of DNA (23). Whether the corresponding structure in Rpn6 serves such a function is unknown, but might be worth further investigation. The 26S proteasome has been implicated to play a role in transcription (24) and DNA double-strand repair (25), which could require physical association of the 26S proteasome to nucleic acid. Comparison with the other known structures of PCI module proteins, Csn7 and eIF3κ (13, 15), indicated that the winged-helix subdomains are less divergent than the N-terminal helix bundles (Fig. S1). The elongated helices in the Rpn6 helix bundle (helices α12, α14, α16) appear to ensure a rigid connection to the α-solenoid; these elongations are absent in Csn7 and eIF3κ. In addition, the proximal part of the helical bundle subdomain in all three structures appears to function as a buttress for the winged-helix domain.

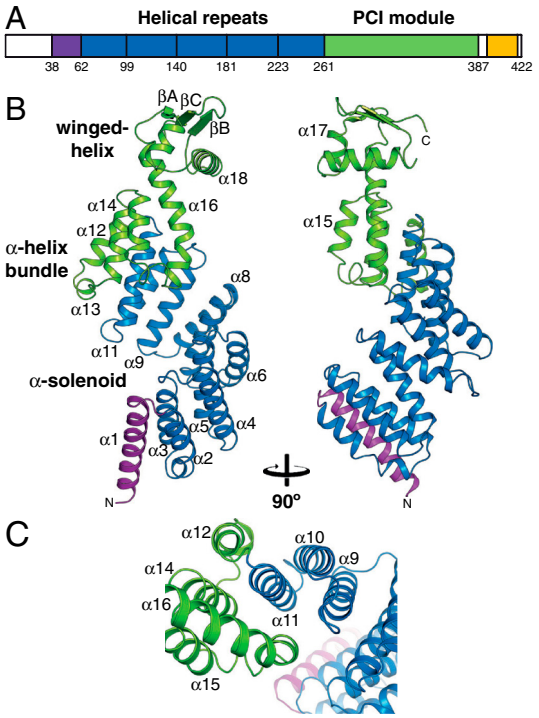

Fig. 1. Crystal structure of Rpn6. (*A*) Domain structure of Rpn6. The purple region denotes a capping helix; the yellow region is predicted to be α-helical. (*B*) Ribbon representation of Rpn6, colored by domain structure. Two views related by 90° rotation are shown. N and C termini and selected secondary structure elements are indicated. (*C*) Detailed view of the interface between the solenoid fold and the PCI module.

Rpn6 Surface Conservation. To identify functionally important regions, we performed an extensive sequence alignment of 21 putative Rpn6 sequences (Fig. S2) and mapped the similarity score onto the surface of the crystal structure (Fig. 2*A*). In the solenoid segment, a large continuous area of increased surface conservation was found on the convex outer face between helix α8 and α10 (region I, Fig. 2*A*). This area has few surface charges (Fig. S3*B*). The adjacent loop connection between helices α6 and α7 (residues 158–162) is also highly conserved. On the concave face, the adjacent residues Lys82, Lys84, Lys87, Arg90, and Phe124 are almost invariant. All these areas face approximately in the same direction, while there is essentially no surface conservation on the opposite (convex) side (Fig. 2*A*), strongly suggesting that the former is involved in contacts with other subunits of the 26S proteasome complex, while the latter is exposed to solvent.

Surface conservation in the PCI module of Rpn6 is limited to two smaller areas located at the flanks on the β-sheet (regions II and III, Fig. 2*B*). Region II includes the end of helix α16, strand βA and the connecting linker. Region III is composed of helix α18 and strand βB. Both are predominantly hydrophobic, implying that they might serve as protein–protein interfaces (Fig. S3). Interestingly, region II and region III of adjacent Rpn6 chains contact each other in the crystal lattice. The alignment of the β-sheets creates a continuous β-ribbon that traverses the crystals along the 6-fold screw axis (Fig. S4*A*), suggesting that the six PCI subunits in the lid might be arranged similarly within the complex. The buried surface area of approximately 460 $Å^2$ on each partner is probably too small for a stable interaction consistent with our finding that Rpn6 is monomeric in solution. This observation suggests that other interactions must contribute to complex formation. A likely candidate for this additional interface is a conserved region at the C-terminus (residues 396–419) that was disordered in the crystal structure. In agreement, the sequence alignment suggests that this segment is flexibly attached to the PCI module via a poorly conserved linker (Fig. S2). Secondary structure prediction strongly suggests that the respective

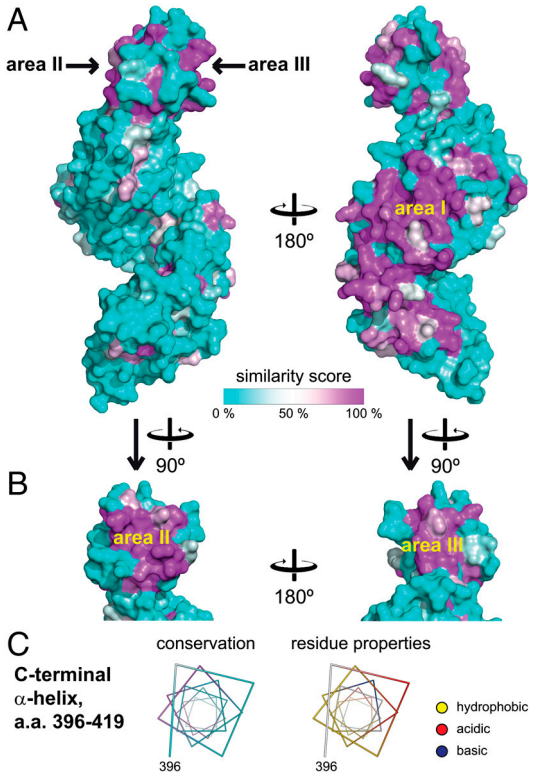

Fig. 2. Surface analysis of Rpn6. (*A*) Surface conservation mapped onto the surface of Rpn6. On the left, the same orientation as in Fig. 1*A* is shown. The similarity score from a multiple alignment of 21 related sequences (Fig. S2) was mapped onto the molecular surface of Rpn6. A cyan-white-magenta color gradient indicates increasing surface conservation. Regions I, II, and III are indicated. (*B*) Side views on the winged-helix subdomain. (*C*) The predicted C-terminal helix. The helix is represented as a helical wheel, and residue properties are indicated. (*Left*) Conservation is represented using the same color scheme as in panel *A*. (*Right*) Hydrophobic side chains are indicated in yellow. Positively and negatively charged functional groups are colored blue and red, respectively. The rest of the surface is shown in white.

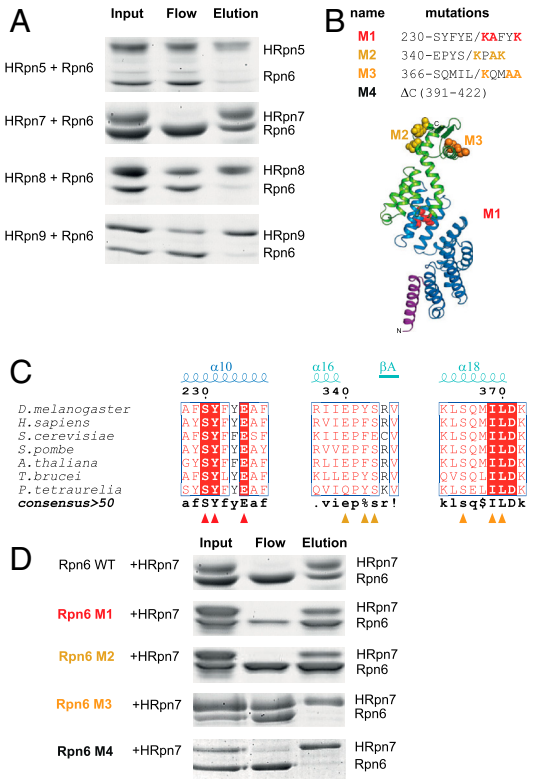

Fig. 3. Binary interaction of Rpn6 and Rpn7. (*A*) Probing for direct interactions of Rpn6 with lid particle subunits. Purified Rpn6 was incubated individually with His-tagged Rpn5, Rpn7, Rpn8, or Rpn9 from *D. melanogaster*. The Coomassie-stained SDS-PAGE gels show the initial mixtures, unbound proteins, and proteins precipitated with Ni-affinity resin. (*B*) Location of Rpn6 mutations in the structure. The respective amino acid residue substitutions are indicated. Mutated residues are shown in space-filling mode. (*C*) Excerpts from Rpn6 sequence alignment showing the mutated regions. (*D*) Both the PCI module interface region III and the C-terminal helix of Rpn6 are required for the interaction with Rpn7. His-tagged Rpn7 was incubated with either wild-type Rpn6(30–422) or Rpn6(30–422) mutants M1, M2, M3, or M4 and analyzed as described for panel *A*.

region forms an amphipathic α-helix (4). Mapping conservation and surface properties on this predicted helix shows that conservation is limited to the hydrophobic face (Fig. 2*C*), suggesting that it is involved in interactions with other subunits, probably in a coiled-coil conformation. Intriguingly, all proteasomal PCI subunits were predicted to comprise such a helical segment C-terminal to the PCI module (4).

Interactions of Rpn6 Within the Lid. To test whether or not the PCI subunits interact with each other in the lid subcomplex, we incubated Rpn6 separately with 6xHis-tagged Rpn5, Rpn7, or Rpn9 of *D. melanogaster*, followed by Ni-affinity precipitation (Fig. 3*A*). Under the conditions tested, only Rpn6 and Rpn7 formed a stable binary complex. To analyze this interaction in more detail, mutations were introduced into Rpn6 (Fig. 3*B*). At the center of region I, we replaced the highly conserved peptide sequence 230-SYFYE-234 with KAFYK, yielding mutant M1 (Fig. 3*C*). Similarly, Rpn6 mutants M2 and M3 were generated by analogous substitutions of conserved peptide motifs in regions II and III, respectively. Finally, we removed the putative C-terminal α-helix by truncation at position 391 (M4). Interaction analysis of these mutant Rpn6 forms with 6xHis-tagged Rpn7 clearly showed that both an intact region III and the putative C-terminal helix are required for the interaction (Fig. 3*D*). This finding strongly suggests that the observed interaction is specific. Rpn6 and Rpn7 are thus likely to be in direct contact with each other in the lid, probably employing a bipartite interface.

Location of Rpn6 in the 26S Proteasome. Finally, we fitted the crystal structure of Rpn6 into the 9.1 Å cryo-EM density of the 26S proteasome from *S. pombe*, which is the highest-resolution map available so far (10) (Fig. 4*A*). An exhaustive six-dimensional real-space search yielded a single solution, with high confidence (Fig. S5). The size of Rpn6 (49 kDa), its distinctive shape, and the prevalence of α-helices enabled the high-precision fit into the map (Fig. S6). We estimate that the accuracy of the fit considerably exceeds the resolution of the map (9 Å), probably by an order of magnitude. In the resulting model, Rpn6 forms a protrusion that is located at the outer rim of the lid particle, reaching down to the ATPase and alpha rings with its α-solenoid segment (Fig. 4*A*). This interface appears to be the most extensive direct contact between the lid and core particles (a second contact formed by a protrusion to the left of Rpn6 appears weaker). There is additional density at the N-terminus of the Rpn6 model that might correspond to residues 1–37, most of which were not included in the crystallization construct. For Rpn6 of *S. pombe*, an additional pair of helices was predicted for this segment and included in our homology model (Fig. 4*B*). Regions on Rpn6 with high surface conservation match almost perfectly with the areas buried in the complex, while the rather poorly conserved face projects toward the solvent (compare Figs. 2*A* and 4*A*).

The subunits contacted by the solenoid domain of Rpn6 were previously assigned as Rpt6 and Pre8 (alpha2) using the 9.1 Å cryo-EM density of the 26S proteasome from *S. pombe* and

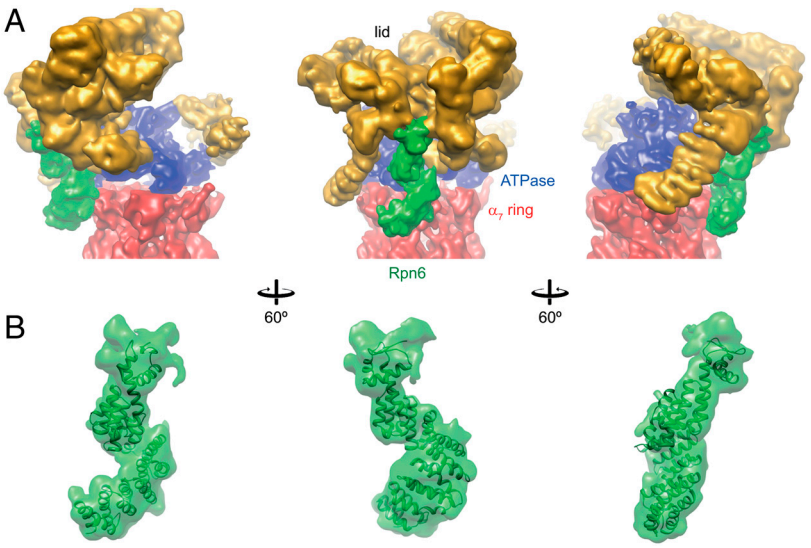

Fig. 4. Location of Rpn6 in the 26S proteasome. (*A*) Rpn6 density within the 9 Å cryo-EM density of the 26S proteasome from *S. pombe*. Three views are shown. The lid, base, and core subcomplex densities are indicated in gold, blue, and red, respectively. Density ascribed to Rpn6 is colored green. The core particle is clipped off at the β_7 ring. (*B*) Detailed view of the Rpn6 fitted into the EM envelope. Density assigned for Rpn6 was segmented from the map. The homology model of Rpn6 from *S. pombe* including the predicted N-terminal helices $\alpha(-1)$ and α0 are included. Similar orientations as in panel *A* are shown.

cross-linking data (10). For both, high-confidence molecular models are available (7, 26–28). Both subunits share a conspicuous surface conservation in the Rpn6 contact areas, which is indicative of coevolution of the interface residues (Fig. 5 *A–E*). Interestingly, conditional mutation of Rpt6 in *S. cerevisiae* resulted in the same G2/M phase transition arrest as the Rpn6 deletion (20, 29). Closer inspection reveals that the CP subunit Pre8 is in proximity to the N-terminus of α3 (residues 79–85), the loop between α4 and α5 (118–122), and the loop between α6 and α7 (157–160) (Fig. 5 *B* and *C*). Together, these elements form an extensive, conserved interface. Under the reasonable assumption that the peptide backbones in the complex are similar to those in the individual crystal structures, a tentative assignment of molecular interactions is possible: The small side chains of $Ser79^{Rpn6}$ and $Ala81^{Rpn6}$ (*S. pombe* numbering, add 2 for *D. melanogaster*) enable tight contacts to α7 of Pre8. The adjacent residues $Lys80^{Rpn6}$, $Lys82^{Rpn6}$, and $Lys85^{Rpn6}$ are in hydrogen-bonding distance to $Glu183^{Pre8}$/$Asp185^{Pre8}$, $Asp240^{Pre8}$, and $Asp243^{Pre8}$, respectively. Because of the proximity to $Asp159^{Rpn6}$ and $Asp160^{Rpn6}$, the C-terminal $Val245^{Pre8}$ might rearrange to form a salt bridge with its carboxylate group to $Arg88^{Rpn6}$. The $Val245^{Pre8}$ side chain would then point into a hydrophobic pocket formed by $Phe122^{Rpn6}$, $Ala126^{Rpn6}$, and $Arg88^{Rpn6}$. In an alternative scenario, the side chains of $Phe122^{Rpn6}$ and $Met158^{Rpn6}$ might rearrange locally and engage in contacts with two hydrophobic pockets located between helices α7 and α6, and at the loop connection between α5 and α6 of Pre8, respectively. Moreover, $Asp159^{Rpn6}$ is in hydrogen-bonding distance to $Arg177^{Pre8}$ and $His189^{Pre8}$; $Lys119^{Rpn6}$ may form a salt bridge with $Glu183^{Pre8}$. The exposed side chain of residue $Tyr199^{Rpn6}$, which is located in the strongly conserved loop between helices α8 and α9 (residues 186–202), could reach toward the highly conserved $Lys196^{Pre8}$.

The Rpt6–Rpn6 interface involves Rpn6 helices α8 and α10 (Fig. 2, area I), which are located opposite to Rpt6 helices α12 and α13 (i.e. helices 3 and 4 in its four-helical bundle subdomain) (Fig. 5 *D* and *E*). Specifically, the conserved helix α8 of Rpn6 aligns with helix α12 in Rpt6. Residues $Thr234^{Rpn6}$, $Ser227^{Rpn6}$, $Tyr228^{Rpn6}$, and $Glu231^{Rpn6}$ (the latter three mutated in Rpn6-M1, Fig. 3) at the groove between helices α8 and α10 of Rpn6 cradle the highly conserved C terminus of Rpt6 helix α12, extending the contact area. While $Tyr228^{Rpn6}$ is placed for con-

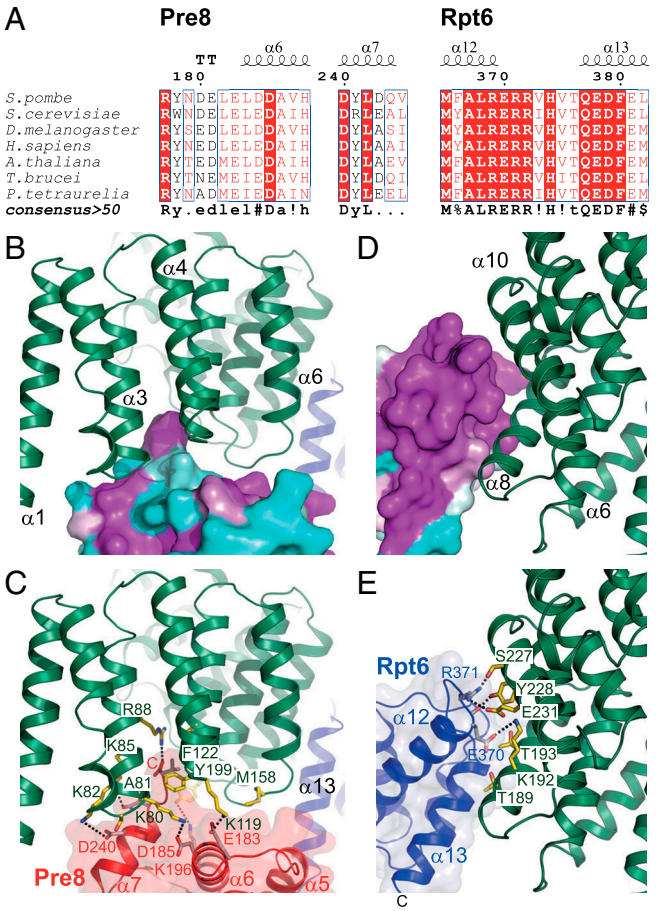

Fig. 5. Putative interactions of Rpn6 with Pre8 and Rpt6. (*A*) Excerpts from Pre8 and Rpt6 sequence alignments for the Rpn6 contact regions. (*B* and *C*) Detailed view of the interactions with Pre8. (*Upper*) The similarity score of an extensive alignment of Pre8 sequences mapped onto the homology model surface. Rpn6 is shown as a green ribbon. (*Lower*) Putative key interactions at the interface. Both proteins are shown in ribbon representation. Selected side chains are shown as sticks. Putative hydrogen bonds are indicated by dashed lines. (*D* and *E*) Detailed view of the interactions with Rpt6.

tacting the backbone at Rpt6 residue 370, the Arg371^{Rpt6} side chain is in hydrogen-bonding distance to both Ser227^{Rpn6} and Glu231^{Rpn6}. Glu370^{Rpt6} could form hydrogen bonds with Lys192^{Rpn6} and Asn196^{Rpn6}.

Interestingly, surface conservation on Rpn6 extends toward the lid beyond the observed contact area—for example, Ala186^{Rpn6} is extending the conserved edge of helix α8 continuing from Thr189^{Rpn6} and Thr193^{Rpn6}. This conservation suggests that Rpn6 could accommodate different conformational states of the ATPase ring. "Wobbling" or "wagging" motions of the active ATPase ring relative to the CP have been proposed (30, 31), and ATP-dependent structural changes involve binding of ubiquitin conjugates (32). In addition, there is structural evidence for a wagging motion of the whole RP (30).

The tip of the PCI module of Rpn6 is part of a horseshoe structure with six radially projecting protrusions that are included in the lid density (Fig. 4*A*). The contact points within the horseshoe coincide with the conserved regions II and III at the flanks of the β-sheet in Rpn6 (Fig. 4*B*). Region III, which was implicated in direct interactions of Rpn6 with Rpn7 (Fig. 3*D*), is situated to the right (Fig. 4*B*), suggesting that this density corresponds to Rpn7. Furthermore, yeast-two hybrid assays indicate a physical interaction of Rpn6 and Rpn5 via their PCI modules (21), suggesting that the density to the left of Rpn6 represents Rpn5. It is thus tempting to speculate that the horseshoe represents the density for the six proteasome PCI subunits, arranged like the Rpn6 chains in the crystal (Fig. S4*A*). According to this hypothesis, the interacting winged-helix subdomains form the inner rim, and the N-terminally adjacent α-helical bundles and solenoids form the protrusions. At the current resolution, the density for the C-terminal helix of Rpn6 cannot be assigned with confidence.

Arrangement of the PCI Subunits in the RP. Our mutational analysis showed that the winged-helix subdomain in the PCI module of Rpn6 is important for interactions with the PCI subunit Rpn7, consistent with the proposed function as a PCI:PCI interaction module (14). In addition to an intact winged-helix motif, the conserved C-terminal helix of Rpn6 is required for the interaction with Rpn7. This requirement for an additional contact might explain why we were not able to identify a second PCI binding partner of Rpn6. Rpn5, Rpn6, and Rpn9 form a subcomplex together with Rpn8 and Rpn11 (33), suggesting that one of the latter non-PCI subunits is required for the attachment of Rpn6 to Rpn5 in addition to the subunit II–III interface. The assembly pathway of the lid suggests that the PCI subunits Rpn3 and Rpn7 form a dimer, and PCI subunit Rpn12 attaches to the Rpn3/Rpn7 dimer after its binding to the Rpn6/Rpn5/Rpn8/Rpn9/Rpn11 pentamer (33). Thus, Rpn6 and Rpn7 followed by Rpn3 and Rpn12 could form the right end of the horseshoe, perhaps stabilized by coiled-coil interactions of their C-terminal helices; the interaction of Rpn6 with Rpn5 would require Rpn8 and Rpn11, resulting in the second subcomplex. The sequence of PCI subunits in the horseshoe structure would thus be (from the left) Rpn9-Rpn5-Rpn6-Rpn7-Rpn3-Rpn12 (Fig. S4*B*). Such a model is consistent with native MS analysis of the COP9/signalosome, in which each subunit of the lid subcomplex has a homolog (34). Thus, the lid and COP9/signalosome architectures might be evolutionarily conserved.

Conclusions

In our hybrid structure, Rpn6 contacts at least four subunits from three functional units of the proteasome, the lid, the ATPase, and the proteolytic core particle. Interactions with Rpn6 thus appear to reinforce the contacts between the lid and base and also between the regulatory and core particles. This Rpn6 role is consistent with increased occurrence of partially assembled proteasome particles in the temperature-sensitive *rpn6-2* mutant of budding yeast (21). Interestingly, this mutant harbors mutations both at the interface to the alpha ring, F132L (residue F122 in *S. pombe*) and the lid subunits Rpn5 and Rpn7, L377P (residue L365 in *D. melanogaster*). The latter mutation would presumably interrupt helix α18, compromising the structural integrity of the winged-helix subdomain.

Because of the symmetry mismatch between the heptameric alpha ring and the hexameric AAA-ATPase, their contacts appear rather sparse and weak, thus enabling relative motions. Indeed, symmetry mismatches have often evolved to allow for motions of macromolecules during their functional cycle (35). Thus, Rpn6 appears to have a pivotal role in holding the complex together by acting as an additional clamp between RP and CP. Monomeric Rpn6 might also be functionally important. The reported interactions of Rpn6 with the ubiquitin ligase regulatory complex COP9/signalosome probably control its own degradation (19, 36), which might in turn regulate the assembly and activation of 26S proteasomes through the availability of monomeric Rpn6. Such a regulation is consistent with the critical role of Rpn6 for the integrity of the 26S proteasomes complex.

Materials and Methods

Detailed experimental procedures are given in *SI Materials and Methods*. Briefly, Rpn6 from *D. melanogaster* was expressed as a His_6-tag fusion protein including a tobacco etch virus (TEV) protease site in *R. erythropolis (L-88)* cells and purified by Ni^{2+}-immobilized metal affinity chromatography, TEV cleavage, Mono-Q anion exchange chromatography, and Superose-12 size-exclusion chromatography. Crystals were grown using 100 mM Tris-HCl pH 7.5 200 mM Li_2SO_4 and 12% PEG-3350 as a precipitant. The Rpn6 crystal structure was solved by multiwavelength anomalous dispersion using gadolinium(3+), using diffraction data acquired at the European Synchrotron Radiation Facility (ESRF), Grenoble, France. The exact position and orientation of Rpn6 in the 9.1 Å electron density map of the 26S proteasome was determined by an exhaustive six-dimensional search procedure.

ACKNOWLEDGMENTS. We thank the staff of the Joint Structural Biology Group at the European Synchrotron Radiation Facility, Grenoble, France, of the Max-Planck-Institute of Biochemistry Crystallization Facility and the Max-Planck-Institute of Biochemistry Core Facility for their excellent support; and Johannes Söding for valuable discussions. Materials for the *R. erythropolis* expression system were kindly provided by Khalid Ibrahim Sallam and Noriko Tamura, Sapporo, Japan. This work was supported in part by funding from the European Union 7th Framework Program PROSPECTS (Proteomics Specification in Space and Time Grant HEALTH-F4-2008-201648). F.F. is grateful to a Career Development Award from the Human Frontier Science Project. K.L. was supported by continuous mentorship from Prof. Haim J. Wolfson as well as a fellowship from the Clore Foundation Ph.D. Scholars program.

1. Buchberger A, Bukau B, Sommer T (2010) Protein quality control in the cytosol and the endoplasmic reticulum: Brothers in arms. *Mol Cell* 40:238–252.
2. Glickman MH, Ciechanover A (2002) The ubiquitin-proteasome proteolytic pathway: Destruction for the sake of construction. *Physiol Rev* 82:373–428.
3. Hershko A, Ciechanover A, Varshavsky A (2000) Basic Medical Research Award. The ubiquitin system. *Nat Med* 6:1073–1081.
4. Förster F, Lasker K, Nickell S, Sali A, Baumeister W (2010) Toward an integrated structural model of the 26S proteasome. *Mol Cell Proteomics* 9:1666–1677.
5. Tanaka K (2009) The proteasome: Overview of structure and functions. *Proc Jpn Acad Ser B Phys Biol Sci* 85:12–36.
6. Voges D, Zwickl P, Baumeister W (1999) The 26S proteasome: A molecular machine designed for controlled proteolysis. *Annu Rev Biochem* 68:1015–1068.
7. Groll M, et al. (1997) Structure of 20S proteasome from yeast at 2.4 A resolution. *Nature* 386:463–471.
8. Löwe J, et al. (1995) Crystal structure of the 20S proteasome from the archaeon T. acidophilum at 3.4 A resolution. *Science* 268:533–539.
9. Unno M, et al. (2002) The structure of the mammalian 20S proteasome at 2.75 A resolution. *Structure* 10:609–618.
10. Bohn S, et al. (2010) Structure of the 26S proteasome from Schizosaccharomyces pombe at subnanometer resolution. *Proc Natl Acad Sci USA* 107:20992–20997.
11. Glickman MH, et al. (1998) A subcomplex of the proteasome regulatory particle required for ubiquitin-conjugate degradation and related to the COP9-signalosome and eIF3. *Cell* 94:615–623.
12. Kim T, Hofmann K, von Arnim AG, Chamovitz DA (2001) PCI complexes: Pretty complex interactions in diverse signaling pathways. *Trends Plant Sci* 6:379–386.
13. Dessau M, et al. (2008) The Arabidopsis COP9 signalosome subunit 7 is a model PCI domain protein with subdomains involved in COP9 signalosome assembly. *Plant Cell* 20:2815–2834.

14. Scheel H, Hofmann K (2005) Prediction of a common structural scaffold for proteasome lid, COP9-signalosome and eIF3 complexes. *BMC Bioinformatics* 6:71.
15. Wei Z, et al. (2004) Crystal structure of human eIF3k, the first structure of eIF3 subunits. *J Biol Chem* 279:34983–34990.
16. Saito A, et al. (1997) cDNA cloning and functional analysis of p44.5 and p55, two regulatory subunits of the 26S proteasome. *Gene* 203:241–250.
17. Li Z, Wang CC (2002) Functional characterization of the 11 non-ATPase subunit proteins in the trypanosome 19 S proteasomal regulatory complex. *J Biol Chem* 277:42686–42693.
18. Muralidharan V, Oksman A, Iwamoto M, Wandless TJ, Goldberg DE (2011) Asparagine repeat function in a Plasmodium falciparum protein assessed via a regulatable fluorescent affinity tag. *Proc Natl Acad Sci USA* 108:4411–4416.
19. Lier S, Paululat A (2002) The proteasome regulatory particle subunit Rpn6 is required for Drosophila development and interacts physically with signalosome subunit Alien/CSN2. *Gene* 298:109–119.
20. Santamaria PG, Finley D, Ballesta JP, Remacha M (2003) Rpn6p, a proteasome subunit from Saccharomyces cerevisiae, is essential for the assembly and activity of the 26 S proteasome. *J Biol Chem* 278:6687–6695.
21. Isono E, Saito N, Kamata N, Saeki Y, Toh EA (2005) Functional analysis of Rpn6p, a lid component of the 26 S proteasome, using temperature-sensitive rpn6 mutants of the yeast Saccharomyces cerevisiae. *J Biol Chem* 280:6537–6547.
22. Nakashima N, Tamura T (2004) A novel system for expressing recombinant proteins over a wide temperature range from 4 to 35 degrees C. *Biotechnol Bioeng* 86:136–148.
23. Gajiwala KS, Burley SK (2000) Winged helix proteins. *Curr Opin Struct Biol* 10:110–116.
24. Collins GA, Tansey WP (2006) The proteasome: A utility tool for transcription? *Curr Opin Genet Dev* 16:197–202.
25. Krogan NJ, et al. (2004) Proteasome involvement in the repair of DNA double-strand breaks. *Mol Cell* 16:1027–1034.
26. Djuranovic S, et al. (2009) Structure and activity of the N-terminal substrate recognition domains in proteasomal ATPases. *Mol Cell* 34:580–590.
27. Zhang F, et al. (2009) Structural insights into the regulatory particle of the proteasome from Methanocaldococcus jannaschii. *Mol Cell* 34:473–484.
28. Förster F, et al. (2009) An atomic model AAA-ATPase/20S core particle sub-complex of the 26S proteasome. *Biochem Biophys Res Commun* 388:228–233.
29. Ghislain M, Udvardy A, Mann C (1993) S. cerevisiae 26S protease mutants arrest cell division in G2/metaphase. *Nature* 366:358–362.
30. Walz J, et al. (1998) 26S proteasome structure revealed by three-dimensional electron microscopy. *J Struct Biol* 121:19–29.
31. Saeki Y, Tanaka K (2007) Unlocking the proteasome door. *Mol Cell* 27:865–867.
32. Peth A, Uchiki T, Goldberg AL (2010) ATP-dependent steps in the binding of ubiquitin conjugates to the 26S proteasome that commit to degradation. *Mol Cell* 40:671–681.
33. Fukunaga K, Kudo T, Toh-e A, Tanaka K, Saeki Y (2010) Dissection of the assembly pathway of the proteasome lid in Saccharomyces cerevisiae. *Biochem Biophys Res Commun* 396:1048–1053.
34. Sharon M, et al. (2009) Symmetrical modularity of the COP9 signalosome complex suggests its multifunctionality. *Structure* 17:31–40.
35. Zwickl P, Baumeister W, Steven A (2000) Dis-assembly lines: The proteasome and related ATPase-assisted proteases. *Curr Opin Struct Biol* 10:242–250.
36. Kwok SF, Staub JM, Deng XW (1999) Characterization of two subunits of Arabidopsis 19S proteasome regulatory complex and its possible interaction with the COP9 complex. *J Mol Biol* 285:85–95.

Supporting Information

Pathare et al. 10.1073/pnas.1117648108

SI Materials and Methods

Cloning and Purification of Rpn6. Rpn6 from *Drosophila melanogaster* was cloned as N-terminal 6xHis-tag fusion protein into a modified pTipRC1 plasmid with a tobacco etch virus (TEV) protease cleavage site in between 6xHis-tag and the *rpn6* gene. Protein expression was carried out in *Rhodococcus erythropolis (L-88)* (1), where the resulting strain was grown at 30 °C in 5 L of LB medium. Protein production was induced with 0.5 $\mu g\,mL^{-1}$ thiostrepton for another 24 to 48 h. Cells were sedimented at 4,000 g and washed with sterile water. The pellet (20 g) was resuspended in 50 mL lysis buffer (50 mM sodium phosphate pH 8.0, 10 mM imidazole, 300 mM NaCl). Complete protease inhibitor cocktail (Roche Biotech) and 1 $mg\,mL^{-1}$ lysozyme were added, and the mixture incubated for 2 h on ice. Subsequently, 100 ppm Benzonase was added, followed by ultrasonication on ice. Cell debris was removed by ultracentrifugation at 28,000 × *g*. His-tagged Rpn6 was purified by affinity chromatography using Ni-NTA beads (GE Healthcare) according to the supplier recommendations. Fractions containing Rpn6 were pooled, augmented with TEV protease for removal of the 6xHis-tag, and incubated for 12 h at 4 °C in a dialysis chamber equilibrating against 25 mM Tris HCl pH 7.5. TEV protease was removed by MonoQ anion exchange chromatography, using a linear salt gradient to 1 M NaCl in 25 mM Tris HCl pH 7.5. Size-exclusion chromatography (SEC), using Superose-12 (GE Healthcare) equilibrated with 20 mM Hepes NaOH pH 7.5, 300 mM NaCl, and 1 mM DTT was used as final purification step.

Limited proteolysis. Full-length Rpn6 at 0.5 $mg\,mL^{-1}$ was subjected to limited proteolysis, using increasing concentrations of Proteinase-K (0.025–0.1 $mg\,mL^{-1}$). After 30 min incubation at 20 °C, samples were analyzed by SDS-PAGE followed by in-gel digestion and peptide mass spectrometry. Samples with prominent digestion products were subjected to liquid chromatography–mass spectrometry analysis to measure apparent molecular masses to be able to determine actual proteolytic sites.

Crystallization. Crystals of Rpn6(30–422) were grown by the sitting drop vapor diffusion method at 4 °C and 18 °C, mixing equal volumes of Rpn6(30–422) (25 $mg\,mL^{-1}$ in 20 mM Hepes NaOH pH 7.5, 300 mM NaCl, and 1 mM DTT) with a precipitant containing 100 mM Tris HCl pH 7.5 200 mM Li_2SO_4, 12% PEG-3350. For cryoprotection, crystals were transferred stepwise into 100 mM Tris HCl pH 7.5, 300 mM Li_2SO_4, 15% PEG-3350 and 20% glycerol before being flash-frozen in liquid nitrogen.

Structure Determination. Diffraction data were collected at the European Synchrotron Radiation Facility (ESRF) in Grenoble, France. The data were processed with XDS (2) and transferred into the CCP4 format using Pointless (3), Scala (4), and Truncate (5). The structure was solved using crystals soaked with 0.5 mM $GdCl_3$. Four Gd sites were found in a MAD dataset using SHELXD (6) as implemented in HKL2MAP (7). This solution was further refined with Sharp (8). Density modification was subsequently carried out using Resolve (9). A preliminary model was manually built in the resulting map using Coot (10). For final model building and refinement, nearly isomorphous native data were used. Iterative cycles of manual model building and refinement with Refmac (11), as implemented in the CCP4 interface (12), were carried out. The final model contains Rpn6 residues 38 to 390, two sulphate, two glycerol, and 49 water molecules. Nonglycine residues facing solvent channels without discernable side-chain density were modeled as alanines.

Site-Directed Mutagenesis. Site-directed mutations in Rpn6 were introduced with the QuikChange site-directed mutagenesis kit (Stratagene) using pTipRC-Rpn6 as the template.

Coprecipitation Assay. Different subunits from the *D. melanogaster* regulatory particle were used for the coprecipitation assay. Binary interactions of these subunits were studied by mixing Rpn6 with other subunits having a 6xHis-tag. Proteins were mixed at 1:1 molar ratio and incubated with Ni-NTA Superflow beads at 20 °C for 45 min. The mixtures were applied to spin column bodies (Qiagen), washed with the washing buffer, and the retained proteins were eluted with the elution buffer. The fractions were analyzed by SDS-PAGE.

EM Density Fitting. The exact position and orientation of Rpn6 in the electron density map of the 26S proteasome was determined by an exhaustive six-dimensional search procedure. The atomic coordinates of Rpn6 were converted into a gray-scale volume by assigning the sums of atomic numbers for all atoms contained in the corresponding voxels. This Rpn6 density volume was low-pass filtered to a resolution of 6.4 Å and used as a template for a cross-correlation based search by screening three translational and three rotational parameters. The rotational search was performed with an angular increment of 2° using MOLMATCH (13). The position of the maximal normalized cross-correlation correlation coefficient ($CCC_{max} = 0.48$) and the corresponding rotational parameters were determined, and the original atomic coordinates of Rpn6 were transformed accordingly (see also Fig. S5). In addition, we computed a Z-score for the orientation-specificity for each of the determined positions as described previously (14).

Bioinformatics Methods. A Dali search (15) of the Protein Data Bank (PDB) using the solenoid part of Rpn6 revealed several prokaryotic proteins with structurally similar repeats but disparate biological functions: DrR162B (PDB ID code 3GW4), PlcR [PDB ID code 2QFC (16)], and MalT [PDB ID code 1HZ4 (17)].

HHpred (18) was used for identification of structural templates and their alignment to the target sequence of *Schizosaccharomyces pombe* Rpn6. Our *D.melanogaster* Rpn6 crystal structure covered residues 38 to 387, and TOM70 (PDB ID code 2GW1) was used as an additional template for residues 4 to 100. The C-terminal residues 388–421 were not modeled. Comparative models were built using MODELLER (19) and further refined in the context of the EM map using MDFF (20).

Structural figures were prepared using PyMOL (http://www.pymol.org) and Chimera (http://www.cgl.ucsf.edu/chimera/). Alignment figures were created with ESPript (21).

1. Nakashima N, Tamura T (2004) A novel system for expressing recombinant proteins over a wide temperature range from 4 to 35 degrees C. *Biotechnol Bioeng* 86:136–148.
2. Kabsch W (2010) XDS. *Acta Crystallogr D Biol Crystallogr* 66:125–132.
3. Evans P (2006) Scaling and assessment of data quality. *Acta Crystallogr D Biol Crystallogr* 62:72–82.
4. Evans PR (1997) Scala. *Joint CCP4 + ESF-EACBM Newsletter on Prot Crystallogr* 33:22–24.
5. French G, Wilson K (1978) On the treatment of negative intensity observations. *Acta Crystallogr A* 34:517–525.

6. Schneider TR, Sheldrick GM (2002) Substructure solution with SHELXD. *Acta Crystallogr D Biol Crystallogr* 58:1772–1779.
7. Pape T, Schneider TR (2004) HKL2MAP: A graphical user interface for macromolecular phasing with SHELX programs. *J Appl Crystallogr* 37:843–844.
8. de la Fortelle E, Bricogne G (1997) Maximum-likelihood heavy atom parameter refinement for multiple isomorphous replacement and multiwavelength anomalous diffraction methods. *Methods Enzymol* 276:472–494.
9. Terwilliger TC (2000) Maximum-likelihood density modification. *Acta Crystallogr D Biol Crystallogr* 56:965–972.
10. Emsley P, Cowtan K (2004) Coot: Model-building tools for molecular graphics. *Acta Crystallogr D Biol Crystallogr* 60:2126–2132.
11. Murshudov GN, Vagin AA, Dodson EJ (1997) Refinement of macromolecular structures by the maximum-likelihood method. *Acta Crystallogr D Biol Crystallogr* 53:240–255.
12. Potterton E, Briggs P, Turkenburg M, Dodson E (2003) A graphical user interface to the CCP4 program suite. *Acta Crystallogr D Biol Crystallogr* 59:1131–1137.
13. Förster F, Han BG, Beck M (2010) Visual proteomics. *Methods Enzymol* 483:215–243.
14. Volkmann N (2009) Confidence intervals for fitting of atomic models into low-resolution densities. *Acta Crystallogr D Biol Crystallogr* 65:679–689.
15. Holm L, Rosenström P (2010) Dali server: Conservation mapping in 3D. *Nucleic Acids Res* 38:W545–W549.
16. Declerck N, et al. (2007) Structure of PlcR: Insights into virulence regulation and evolution of quorum sensing in Gram-positive bacteria. *Proc Natl Acad Sci USA* 104:18490–18495.
17. Steegborn C, Danot O, Huber R, Clausen T (2001) Crystal structure of transcription factor MalT domain III: A novel helix repeat fold implicated in regulated oligomerization. *Structure* 9:1051–1060.
18. Söding J, Biegert A, Lupas AN (2005) The HHpred interactive server for protein homology detection and structure prediction. *Nucleic Acids Res* 33:W244–W248.
19. Sali A, Blundell TL (1993) Comparative protein modelling by satisfaction of spatial restraints. *J Mol Biol* 234:779–815.
20. Trabuco LG, Villa E, Mitra K, Frank J, Schulten K (2008) Flexible fitting of atomic structures into electron microscopy maps using molecular dynamics. *Structure* 16:673–683.
21. Gouet P, Courcelle E, Stuart DI, Metoz F (1999) ESPript: multiple sequence alignments in PostScript. *Bioinformatics* 15:305–308.

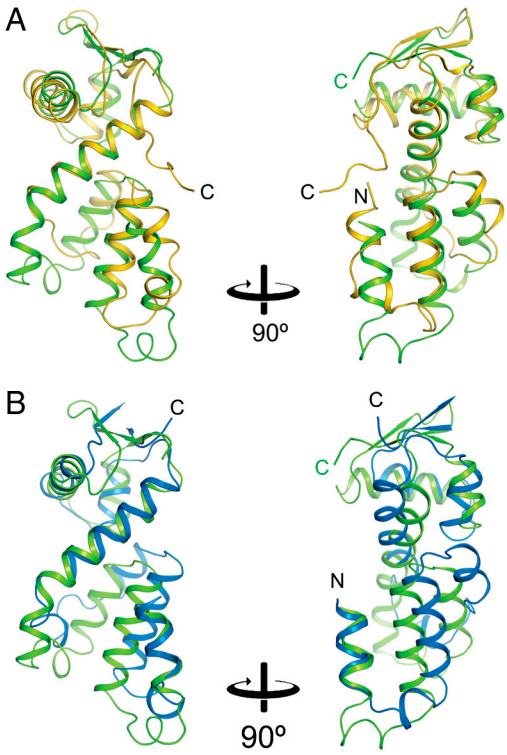

Fig. S1. Comparison of the (proteasome, COP9/signalosome, and eIF3 (PCI) modules of Rpn6, Csn7, and eIF3κ. (*A*) Superposition of Rpn6 and Csn7 [Protein Data Bank (PDB) ID code 3CHM (1)]. The superposed PCI modules of Rpn6 and Csn7 are shown as green and yellow ribbons, respectively. N and C termini are indicated. (*B*) Superposition of Rpn6 and eIF3κ [PDB ID code 1RZ4 (2)]. The superposed PCI modules of Rpn6 and eIF3κ are shown as green and blue ribbons, respectively.

1 Dessau M, et al. (2008) The Arabidopsis COP9 signalosome subunit 7 is a model PCI domain protein with subdomains involved in COP9 signalosome assembly. *Plant Cell* 20:2815–2834.
2 Wei Z, et al. (2004) Crystal structure of human eIF3k, the first structure of eIF3 subunits. *J Biol Chem* 279:34983–34990.

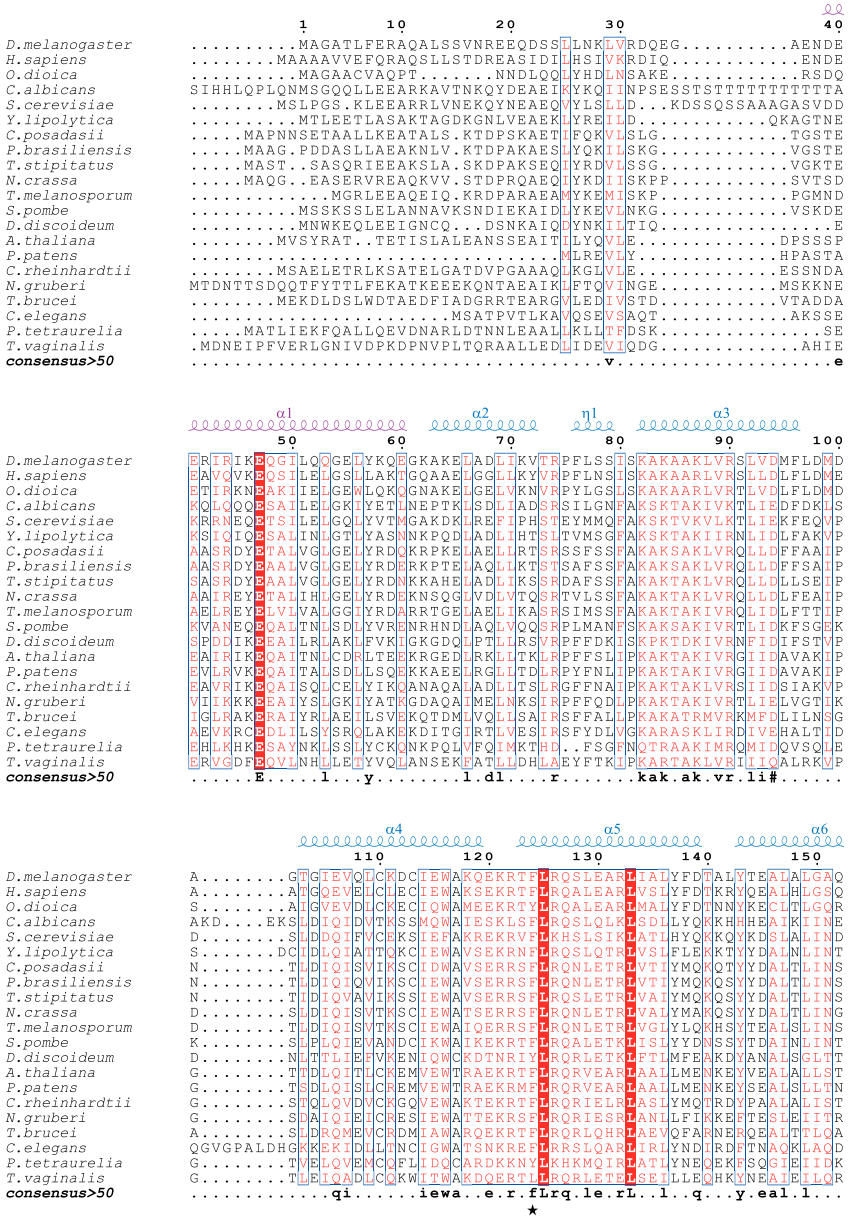
α1
α2
η1
α3
α4
α5
α6
D.melanogaster
H.sapiens
O.dioica
C.albicans
S.cerevisiae
Y.lipolytica
C.posadasii
P.brasiliensis
T.stipitatus
N.crassa
T.melanosporum
S.pombe
D.discoideum
A.thaliana
P.patens
C.rheinhardtii
N.gruberi
T.brucei
C.elegans
P.tetraurelia
T.vaginalis
consensus>50

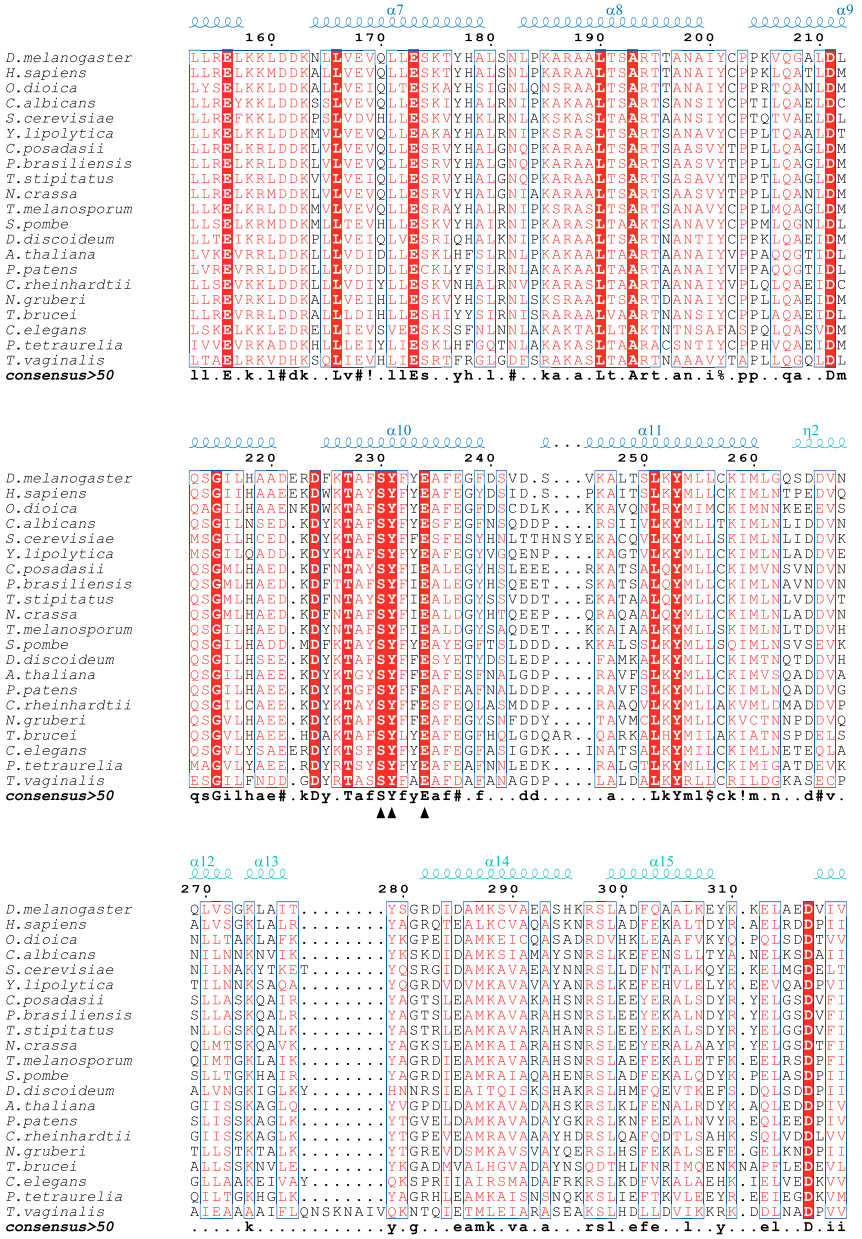
α7
α8
α9
160
170
180
190
200
210
D.melanogaster
H.sapiens
O.dioica
C.albicans
S.cerevisiae
Y.lipolytica
C.posadasii
P.brasiliensis
T.stipitatus
N.crassa
T.melanosporum
S.pombe
D.discoideum
A.thaliana
P.patens
C.rheinhardtii
N.gruberi
T.brucei
C.elegans
P.tetraurelia
T.vaginalis
consensus>50
α10
α11
η2
220
230
240
250
260
α12
α13
α14
α15
270
280
290
300
310

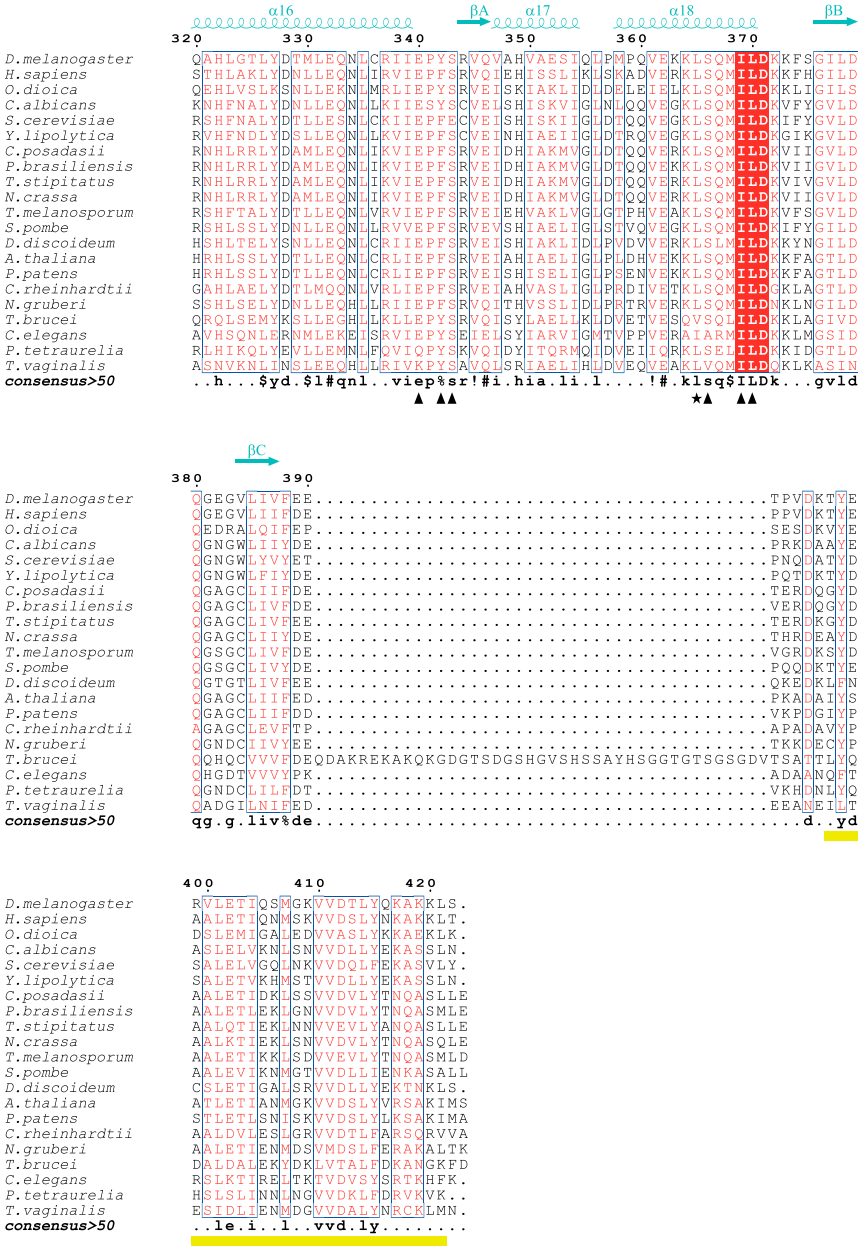

Fig. S2. Alignment of representative Rpn6 sequences. Amino acid sequences of selected Rpn6 homologs were aligned using Clustal-X. Secondary structure elements for the *D. melanogaster* Rpn6 are indicated above the sequences. The Rpn6 domain structure is indicated by purple, blue, and green coloring of secondary structure elements in the capping helix, α-solenoid, and PCI module, respectively. Similar residues are shown in red and identical residues in white on red background. Blue frames indicate homologous regions. The consensus sequence is shown at the bottom. The mutation sites, F132L and L377P, in *Saccharomyces cerevisiae* strain *rpn6-2* are indicated by asterisks. The mutations sites for *D. melanogaster* mutants M1, M2, and M3 are indicated by triangles. The position of the predicted C-terminal helix is indicated by a yellow bar below the alignment. The Uniprot accession codes for the sequences are: Q7KLV9, *Drosophila melanogaster*; O00231, *Homo sapiens*; E4XC34, *Oikopleura dioica*; Q59TN7, *Candida albicans*; Q12377, *Sacharomyces cerevisiae*; Q6C9R4, *Yarrowia lipolytica*; C5P9Z7, *Coccidioides posadasii* (strain C735); C1GHW5, *Paracoccidioides brasiliensis* (strain Pb18); B8M6N4, *Talaromyces stipitatus* (strain ATCC 10500/CBS 375.48/QM 6759/NRRL 1006); Q96U28, *Neurospora crassa*; D5GI46, *Tuber melanosporum* (strain Mel28); Q9P7S2, *Schizosaccharomyces pombe*; Q54UB5, *Dictyostelium discoideum*; Q9LP45, *Arabidobsis thaliana*; A9RB85, *Physcomitrella patens* subsp. patens; A8I274, *Chlamydomonas rheinhardtii*; D2UZW5, *Naegleria gruberi*; Q586L6, *Trypanosoma brucei*; P34481, *Caenorhabditis elegans*; A0BT65, *Paramecium tetraurelia*; A2DYJ9, *Trichomonas vaginalis*.

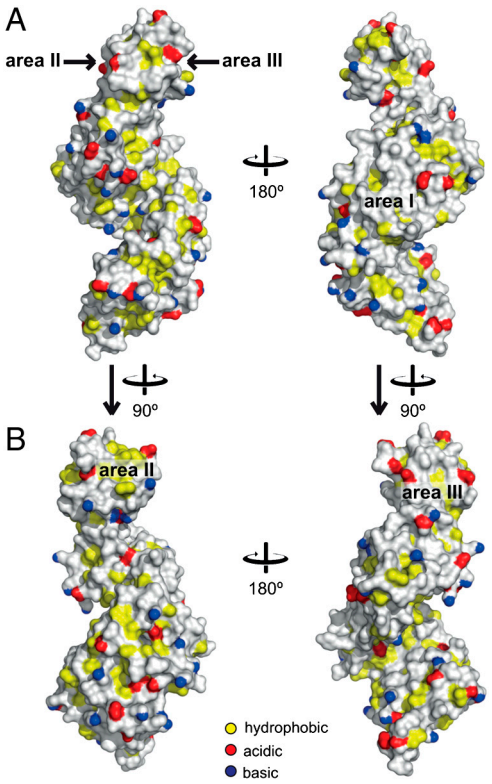

Fig. S3. Surface properties of Rpn6. (*A* and *B*) Physicochemical properties of the Rpn6 surface. Rpn6 is shown in surface representation. The same orientations as in Fig. 2 of the main text are shown. Hydrophobic side chains are indicated in yellow. Positively and negatively charged functional groups are colored blue and red, respectively. The rest of the surface is shown in white.

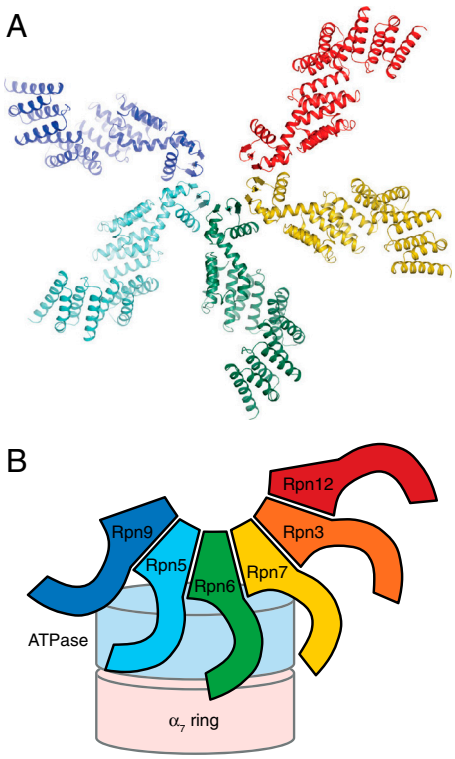

Fig. S4. Rpn6 crystal contacts suggest a linear arrangement of PCI subunits in the proteasome. (*A*) Crystal contacts of Rpn6. Five Rpn6 chains are shown in rainbow colors, as found in the crystal lattice. The sixfold screw axis is oriented perpendicular to the paper plane at the center. The small β-sheets at the tip of the PCI module form a continuous β-ribbon around the screw axis. Slight rearrangements would lead to an open structure. (*B*) Schematic model for the arrangement of the PCI subunits in the proteasome. The proposed PCI subunit order was deduced from (*i*) the lid assembly pathway (1), (*ii*) the PCI-domain-dependent yeast-two hybrid interaction between Rpn5 and Rpn6 (2), and the binary Rpn6–Rpn7 interaction described in this study.

1 Fukunaga K, Kudo T, Toh-e A, Tanaka K, Saeki Y (2010) Dissection of the assembly pathway of the proteasome lid in Saccharomyces cerevisiae. *Biochem Biophys Res Commun* 396:1048–1053.

2 Isono E, Saito N, Kamata N, Saeki Y, Toh EA (2005) Functional analysis of Rpn6p, a lid component of the 26 S proteasome, using temperature-sensitive rpn6 mutants of the yeast Saccharomyces cerevisiae. *J Biol Chem* 280:6537–6547.

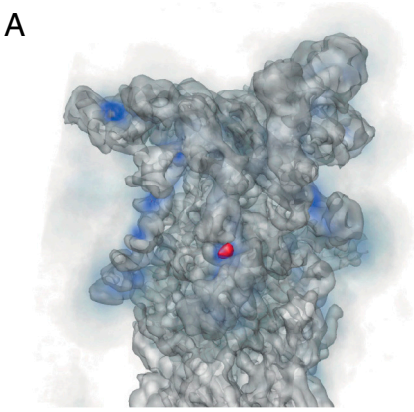

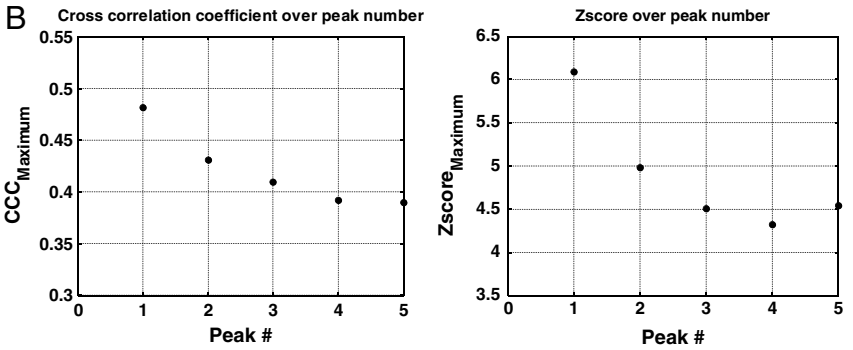

C

Peak #	CCC	z-score
1	0.4813	6.0942
2	0.4308	4.9813
3	0.4097	4.5057
4	0.3923	4.3202
5	0.3898	4.5434

Fig. S5. Docking of Rpn6 into the 26S proteasome EM density map. (*A*) Isosurface representation of the EM density of the 26S proteasome (grayscale) with overlaying cross-correlation function (CCF) (blue). The position of the maximum of the CCF (red) indicates the location of Rpn6. (*B*) Analysis of the highest five peaks of the CCF. (*Left*)The cross-correlation coefficients (CCCs); (*Right*) the corresponding Z-scores (14). (*C*) Table of the five highest CCC peaks and corresponding Z-score.

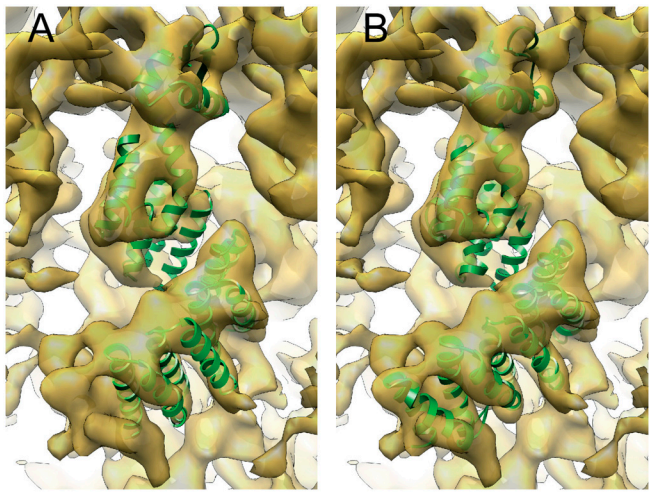

Fig. S6. Colocalization of secondary structure elements in Rpn6 atomic models and cryo-EM density. (*A*) dmRpn6 crystal structure (green) fitted into the EM density (gold). For better visibility of secondary structure elements, we hi-pass filtered the EM map (>1/17 nm). (*B*) Comparative model of spRpn6 (residues 1–387) after flexible fitting.

Table S1. Data collection and refinement statistics

Dataset	MAD			Native
Beamline	ESRF, ID23-1			ESRF, ID29
	peak	*inflection*	*remote*	
Wavelength, Å	1.71024	1.71072	1.03320	1.00686
Space group	$P6_1$			$P6_1$
Cell dimensions, *a*, *b*, *c*; Å	161.25, 161.25, 42.08;			161.30, 161.30, 42.10;
α, β, γ, °	90, 90, 120			90, 90, 120
Resolution limits, Å*	40.42–3.4 (3.58–3.4)	40.47–3.4 (3.58–3.4)	38.89–3.0 (3.16–3.0)	52.78–2.5(2.65–2.5)
R_{merge}*	0.063 (0.335)	0.054 (0.352)	0.048 (0.489)	0.046 (0.303)
I/sigma*	20.1 (5.2)	13.5 (2.9)	14.5 (1.9)	14.4 (2.6)
Multiplicity†	7.3 (7.6)	3.6 (3.7)	3.6 (3.7)	3.3 (3.3)
Completeness, %*	97.9 (98.5)	97.4 (97.7)	97.9 (96.6)	99.3 (99.0)
Phasing				
Sites	4 Gd			—
Phasing power ano	2.172	1.405	0.447	
Phasing power iso	1.158	1.113	—	
Mean FoM			0.277	—
Refinement				
Resolution range	—	—	20–3.0	20–2.5
Reflections (test set)	—	—	11819 (638)	20825 (1146)
R_{work}	—	—	0.205	0.216
R_{free}	—	—	0.251	0.265
No. of atoms	—	—	2731	2788
rmsd bonds, Å	—	—	0.012	0.012
rmsd angles, °	—	—	1.384	1.294
Ramachandran plot†				
% most favored region	—	—	88.7	91.8
% additionally allowed	—	—	11.0	8.2

*Values in parenthesis for outer shell.
†As defined in Procheck (1).

1 Laskowski RA, MacArthur MW, Moss DS, Thornton JM (1993) PROCHECK: A program to check the stereochemical quality of protein structures. *J Appl Crystallogr* 26:283–291.

Part 2:

Crystal structure of the proteasomal deubiquitylation module Rpn8-Rpn11

Crystal structure of the proteasomal deubiquitylation module Rpn8-Rpn11

Ganesh Ramnath Pathare[a], István Nagy[a], Paweł Śledź[a], Daniel J. Anderson[b], Han-Jie Zhou[b], Els Pardon[c,d], Jan Steyaert[c,d], Friedrich Förster[a], Andreas Bracher[e,1], and Wolfgang Baumeister[a,1]

[a]Department of Molecular Structural Biology, Max Planck Institute of Biochemistry, 82152 Martinsried, Germany; [b]Cleave Biosciences, Burlingame, CA 94010; [c]Structural Biology Brussels, Vrije Universiteit Brussel, 1050 Brussels, Belgium; [d]Structural Biology Research Center, Vlaams Instituut voor Biotechnologie, 1050 Brussels, Belgium; and [e]Department of Cellular Biochemistry, Max Planck Institute of Biochemistry, 82152 Martinsried, Germany

Contributed by Wolfgang Baumeister, January 15, 2014 (sent for review December 20, 2013)

The ATP-dependent degradation of polyubiquitylated proteins by the 26S proteasome is essential for the maintenance of proteome stability and the regulation of a plethora of cellular processes. Degradation of substrates is preceded by the removal of polyubiquitin moieties through the isopeptidase activity of the subunit Rpn11. Here we describe three crystal structures of the heterodimer of the Mpr1–Pad1–N-terminal domains of Rpn8 and Rpn11, crystallized as a fusion protein in complex with a nanobody. This fusion protein exhibits modest deubiquitylation activity toward a model substrate. Full activation requires incorporation of Rpn11 into the 26S proteasome and is dependent on ATP hydrolysis, suggesting that substrate processing and polyubiquitin removal are coupled. Based on our structures, we propose that premature activation is prevented by the combined effects of low intrinsic ubiquitin affinity, an insertion segment acting as a physical barrier across the substrate access channel, and a conformationally unstable catalytic loop in Rpn11. The docking of the structure into the proteasome EM density revealed contacts of Rpn11 with ATPase subunits, which likely stabilize the active conformation and boost the affinity for the proximal ubiquitin moiety. The narrow space around the Rpn11 active site at the entrance to the ATPase ring pore is likely to prevent erroneous deubiquitylation of folded proteins.

Mpr1 | POH1 | PSMD7 | PSMD14 | JAMM protease

In eukaryotes, the ubiquitin (Ub) proteasome system (UPS) is responsible for the regulated degradation of proteins (1–5). The UPS plays a key role in the maintenance of protein homeostasis by removing misfolded or damaged proteins, which could impair cellular functions, and by removing proteins whose functions are no longer needed. Consequently, the UPS is critically involved in numerous cellular processes, including cell cycle progression, apoptosis, and DNA damage repair, and malfunctions of the system often result in disease.

The 26S proteasome executes the degradation of substrates that are marked for destruction by the covalent attachment of polyubiquitin chains. It is a molecular machine of 2.5 MDa comprising two subcomplexes, the 20S core particle (CP) and one or two 19S regulatory particles (RPs), which associate with the ends of the cylinder-shaped CP (6–8). The recognition and recruitment of polyubiquitylated substrates, their deubiquitylation, ATP-dependent unfolding, and translocation into the core particle take place in the RP. The structurally and mechanistically well-characterized CP houses the proteolytic activities and sequesters them from the environment, thereby avoiding collateral damage (9).

The RPs attach to the outer α-rings of the CP, which control access to the proteolytic chamber formed by the inner β-subunit rings (10). Recently, the molecular architecture of the 26S holocomplex was established using cryo-EM–based approaches (11, 12), and a pseudoatomic model of the holocomplex was put forward (13). The RP is formed by two subcomplexes, known as the base and the lid, which assemble independently (12, 14). The base contains the hetero-hexameric AAA-ATPase ring (Rpt1–Rpt6), which drives the conformational changes required for substrate processing, including unfolding and translocation into the CP (15, 16). The base also contains the largest RP non-ATPase subunits, Rpn1 and Rpn2, and the Ub receptor Rpn13. The second resident Ub receptor, Rpn10, is not part of either the base or the lid; it binds only to the assembled 26S proteasome and is positioned close to the ATPase module.

The lid scaffold is composed of the Rpn3, Rpn5, Rpn6, Rpn7, Rpn8, Rpn9, Rpn11, and Rpn12 subunits (14). These subunits can be grouped according to their domain structures. Rpn3, Rpn5, Rpn6, Rpn7, Rpn9, and Rpn12 each comprise an N-terminal helix repeat segment, a proteasome-COP9/signalosome-eIF3 (PCI) module, and a long helix at the C terminus (8). The Rpn8 and Rpn11 subunits each consist of an Mpr1–Pad1–N-terminal (MPN) domain, followed by long C-terminal helices (Fig. 1*A*). The PCI subunits form a horseshoe-shaped structure and the MPN domains form a heterodimer, which are connected by a large helical bundle, to which all subunits contribute (13, 17, 18). Each of these eight subunits has paralogs in the COP9/signalosome (CSN) and the elongation initiation factor 3 (eIF3), which likely adopt a similar architecture (18–21).

The lid strengthens the interaction between the CP and RP (17) and deubiquitylates substrates before their processing by the AAA-ATPase module and the CP. Cleavage of polyubiquitin

Significance

The 26S proteasome is a multiprotein complex that degrades proteins marked for destruction by the covalent attachment of polyubiquitin chains. Proteasome activity is essential for the removal of damaged, potentially toxic proteins and for the regulation of numerous cellular processes. Multiple crystal structures of the Rpn8-Rpn11 heterodimer, which is responsible for the removal of polyubiquitin tags before substrate degradation in the proteasome, provide insight into how substrate unfolding and isopeptide bond cleavage might be coupled, and how premature activation of this module is prevented. Its accurate function ensures timely degradation of substrates and, ultimately, the replenishment of the limited cellular pool of free ubiquitin.

Author contributions: G.R.P., I.N., H.-J.Z., F.F., A.B., and W.B. designed research; G.R.P., I.N., P.Ś., D.J.A., and A.B. performed research; E.P. and J.S. contributed new reagents/analytic tools; G.R.P., I.N., P.Ś., D.J.A., F.F., and A.B. analyzed data; and G.R.P., F.F., A.B., and W.B. wrote the paper.

Conflict of interest statement: D.J.A. and H.Z. are full-time employees of Cleave Biosciences.

Freely available online through the PNAS open access option.

Data deposition: The atomic coordinates and structure factors have been deposited in the Protein Data Bank, www.pdb.org (PDB ID codes 4OCL, 4OCM, and 4OCN).

[1]To whom correspondence may be addressed. E-mail: bracher@biochem.mpg.de or baumeist@biochem.mpg.de.

This article contains supporting information online at www.pnas.org/lookup/suppl/doi:10.1073/pnas.1400546111/-/DCSupplemental.

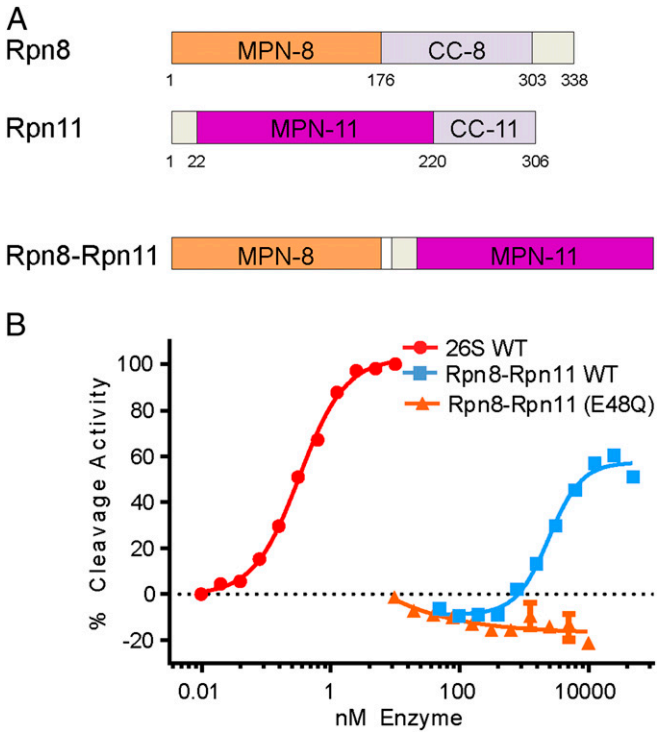

Fig. 1. Biochemical activity of the Rpn8-Rpn11 fusion protein. (*A*) Domain structures of Rpn8, Rpn11 and the fusion protein. (*B*) Ub_4 cleavage activity of 26S proteasome, WT Rpn8-Rpn11 and Rpn8-Rpn11 (E48Q). Cleavage of labeled peptide from Ub_4 was detected by the change in fluorescence polarization after 1hr incubation at 37 °C at the indicated concentrations. Values are normalized to maximum cleavage activity of 26S proteasome. The used 26S proteasome preparation contained only trace amounts of the DUB Ubp6.

chains from the substrate enables recycling of Ub into the cellular pool, and the removal of the unfolding-resistant Ub moieties promotes translocation of substrates. The MPN domain of Rpn11 contains the catalytic site for deubiquitylation (22, 23). Rpn11 belongs to the JAB1/MPN/Mov34 metalloenzyme (JAMM) family of metalloproteases, which provide the isopeptidase activities in the proteasome, CSN, and exo-deubiquitylating enzymes (DUBs), such as associated molecule with the SH3 domain of STAM-like protein (AMSH-LP). The signature motif for this family is a conserved glutamate upstream of a zinc-coordinating catalytic loop, H(S/T)HX_7SXXD, first revealed in the structure of an archaeal homolog, AfJAMM (24). The substrate-binding mode of JAMM DUBs was clarified by the crystal structure of AMSH-LP in complex with Lys63-linked diubiquitin (25). The other proteasomal MPN subunit, Rpn8, is catalytically inactive; it does not contain the JAMM motif and appears to have mainly a supporting role for Rpn11. Isolated Rpn11 is catalytically inactive, as is the isolated lid (22). Rpn11 is activated upon integration into the 26S holocomplex and is dependent on ATP hydrolysis (23). The 26S proteasome was recently shown to undergo large-scale conformational changes from a substrate-accepting conformation to a substrate-engaged conformation that may be critical for Rpn11 function (15, 26), but the mechanistic basis for the regulation of Rpn11 remains unclear. Loss-of-function mutants of the JAMM motif cause stalling of substrates above the mouth of the ATPase module and lead to clogging of the 26S proteasome (23, 26).

Inhibitors of human Rpn11 (hRpn11, also known as POH1) have been proposed as potential antitumor agents working upstream of the β5 proteolytic subunits in the UPS. The β5 subunits have been clinically validated by the approval of bortezomib and carilfzomib for the treatment of hematologic malignancies. siRNA and mutagenesis studies show that expression of the zinc catalytic domain of hRpn11 is essential for cell survival (27). Inhibition of hRpn11 in combination with EGFR inhibition has been suggested to be beneficial in the treatment of nonsmall cell lung cancer (28). Overexpression of hRpn11 in cancer cells has been linked to their tumor escape from cytotoxic agents (29). Thus, hRpn11 is an attractive target for pharmacologic intervention of the UPS.

Here we present three crystal structures of the catalytically active Rpn8/Rpn11 MPN heterodimer from *Saccharomyces cerevisiae*, revealing the details of the Rpn11 active site and the mode of interaction with other subunits. Not all structures show proper active site geometry, hinting at possible mechanisms preventing activation outside of the proteasome complex. The access path for the C-terminal peptide of the substrate-bound Ub is blocked by a highly conserved insertion specific to Rpn11. Fitting of the Rpn8-Rpn11 crystal structure into the cryo-EM density of both the substrate-accepting and substrate-engaged proteasome revealed how the subcomplex is situated between base and PCI domain subunits, which involves long insertions unique to Rpn11 and Rpn8. Contacts to the coiled coils and the oligosaccharide-binding fold (OB) domain ring of the AAA subunits appear to control active site geometry and proper access of the isopeptide bond segment. In the substrate-engaged proteasome, the catalytic center becomes situated just above the maw of the ATPase ring.

Results and Discussion

Structure Determination of the Rpn8-Rpn11 Core Complex. The MPN domains of Rpn8 and Rpn11 were expressed as a fusion protein with a 9-aa-long connecting linker (Fig. 1*A*). The domain limits were selected based on limited proteolysis experiments with proteinase K (residues 1–175 of Rpn8 and residues 1–219 of Rpn11), and the domains were fused to ensure stability and formation of a stoichiometric complex. Notably, this fusion construct, designated Rpn8-Rpn11, cleaves a model substrate, a linear tetraubiquitin (Ub_4)-peptide fusion protein, indicating that this construct samples the catalytically active conformation. It requires a 7,000-fold higher concentration than the complete proteasome, however (Fig. 1*B*).

The Rpn8-Rpn11 crystals suitable for structure determination were grown with the aid of a tailored nanobody (variable domain of camelid heavy chain-only antibodies). Rpn8-Rpn11–specific nanobodies were selected from llama antisera raised against purified yeast 26S proteasome. The successful nanobody Nb1 inhibited the deubiquitylation activity of 26 proteasome in a concentration-dependent manner (Fig. S1).

Crystal Lattices. We obtained three crystal forms, here designated Ia, Ib and II, of the Rpn8-Rpn11 fusion protein complex with the nanobody (Table S1 and Fig. S2 *A* and *B*). Crystal forms Ia and Ib are closely related. All crystal forms contain two Rpn8-Rpn11-nanobody complexes per asymmetric unit. The backbones in the core regions of the complex subunits are very similar, yielding rmsd values between 0.304 and 0.916 Å (Fig. S2 *C* and *D*); only helix α4 of Rpn8 is displaced in one copy of crystal form II (Fig. S2*C*). No density could be assigned to any of the linker regions between the Rpn8 and Rpn11 MPN domains.

A major difference between crystal forms I and II is the presence of bound Zn in the former. In crystal form II, a crystal contact between the two copies of Rpn11 distorts the geometry of the catalytic loop, displacing the Zn-coordinating residue His109 from the Zn-binding site (Fig. S2*F*). Thus, crystal form II appears to be incompatible with Zn binding. Thus, we focus on crystal form Ia, diffracting to the highest resolution (2.0 Å).

Structure of the Rpn8-Rpn11 Complex. The Rpn8-Rpn11 core complex structure exhibits pseudo-twofold symmetry (Fig. 2). Each protomer assumes a MPN domain fold and consists of four α-helices, α1–α4, flanking a circular β-sheet of seven β-strands, βA–βG (Figs. S2*E* and S3). The topology of the β-sheet is βA-βC-βB-βD-βE-βF-βG. The long, twisted β-strand βG makes contacts with both βA and βF. Rpn8 and Rpn11 contact each other via two pseudosymmetrical interfaces, a coiled coil between helices α2 and a four-helix bundle of helices α1 and α4 (Fig. 2). The C-terminal α4 helices are associated mainly with the opposing subunit (Fig. 2), causing the domain swapping first observed in the crystal structure of human Rpn8/Mov34 (30) and anticipated in the pseudoatomic models of the 26S proteasome (11, 12).

Two regions connecting βC-α2 and βF-βG are variable in MPN domain sequences, designated here as insertion 1 and insertion 2 (Fig. 2) (24, 25, 30–32). Insertion 1 of Rpn8 forms a β-hairpin on top of the MPN domain. The corresponding region in Rpn11 forms a poorly ordered loop adjacent to the active site, as discussed in more detail below. The insertion 2 regions of Rpn8 and Rpn11 protrude from the opposite ends of the pseudo-twofold symmetric subcomplex (Fig. 2). Insertion 2 of Rpn8 assumes an elongated β-hairpin structure in crystal form II. The hairpins from two Rpn8 molecules align to create a mixed β-sheet contact in this crystal lattice (Fig. S2*B*). In the form I crystal structures, the tips of the β-hairpin are disordered, suggesting that this region is stably structured only in the presence of a suitable interaction partner. The much longer insertion 2 in Rpn11 forms a helical protrusion with a disordered tip in crystal forms Ia and Ib. The helices from two adjacent Rpn11 molecules form antiparallel three-helix bundles (Figs. S2*A* and S3). In crystal form II, both corresponding segments are disordered, suggesting that insertion 2 of Rpn11 stably folds only in appropriate environments, in line with secondary structure predictions.

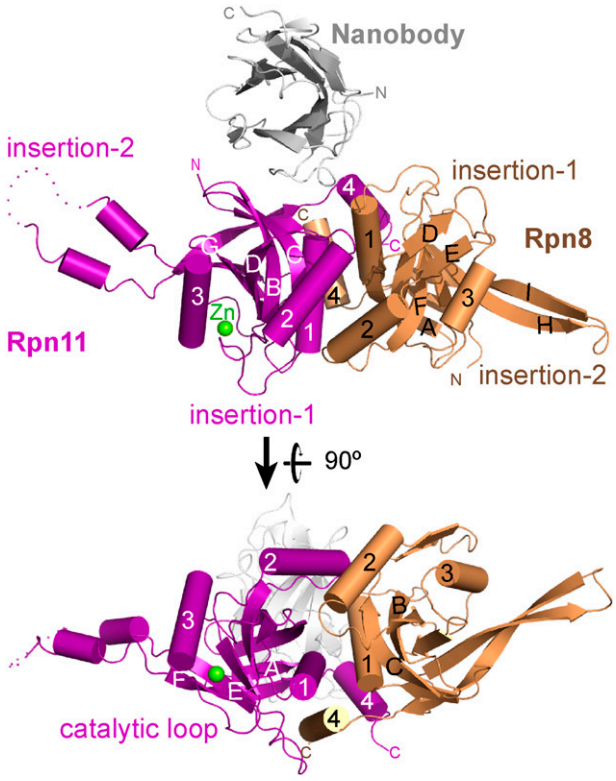

Fig. 2. Crystal structure of the MPN domain fusion protein of Rpn8 and Rpn11 with the attached nanobody. The composite structure of Rpn8 (chain A) from crystal form II superposed on the Rpn8-Rpn11–nanobody complex (chains D, E, and F) from crystal form Ia is shown in side and bottom views. The Rpn8 and Rpn11 units are indicated in purple and brown, respectively; the nanobody is represented in silver. Disordered segments are indicated by dotted lines. Helices are represented by cylinders; the catalytic Zn ion, by a green sphere. The unique insertions into the canonical MPN structure are indicated.

Role of the Nanobody in Crystal Formation. The nanobody contacts an area that involves β-strands βB, βC, and βG and α4 in Rpn11 and a section of helix α1 in Rpn8, thereby establishing additional contacts between the proteins and rigidifying the complex (Fig. 2). This contact area forms a depression on the surface of the Rpn8-Rpn11 complex, providing a concave binding site for the CDR3 loop of the nanobody. Furthermore, in all crystal lattices, the nanobodies contribute important crystal contacts to adjacent Rpn8 molecules. Thus, a combination of both effects might explain why the nanobody is required for the successful crystallization of Rpn8-Rpn11.

Active Site of Rpn11. The active site of MPN domain metalloproteases is located between the N-terminal end of helix α3 and the adjacent β-strands βB and βD (31, 33, 34). Clear density for the catalytic zinc was identified between the sidechains of His109, His111, and Asp122 (Fig. 3*A* and Fig. S4*A*). These sidechains, together with a water molecule, form a slightly distorted tetrahedral coordination shell around the metal ion. This core structure is almost identical to that of the DUB AMSH-LP (25, 33, 34), for which both apo and substrate-bound crystal structures have been characterized at high-resolution (Fig. 3*B* and Fig. S4*E*). In the AMSH-LP cocrystal structure, the isopeptide bond carbonyl group was positioned directly on top of the metal site (Fig. 3*B*) (34), strongly suggesting that this conformation of Rpn8-Rpn11 represents a catalytically active state.

The residue Glu48 at the beginning of β-strand βB corresponds to residue Glu292 of AMSH-LP, which is essential for AMSH-LP activity (25, 33). Mutating this residue to glutamine abolished Ub_4 cleavage activity in Rpn8-Rpn11 (Fig. 1*B*). Glu48 is positioned for activation of the attacking water molecule and protonation of the isopeptide amide group. With the location of Glu48, His109, and His111 in two adjacent β-strands, the respective geometry is largely fixed (Fig. 3*A* and Fig. S4*A*). The conformation of the catalytic loop (residues 109–122) is stabilized by an extended hydrogen bond network in Rpn11 (Fig. 3*A* and Fig. S4*A*), which is also observed in the apo crystal structures of AMSH-LP (25), the Rpn11 paralog Csn5 (31), and the archaeal Rpn11 homolog AfJAMM (24) (Fig. S4 *D*–*F*). Hydrogen bond contacts between the carbonyl group of Gly115 and the imidazole ring of His111 and between the amide group of Ser119 and the carboxyl group of Asp122 orient the coordinating sidechains toward Zn and establish the proper polarity. The imidazole ring of His111 is further buttressed by the sidechains of the catalytic loop residues Phe114 and Trp117 (Fig. 3*A* and Fig. S4*A*). The orientation of the indole group of Trp117 is stabilized by a hydrogen bond to the carbonyl group of Phe114. In addition, the carboxyl group of Asp142 links the amide groups of Gly115 and Ile144. These two interactions are conserved in Csn5 as well (31, 32) (Fig. S4*F*). Asp142 and Ile144 belong to the highly conserved loop connection between βE and βF in Rpn11. The respective loop is much shorter in AMSH-LP. Other important hydrogen bond contacts with the backbone are formed by the JAMM motif residues Ser110 and Ser119. The former extends the β-sheet contacts between βB and βD, and the latter stabilizes the N-terminal part of helix α3 and buttresses Asp122.

Alternative conformations of the catalytic loop were found in one of the two copies of Rpn11 in crystal forms Ia and Ib each (Fig. 3*C* and Fig. S4 *B* and *C*). Both conformers are characterized by a wider separation of the His111 imidazole ring from Zn (2.9 Å vs. 2.1 Å), whereas His109 and Asp122 remain virtually

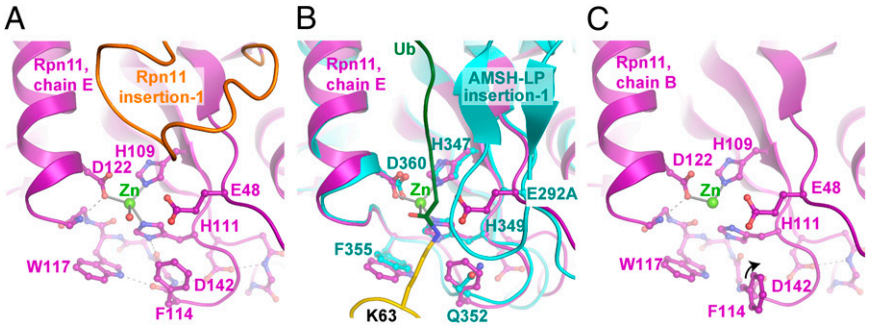

Fig. 3. Active site of Rpn11. (*A*) Detailed view of the Rpn11 active site. The catalytic residues are shown in ball-and-stick representation. Hydrogen bonds are indicated by dashed lines. This represents the active conformation found in complex DEF of crystal form Ia. Insertion 1 in Rpn11 is highlighted in orange. (*B*) Superposition with the AMSH-LP-Ub_2 complex showing the likely orientation of the isopeptide bond in the substrate complex. AMSH-LP, the proximal and distal Ub are shown in cyan, gold, and green, respectively. Insertion 1 of Rpn11 has been removed for clarity. (*C*) Distorted active site geometry in complex ABC of crystal form Ia.

unchanged. This rearrangement should alter the properties of the Zn ion and thereby decrease catalytic activity. The expected water ligands bound to Zn are poorly defined in these conformations and are not included in the model. The reorientation of the His111 sidechain largely disrupts the hydrogen bond network of the catalytic loop. Thus, this mechanism may render the catalytic center geometry sensitive to local changes. In the crystal lattice, the active conformation likely is stabilized by a crystal contact with the sidechain of Phe114. In the context of the 26S proteasome, the adjacent highly conserved loop connection between βE and βF is a good candidate for the regulation of activity; it is in contact with helix α4 of Rpn8, and its conformation is likely to be sensitive to rearrangements in the RP.

Ub Binding. Superposition with the AMSH-LP-Ub_2 structure suggests that the binding site for the substrate-ligated Ub moiety is located in the shallow groove between helices α2 and α3 of Rpn11 (Fig. 3*B*). Compared with AMSH-LP, helix α2 is differently oriented in Rpn11 (Fig. 4*A*). This orientation is enforced by conserved hydrophobic interactions with the α2 helix of Rpn8 in the Rpn8-Rpn11 complex (Fig. 4*B*). Thus, a reorientation to the conformation observed in AMSH-LP seems improbable.

The putative Ub-binding site is largely hydrophobic in character, with the notable exception of Asp85, which is replaced by Pro in the majority of Rpn11 sequences (Fig. 4*C*). The highly conserved Asp84 might functionally replace AMSH-LP residue Glu329, which contacts Lys48 of the distal Ub. The other key contact residues in AMSH-LP, Val328, Phe332, Thr342, and Met370, are replaced by Val86, Ala89, Val104, and Leu132, respectively, in Rpn11. The putative Ub-contacting Rpn11 residues Asp85, Val86, Gln88, Ala89, Met92, Met103, Val104, Ser128, Gln131, Leu132, and Asn133 are less conserved compared with the residues facing other subunits of the RP, suggesting evolutionary pressure against high-affinity binding at this site in Rpn11 (see below) (Fig. 4*B*). Only charged residues seem to be forbidden in the Ub contact area.

In the AMSH-LP-Ub_2 structure, the C terminus of the distal Ub aligns with helix α3 and forms β-contacts with insertion 1, which assumes a β-hairpin conformation (Fig. 3*B*). The contact residues in helix α3 are conserved between AMSH-LP and Rpn11. Insertion 1 of AMSH-LP also forms a β-hairpin conformation in the absence of Ub (25). In the Rpn8-Rpn11 structures, insertion 1 forms a loop structure including a helical turn, which blocks the path of the Ub C terminus (Fig. 3*A*). The loop conformation, which is stabilized by hydrogen bonds between the hydroxyl group of Ser79 with the amide of Glu81 and the carbonyl of Thr76, is rather poorly defined in the structures. It makes few van der Waals contacts to the remainder of Rpn11, suggesting considerable structural plasticity. Moreover, the loop has the same length and a similar polarity pattern in AMSH-LP and Rpn11. Glu81 in Rpn11 replaces Asp324 in AMSH-LP, which forms an electrostatic interaction with Arg74 of Ub. Thus, remodeling to a conformation similar to that of AMSH-LP seems possible in Rpn11. Regulated rearrangement of this highly conserved segment in the context of the RP might provide another layer of control against premature Rpn11 activation.

Contacts of Rpn8-Rpn11 in the 26S Proteasome. We next fitted the Rpn8-Rpn11 core complex crystal structure into the EM densities of the *S. cerevisiae* 26S proteasome in the substrate-accepting (13) and the substrate-engaged states (27) (Fig. 5 *A* and *B*). The resolved secondary structure elements of both maps are in excellent agreement, with the notable exception of insertion 2 of Rpn11, which also varies significantly in the different crystal forms (Fig. S2*D*). Thus, the structure of the Rpn8-Rpn11 core complex in isolation is indistinguishable from that in the different 26S conformers at the level of resolution of the cryo-EM maps (Fig. 5 *A* and *B*). Nb1 would severely clash with Rpn2 helices H28 and H30 in both proteasomal conformations

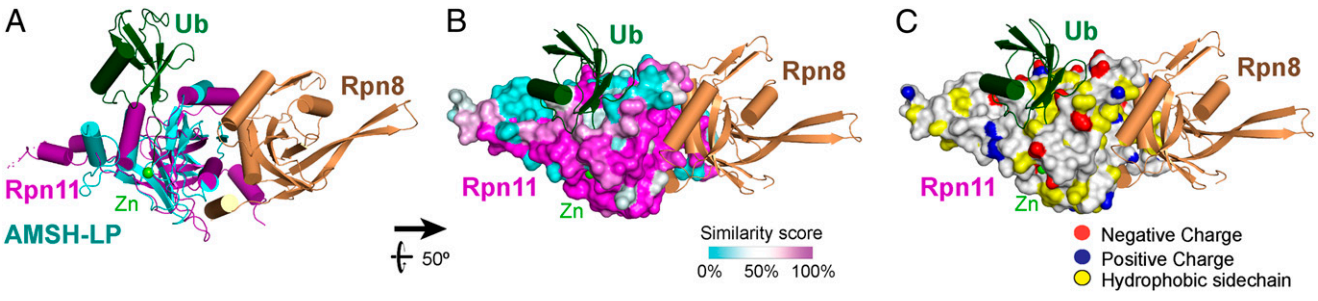

Fig. 4. Binding site for the proximal Ub. (*A*) Superposition of Rpn11 with the AMSH-LP-Ub_2 complex. AMSH-LP and the distal Ub are shown in cyan and green, respectively. (*B*) Surface conservation at the Rpn11 Ub-binding site. The similarity score from the sequence alignment shown in Fig. S3 was mapped onto the surface of Rpn11. A magenta-white-cyan color gradient represents decreasing surface conservation. (*C*) Surface view of Rpn11 showing the residue properties at the putative Ub-binding site. Hydrophobic sidechains are highlighted in yellow; positive and negative charged groups are shown in blue and red, respectively.

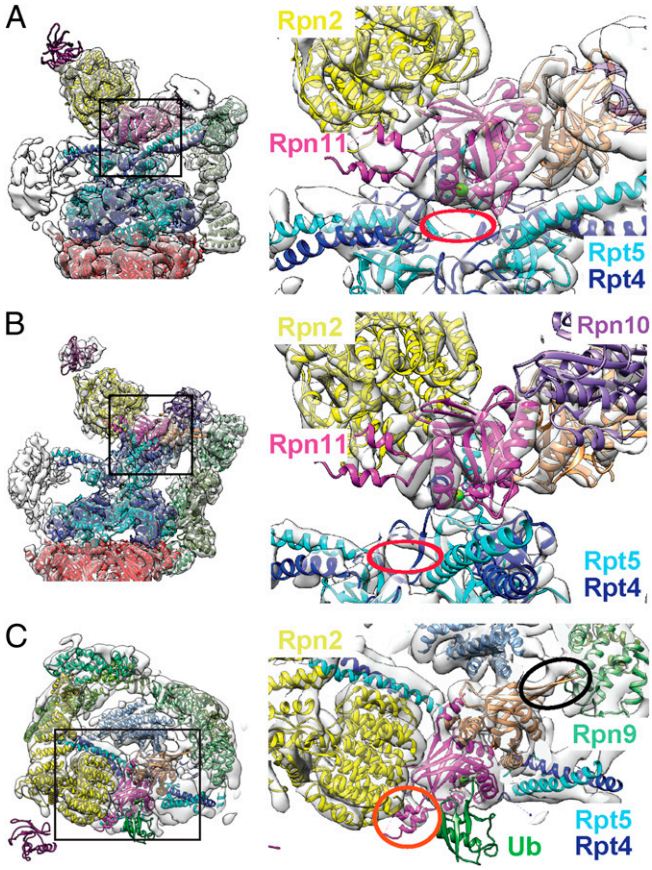

Fig. 5. Docking of the Rpn8-Rpn11 MPN domain complex into 26S proteasome EM density. (*A* and *B*) Rpn8-Rpn11 MPN domain dimer docked into the cryo-EM density of the substrate-engaged and -accepting states of the 26S proteasome, respectively. The green sphere represents the active site zinc ion. The red ring indicates the AAA ATPase pore entrance. Contacting subunits to Rpn8-Rpn11 are indicated. (*C*) Top view of the substrate-engaged state. Insertion 2 of Rpn8 fits into density bridging the gap toward the PCI horseshoe complex at subunit Rpn9 (circled in black). Insertion 2 of Rpn11 fits into an unassigned density close to the PC domain of Rpn2 (circled in orange).

(see Fig. S6 *A* and *B*), suggesting that its inhibitory effect may be related to a perturbation of the holocomplex. In fact, addition of the nanobody to purified 26S proteasomes appeared to largely disrupt the particles, as observed in cryo-EM.

In both 26S states, the MPN domain of Rpn11 makes extensive contacts with the central torus-shaped domain of Rpn2 on one side and the coiled-coil extensions of Rpt3, Rpt4, and Rpt5 and the OB domains of Rpt4 on the other side. The contact areas are highly conserved in Rpn11 and its binding partners (Figs. S5 *A*–*D* and S6 *C* and *D*). The interface with Rpn2 likely involves Rpn11 βA, the βB-βC hairpin, and insertion 2, all of which appear to be flexible in the crystal structures. A flexibly attached, highly conserved segment is found at the tip of insertion 2 in Rpn11, residues 169–178 (EPRQTTSNTG) (Fig. S3), which might insert into a conspicuously conserved groove between helices H20 and H22 on the outer surface of the Rpn2 torus (Fig. S6*A*). Between this patch and the MPN domain proper, an as-yet unassigned density was observed that likely corresponds to the Rpn11 insertion 2 helices and possibly also the N-terminal 22 residues of Rpn11 that are disordered in all crystallographic models. This density appears to be best resolved for the GFP substrate-bound 26S proteasome structure (26).

The contacts to the ATPases involve the catalytic loop, insertion 1, and the βE-βF connecting loop, which are important for substrate access and Rpn11 active site geometry, and the link between α1 and βB. During the transition from the substrate-accepting to the substrate-engaged state, the Rpt4-Rpt5 coiled coil slides away from insertion 1, perhaps stabilizing the insertion 1 on substrate isopeptide link intrusion. The N-terminal end of the Rpt3 coiled coil buttresses the βE-βF loop, and the OB domain of Rpt4 moves in close vicinity to the catalytic loop, presumably stabilizing its active conformation. The C terminus of the docked Ub moiety would be surrounded by protein in the substrate-engaged state.

Insertion 2 of Rpn8 reaches toward the solenoid segment of the PCI domain subunit Rpn9 (Fig. 5*C*). Density for this connection is clearly discernible in the cryo-EM maps. Apart from this interaction, the MPN domain of Rpn8 serves as attachment site for the von Willebrand (VWA) domain of Rpn10 together with Rpn9 (Figs. S5 and S6 *A* and *B*). The Rpn10 contact region, largely identical to insertion 1, represents the most highly conserved surface region within Rpn8 on the Rpn8-Rpn11 complex (Fig. S5 *A* and *B*). In the 26S holocomplex, Rpn10 is situated next to the exposed binding site for the substrate-ligated Ub and might engage in additional contacts with the polyubiquitin chain. A Lys48-linked Ub would be in close contact with the VWA domain of Rpn10 and the N-terminal part of the Rpt4-Rpt5 coiled-coil bundle (35). Further Lys-48–linked Ub moieties could be bound by the C-terminal Ub-interaction motifs (UIMs) in Rpn10 in the committed proteasome (Fig. 6) (36).

Regulation of Rpn11 Activity in the 26 Proteasome. Through the analysis of fusion protein crystal structures, we have identified three potential mechanisms for preventing premature activation of the isopeptidase activity of Rpn11: (*i*) establishment of the correct active site geometry, (*ii*) rearrangement of Rpn11 insertion 1 to allow access of the proximal Ub C terminus to the catalytic site, and (*iii*) low affinity of the proximal Ub to its docking site on Rpn11. The basal isopeptidase activity of the Rpn8-Rpn11 fusion protein indicates that in principle, all of these obstacles can be overcome outside of the 26S proteasome, albeit with low efficiency. The Rpn8-Rpn11 conformers in the

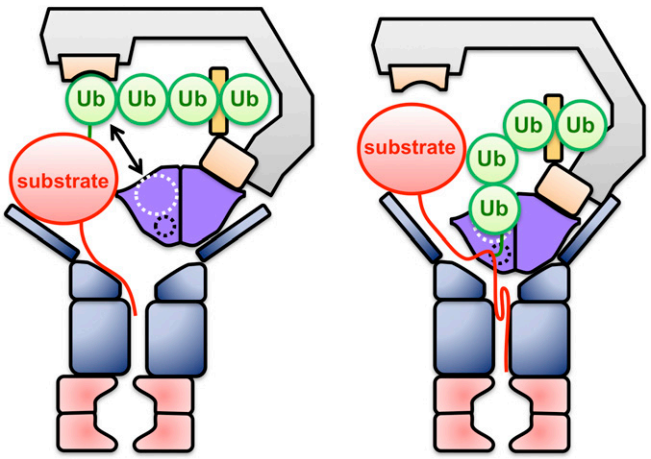

Fig. 6. Schematic model for 26S proteasome isopeptide bond cleavage. Models for the substrate-accepting and -engaged state of the proteasome are shown. Folded and extended parts of the substrate are indicated by red spheres and red lines, respectively. Poly-Ub–tagged substrate proteins are recognized by the Ub receptors Rpn13 and Rpn10 (pale yellow) and Rpn10 UIM (yellow). Rpn11 reaches the isopeptide bond only when the substrate is already partially unfolded (Rpn8-Rpn11; purple). The white and black dashed circles designate the primary Ub-binding site and active site of Rpn11, respectively.

crystal structures show that proper active site geometry is accessible, but not stable. Similarly, insertion 1 of Rpn11 blocks the access path for Ub in our structures; however, this element appears to be mobile, as suggested by the high B-factors and disorder in several conformers, and thus it should rearrange easily once the Ub C terminus enters the access path.

The affinity of the Rpn8-Rpn11 fusion protein for Ub appears to be modest at best (Fig. 1*B*). Simultaneous contacts with both sites should allow efficient substrate binding only in the close presence of Ub receptors, particularly the Rpn10 UIM motif, in the assembled proteasome. In support of this idea, a 26S complex without Rpn10 and Rpn13 demonstrated greatly reduced Ub_4 cleavage activity (Fig. S8). Another mechanism of preventing cleavage of noncommitted substrates is limited access for bulky folded domains to the narrow surroundings of the Rpn11 active site in both 26S conformations.

Full activation of Rpn11 is presumably realized by contacts with the coiled coils and the OB ring of the AAA subunits, which have been proposed to have chaperone activity (37) and furthermore could stabilize the active conformation in Rpn11 and thereby increase the affinity for the primary Ub by opening the binding site for the C-terminal tail. The strong sequence conservation of the involved elements suggests tight coevolution of a defined functional interface (Figs. S5 *A–D* and S6 *C* and *D*). Therefore, the 26S proteasome might have an extended "composite" deubiquitylase active site, converting the access groove for the C-terminal end of the Ub chain in AMSH-LP into a channel, which allows exact control of substrate orientation; this is necessary because the sequences flanking Ub acceptor sites are variable in proteasomal substrates. Only the structure of polyubiquitylated substrate bound to Rpn11 in the context of a stalled proteasome will reveal the molecular mechanism of deubiquitylation in full detail.

Materials and Methods

The experimental procedures are described in detail in *SI Materials and Methods*. In brief, Rpn8-Rpn11 from *S. cerevisiae* was expressed as a His6 tag fusion protein including a tobacco etch virus (TEV) protease site in *E. coli* BL21 (DE3) cells and purified by Ni-affinity chromatography, TEV cleavage, and Superose-12 size exclusion chromatography. Crystals were grown using 50 mM MES pH 6.0, 200 mM Ca acetate, and 22% (wt/vol) PEG-3350 or with 50 mM MES pH 6.0, 100 mM $MgCl_2$, and 21% (wt/vol) PEG-3350. The Rpn8-Rpn11-nanobody crystal structure was solved by molecular replacement. The isopeptidase activity assay was performed with a fluorogenic Ub_4 fusion protein, with reaction progress monitored by fluorescence polarization. The nanobody was selected and produced following standard procedures (38).

ACKNOWLEDGMENTS. We thank Yousuf Mohiuddin Mohammed, André Mourão, Günter Pfeifer, Oana Mihalache, Sándor Varga, Ágnes Hubert, Jan Schuller, Antje Aufderheide, Andreas Schweitzer, Pia Unverdorben, and Roman Körner (Max Planck Insitute of Biochemistry); Alison Lundquist (Vrije Universiteit Brussels); Ethan Emberley, Brajesh Kumar, and David J. Wustrow (Cleave Biosciences); the Joint Structural Biology Group group at the Electron Synchrotron Radiation Facility Grenoble; and staff at Swiss Light Source X10SA Villigen, the MPIB Crystallization Facility, and the MPIB Core Facility for their excellent support. Our research is supported by funding from the Deutsche Forschungsgemeinschaft Excellence Cluster Center for Integrated Protein Science Munich and SFB-1035/Project A01 (to W.B.), Instruct (part of the European Strategy Forum on Research Infrastructures and supported by national member subscriptions) through a Research and Development Pilot Project grant (to J.S., I.N., and P.Ś.), as well as Graduiertenkolleg 1721 (to F.F.) and European Molecular Biology Organization (to P.Ś.).

1. Finley D (2009) Recognition and processing of ubiquitin-protein conjugates by the proteasome. *Annu Rev Biochem* 78:477–513.
2. Goldberg AL (2003) Protein degradation and protection against misfolded or damaged proteins. *Nature* 426(6968):895–899.
3. Varshavsky A (2012) The ubiquitin system, an immense realm. *Annu Rev Biochem* 81:167–176.
4. Buchberger A, Bukau B, Sommer T (2010) Protein quality control in the cytosol and the endoplasmic reticulum: Brothers in arms. *Mol Cell* 40(2):238–252.
5. Hershko A, Ciechanover A, Varshavsky A (2000) Basic Medical Research Award: The ubiquitin system. *Nat Med* 6(10):1073–1081.
6. Tanaka K (2009) The proteasome: Overview of structure and functions. *Proc Jpn Acad, Ser B, Phys Biol Sci* 85(1):12–36.
7. Voges D, Zwickl P, Baumeister W (1999) The 26S proteasome: A molecular machine designed for controlled proteolysis. *Annu Rev Biochem* 68:1015–1068.
8. Förster F, Unverdorben P, Sledź P, Baumeister W (2013) Unveiling the long-held secrets of the 26S proteasome. *Structure* 21(9):1551–1562.
9. Baumeister W, Walz J, Zühl F, Seemüller E (1998) The proteasome: Paradigm of a self-compartmentalizing protease. *Cell* 92(3):367–380.
10. Peters JM, Cejka Z, Harris JR, Kleinschmidt JA, Baumeister W (1993) Structural features of the 26 S proteasome complex. *J Mol Biol* 234(4):932–937.
11. Lasker K, et al. (2012) Molecular architecture of the 26S proteasome holocomplex determined by an integrative approach. *Proc Natl Acad Sci USA* 109(5):1380–1387.
12. Lander GC, et al. (2012) Complete subunit architecture of the proteasome regulatory particle. *Nature* 482(7384):186–191.
13. Beck F, et al. (2012) Near-atomic resolution structural model of the yeast 26S proteasome. *Proc Natl Acad Sci USA* 109(37):14870–14875.
14. Glickman MH, et al. (1998) A subcomplex of the proteasome regulatory particle required for ubiquitin-conjugate degradation and related to the COP9-signalosome and eIF3. *Cell* 94(5):615–623.
15. Śledź P, et al. (2013) Structure of the 26S proteasome with ATP-γS bound provides insights into the mechanism of nucleotide-dependent substrate translocation. *Proc Natl Acad Sci USA* 110(18):7264–7269.
16. Beckwith R, Estrin E, Worden EJ, Martin A (2013) Reconstitution of the 26S proteasome reveals functional asymmetries in its AAA+ unfoldase. *Nat Struct Mol Biol* 20(10):1164–1172.
17. Pathare GR, et al. (2012) The proteasomal subunit Rpn6 is a molecular clamp holding the core and regulatory subcomplexes together. *Proc Natl Acad Sci USA* 109(1):149–154.
18. Estrin E, Lopez-Blanco JR, Chacón P, Martin A (2013) Formation of an intricate helical bundle dictates the assembly of the 26S proteasome lid. *Structure* 21(9):1624–1635.
19. Enchev RI, Schreiber A, Beuron F, Morris EP (2010) Structural insights into the COP9 signalosome and its common architecture with the 26S proteasome lid and eIF3. *Structure* 18(4):518–527.
20. Sun C, et al. (2011) Functional reconstitution of human eukaryotic translation initiation factor 3 (eIF3). *Proc Natl Acad Sci USA* 108(51):20473–20478.
21. Querol-Audi J, et al. (2013) Architecture of human translation initiation factor 3. *Structure* 21(6):920–928.
22. Yao T, Cohen RE (2002) A cryptic protease couples deubiquitination and degradation by the proteasome. *Nature* 419(6905):403–407.
23. Verma R, et al. (2002) Role of Rpn11 metalloprotease in deubiquitination and degradation by the 26S proteasome. *Science* 298(5593):611–615.
24. Ambroggio XI, Rees DC, Deshaies RJ (2004) JAMM: A metalloprotease-like zinc site in the proteasome and signalosome. *PLoS Biol* 2(1):E2.
25. Sato Y, et al. (2008) Structural basis for specific cleavage of Lys 63-linked polyubiquitin chains. *Nature* 455(7211):358–362.
26. Matyskiela ME, Lander GC, Martin A (2013) Conformational switching of the 26S proteasome enables substrate degradation. *Nat Struct Mol Biol* 20(7):781–788.
27. Gallery M, et al. (2007) The JAMM motif of human deubiquitinase Poh1 is essential for cell viability. *Mol Cancer Ther* 6(1):262–268.
28. Bivona TG, et al. (2011) FAS and NF-κB signalling modulate dependence of lung cancers on mutant EGFR. *Nature* 471(7339):523–526.
29. Spataro V, Simmen K, Realini CA (2002) The essential 26S proteasome subunit Rpn11 confers multidrug resistance to mammalian cells. *Anticancer Res* 22(6C):3905–3909.
30. Sanches M, Alves BS, Zanchin NI, Guimarães BG (2007) The crystal structure of the human Mov34 MPN domain reveals a metal-free dimer. *J Mol Biol* 370(5):846–855.
31. Echalier A, et al. (2013) Insights into the regulation of the human COP9 signalosome catalytic subunit, CSN5/Jab1. *Proc Natl Acad Sci USA* 110(4):1273–1278.
32. Zhang H, et al. (2012) The crystal structure of the MPN domain from the COP9 signalosome subunit CSN6. *FEBS Lett* 586(8):1147–1153.
33. Davies CW, Paul LN, Kim MI, Das C (2011) Structural and thermodynamic comparison of the catalytic domain of AMSH and AMSH-LP: Nearly identical fold but different stability. *J Mol Biol* 413(2):416–429.
34. Kikuchi K, Ishii N, Asao H, Sugamura K (2003) Identification of AMSH-LP containing a Jab1/MPN domain metalloenzyme motif. *Biochem Biophys Res Commun* 306(3):637–643.
35. Rani N, Aichem A, Schmidtke G, Kreft SG, Groettrup M (2012) FAT10 and NUB1L bind to the VWA domain of Rpn10 and Rpn1 to enable proteasome-mediated proteolysis. *Nat Commun* 3:749.
36. Riedinger C, et al. (2010) Structure of Rpn10 and its interactions with polyubiquitin chains and the proteasome subunit Rpn12. *J Biol Chem* 285(44):33992–34003.
37. Djuranovic S, et al. (2009) Structure and activity of the N-terminal substrate recognition domains in proteasomal ATPases. *Mol Cell* 34(5):580–590.
38. Pardon E, et al. (2014) A general protocol for the generation of nanobodies for structural biology. *Nat Protoc*, in press.

Supporting Information

Pathare et al. 10.1073/pnas.1400546111

SI Materials and Methods

Purification of the Rpn8-Rpn11 Fusion Protein. The Rpn8-Rpn11 expression construct consisted of an N-terminal His_8-tag, RAAR protein, a tobacco etch virus (TEV) protease cleavage site, residues 1–176 of Rpn8, a nine-residue linker (GSGGSGGSG), and residues 1–220 of Rpn11. The *Saccharomyces cerevisiae* subunit DNA sequences were codon-optimized for *Escherichia coli* expression. The resulting sequence was cloned between the NcoI and XhoI sites of a modified pRSFDuet DNA (Merck Millipore).

To express the fusion protein, *E. coli* BL21 (DE3) was transformed with the plasmid and grown overnight in a shaking culture on LB medium containing 50 μg mL^{-1} kanamycin at 37 °C. At OD_{600} = 0.8, protein expression was induced with 0.5 mM isopropyl β-D-1-thiogalactopyranoside, and the temperature was lowered to 25 °C for 12 h. Subsequently, cells were harvested by sedimentation at 4,000 × *g*, washed with sterile water, resuspended with 2.5 mL of lysis buffer (50 mM Tris pH 8.0, 10 mM imidazole, 150 mM NaCl, and 1 mg mL^{-1} lysozyme) per gram, and incubated on ice for 1 h. Then 100 ppm Benzonase (Sigma-Aldrich) was added, followed by ultrasonication on ice. Cell debris was removed by ultracentrifugation at 28,000 × *g* at 4 °C for 30 min. His_8-tagged Rpn8-Rpn11 was purified on Ni-nitrilotriacetic acid (NTA) fast-flow beads (Qiagen) according to the supplier's recommendations. Fractions containing His_8-Rpn8-Rpn11 were merged, His_8-TEV protease was added, and the mixture was incubated for 12 h at 4 °C in a dialysis chamber equilibrating against 25 mM Tris·HCl pH 7.5. Uncleaved protein, the affinity tag, and His_8-TEV protease were removed by Ni-affinity purification using Ni-NTA fast-flow beads (Qiagen), as described above. The unbound protein was subjected to a Superose-12 column (GE Healthcare) equilibrated with 10 mM Tris pH 7.5, 150 mM NaCl, and 90 mM KCl. Rpn8-Rpn11–containing fractions were merged and concentrated.

Cloning and Purification of Rpn8-Rpn11–Targeted Nanobodies. The use of protein complexes for animal immunization (1) was implemented to obtain nanobodies against epitopes of 26S proteasome subunits in their biologically relevant conformation. For this, a llama was immunized six times with 100 μg of intact 26S proteasomes of *S. cerevisiae* essentially as described by Pardon et al. (2). Peripheral blood lymphocytes were extracted, and their RNA was purified and converted into cDNA via RT-PCR. The cDNA was cloned into phage-display vector pMESy4 containing a C-terminal 6X His tag followed by the CaptureSelect C-tag. Several nanobodies that bind to the Rpn8-Rpn11 subcomplex were identified by biopanning on the unmodified Rpn8-Rpn11 heterodimer immobilized using an anti-streptavidin monoclonal antibody that was solid-phase–coated on the ELISA plate. Antigen-bound phages were recovered by proteolysis with trypsin. After each round of selection, ELISA was performed on periplasmic extracts of 48 individual colonies to screen for Rpn8-Rpn11–specific nanobodies. Nb1, which was used to solve the structure of the Rpn8-Rpn11 complex, was selected after one round of biopanning.

Phagemids (pMESy4) encoding for specific nanobodies were transformed into *E. coli* WK6 Su^- cells for periplasmic expression. Protein expression was carried out as described for the expression of His_8-Rpn8-Rpn11 in *E. coli* BL21 (DE3) cells. The cell pellet was resuspended in 15 mL of hypotonic TES buffer (200 mM Tris pH 8.0, 0.5 mM EDTA, and 500 mM sucrose) per gram and stirred for 1 h on ice. Subsequently, twice the volume of TES/4 (TES buffer diluted four times) was added, followed by 45 min of incubation on ice. Cell debris was sedimented by centrifugation at 28,000 × *g* for 30 min. The supernatant was applied to Ni-NTA (Qiagen) and incubated for several min at 4 °C. The column was washed with 20 mM Tris pH 7.4 buffer containing 20 mM imidazole and 150 mM NaCl. Bound nanobody protein was eluted with 20 mM Tris pH 7.4, 500 mM imidazole, and 150 mM NaCl and then further purified on Superose-12 equilibrated with 10 mM Tris pH 7.5, 150 mM NaCl, and 90 mM KCl.

Nanobodies were tested for inhibition of the 26S proteasome holoenzyme complex using a deubiquitylation assay. The deubiquitylation-inhibitory nanobodies were used for further experiments.

Tetraubiquitin Cleavage Activity Assays. A fusion protein containing four ubiquitin (Ub) copies followed by the sequence MQIFVKTSQSSCVDKLAALEHHHHHH was expressed and purified from a single transcript in *E. coli* and then labeled with Oregon Green 488 using maleimide labeling. Then 5 nM tetraubiquitin (Ub_4) peptide was combined with purified 26S proteasome from *S. cerevisiae*, Rpn8-Rpn11 fusion protein, or mutant forms of these macromolecules in 50 mM Tris·HCl pH 7.5, 0.01% Nonidet P-40, 50 μM $MgCl_2$, 50 mM ATP, and 1 mM DTT. The reaction was incubated at 37 °C for the indicated times, and fluorescence polarization was determined.

Crystallization. For formation of the Rpn8-Rpn11 fusion protein–nanobody complex, the nanobody Nb1 and the Rpn8-Rpn11 fusion protein were mixed at a 2:1 ratio, and the stoichiometric complex was purified by size exclusion chromatography on Superose-12 equilibrated with 10 mM Tris pH 7.5, 150 mM NaCl, and 90 mM KCl.

Crystals of the Rpn8-Rpn11–nanobody complex were grown by the sitting drop vapor diffusion method at 4 °C or 18 °C, equilibrating equal volumes of 10 mg mL^{-1} protein and precipitant against a large volume of precipitant. Crystal forms Ia and Ib grew with precipitant containing 50 mM Mes pH 6.0, 200 mM Ca-acetate, and 22% (wt/vol) PEG-3350. Crystal form II was obtained with a precipitant containing 50 mM MES pH 6.0, 100 mM $MgCl_2$, and 21% (wt/vol) PEG-3350. For cryoprotection, crystals were transferred stepwise into an otherwise unmodified precipitant solution containing 15% (vol/vol) glycerol before being flash-frozen in liquid nitrogen.

Structure Determination. Diffraction data were collected at the Electron Synchrotron Radiation Facility (ESRF) in Grenoble, France, and Swiss Light Source (SLS) in Switzerland. The data were processed with XDS (3) and transferred into the CCP4 format using Pointless (4), Scala (5), and Truncate as implemented in the CCP4 interface (6). The structure of crystal form Ib was solved by molecular replacement with MOLREP (7) using the Rpn8 homodimer (8) and 2X1P nanobody (9) structures as search models for the Mpr1–Pad1–N-terminal (MPN) domain dimers and the nanobody, respectively. Starting from this initial phase information, a greatly improved model was automatically built by ArpWarp 7.2 (10). Subsequently, the model was improved by iterative cycles of manual model building in Coot (11) and refinement with Refmac5 (12). The remaining crystal forms were solved by molecular replacement with the crystal form Ia model. The presence of Zn in crystal form Ib was confirmed by X-ray fluorescence.

Site-Directed Mutagenesis. Site-directed mutations in Rpn11 were introduced with the QuikChange Site-Directed Mutagenesis Kit (Stratagene) using pRSF-Rpn8-Rpn11 as a template.

EM Density Fitting. The Rpn8-Rpn11 complex was fitted into the cryo-EM density maps of the 26S proteasome starting from the previously assigned position (13, 14) using UCSF Chimera (15).

Figure Preparation. Structure figures were prepared using PyMOL (www.pymol.org) and UCSF Chimera (15). Alignment figures were created with ESPript (16).

1. Rasmussen SG, et al. (2011) Crystal structure of the β2 adrenergic receptor-Gs protein complex. *Nature* 477(7366):549–555.
2. Pardon E, et al. (2014) A general protocol for the generation of nanobodies for structural biology. *Nat Protoc*, in press.
3. Kabsch W (2010) XDS. *Acta Crystallogr D Biol Crystallogr* 66(Pt 2):125–132.
4. Evans P (2006) Scaling and assessment of data quality. *Acta Crystallogr D Biol Crystallogr* 62(Pt 1):72–82.
5. Evans PR (1997) Scala. *Joint CCP4 and ESF-EACBM Newslett* 33:22–24.
6. Collaborative Computational Project, Number 4 (1994) The CCP4 suite: Programs for protein crystallography. *Acta Crystallogr D Biol Crystallogr* 50(Pt 5):760–763.
7. Vagin AA, Isupov MN (2001) Spherically averaged phased translation function and its application to the search for molecules and fragments in electron-density maps. *Acta Crystallogr D Biol Crystallogr* 57(Pt 10):1451–1456.
8. Sanches M, Alves BS, Zanchin NI, Guimarães BG (2007) The crystal structure of the human Mov34 MPN domain reveals a metal-free dimer. *J Mol Biol* 370(5):846–855.
9. Van den Abbeele A, et al. (2010) A llama-derived gelsolin single-domain antibody blocks gelsolin–G-actin interaction. *Cell Mol Life Sci* 67(9):1519–1535.
10. Perrakis A, Morris R, Lamzin VS (1999) Automated protein model building combined with iterative structure refinement. *Nat Struct Biol* 6(5):458–463.
11. Emsley P, Cowtan K (2004) Coot: Model-building tools for molecular graphics. *Acta Crystallogr D Biol Crystallogr* 60(Pt 12 Pt 1):2126–2132.
12. Murshudov GN, Vagin AA, Dodson EJ (1997) Refinement of macromolecular structures by the maximum-likelihood method. *Acta Crystallogr D Biol Crystallogr* 53(Pt 3):240–255.
13. Lasker K, et al. (2012) Molecular architecture of the 26S proteasome holocomplex determined by an integrative approach. *Proc Natl Acad Sci USA* 109(5):1380–1387.
14. Lander GC, et al. (2012) Complete subunit architecture of the proteasome regulatory particle. *Nature* 482(7384):186–191.
15. Goddard TD, Huang CC, Ferrin TE (2007) Visualizing density maps with UCSF Chimera. *J Struct Biol* 157(1):281–287.
16. Gouet P, Courcelle E, Stuart DI, Métoz F (1999) ESPript: Analysis of multiple sequence alignments in PostScript. *Bioinformatics* 15(4):305–308.
17. Ambroggio XI, Rees DC, Deshaies RJ (2004) JAMM: A metalloprotease-like zinc site in the proteasome and signalosome. *PLoS Biol* 2(1):E2.
18. Sato Y, et al. (2008) Structural basis for specific cleavage of Lys 63-linked polyubiquitin chains. *Nature* 455(7211):358–362.
19. Echalier A, et al. (2013) Insights into the regulation of the human COP9 signalosome catalytic subunit, CSN5/Jab1. *Proc Natl Acad Sci USA* 110(4):1273–1278.

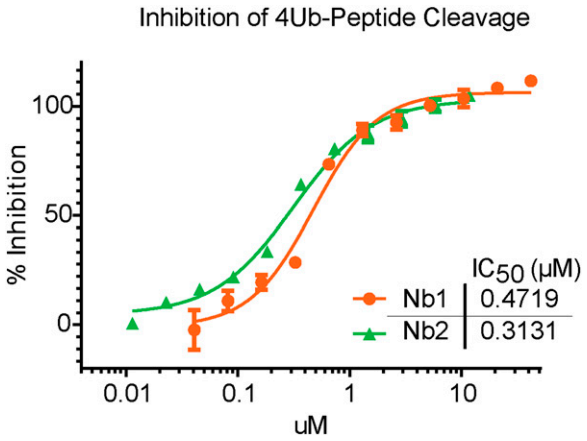

Fig. S1. Inhibition of 26S-mediated Ub_4-peptide cleavage by nanobodies. Twofold serial dilutions of Nb1 and Nb2 were added to the purified 26S proteasome and Ub_4-peptide cleavage activity was monitored after 1 h of incubation at 37 °C. Values are normalized to activity of 26S proteasome in the absence of effector.

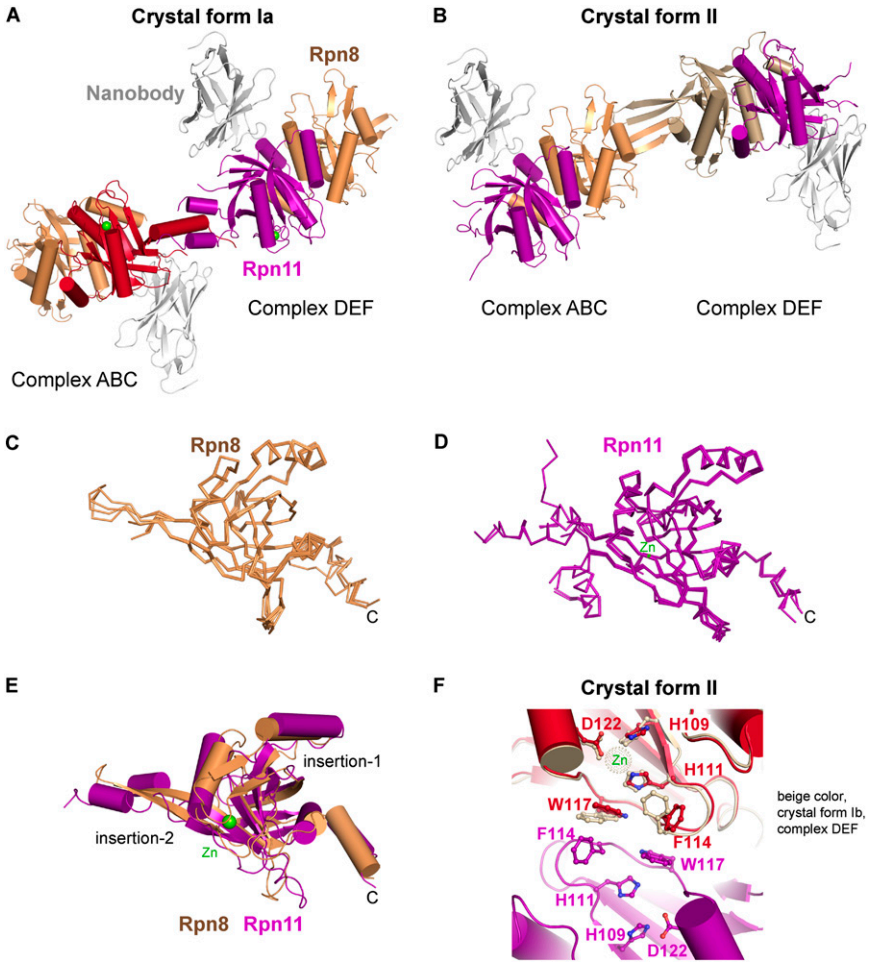

Fig. S2. Comparison of the different Rpn8-Rpn11-nanobody crystal forms. (*A* and *B*) Asymmetric units of crystal forms Ia and II. Each contains two complexes linked by characteristic crystal contacts. The Rpn8 and Rpn11 units are shown in hues of purple and sandy brown, respectively; the nanobody is represented in silver. The catalytic zinc ions are shown as green spheres. (*C*) Superposition of Rpn8 conformations observed the different crystal forms. The Rpn8 chains are indicated by Cα traces. In one copy of crystal form II, helix α4 is displaced. (*D*) Superposition of Rpn11 conformations. Bound zinc ions are represented by green crosshairs. (*E*) Superposition of Rpn11 and Rpn8 MPN domains. Color-coding is as in *A* and *B*. (*F*) Catalytic loop contacts in crystal form II. The two copies on Rpn11 are shown in purple and red; the active conformation is superposed in beige. Sidechains of key catalytic residues are shown in ball-and-stick representation. The tight contact distorts the active site loop, pushing His109 away the zinc-binding site (indicated by a dotted sphere).

A

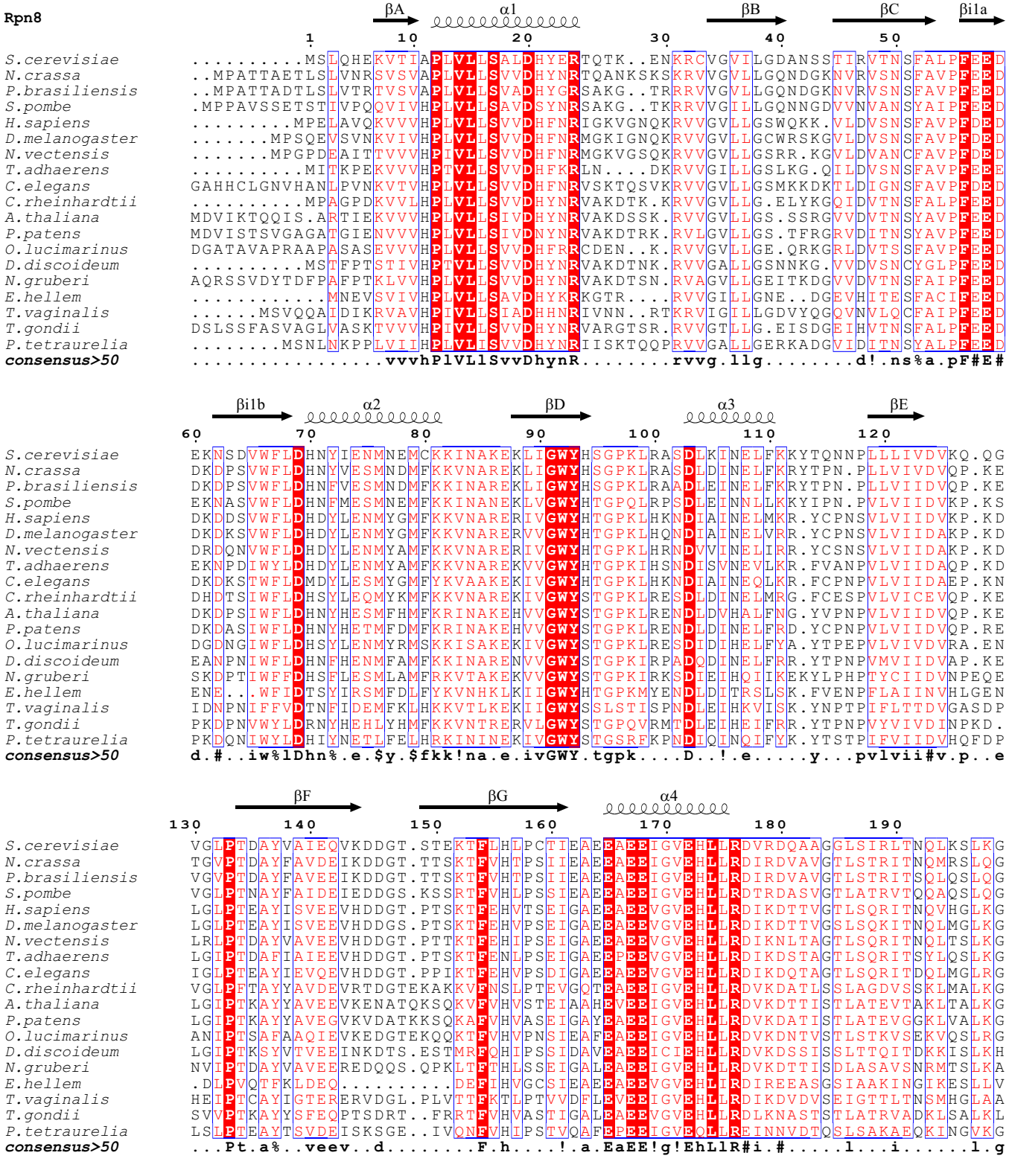

Fig. S3. (Continued)

Rpn8

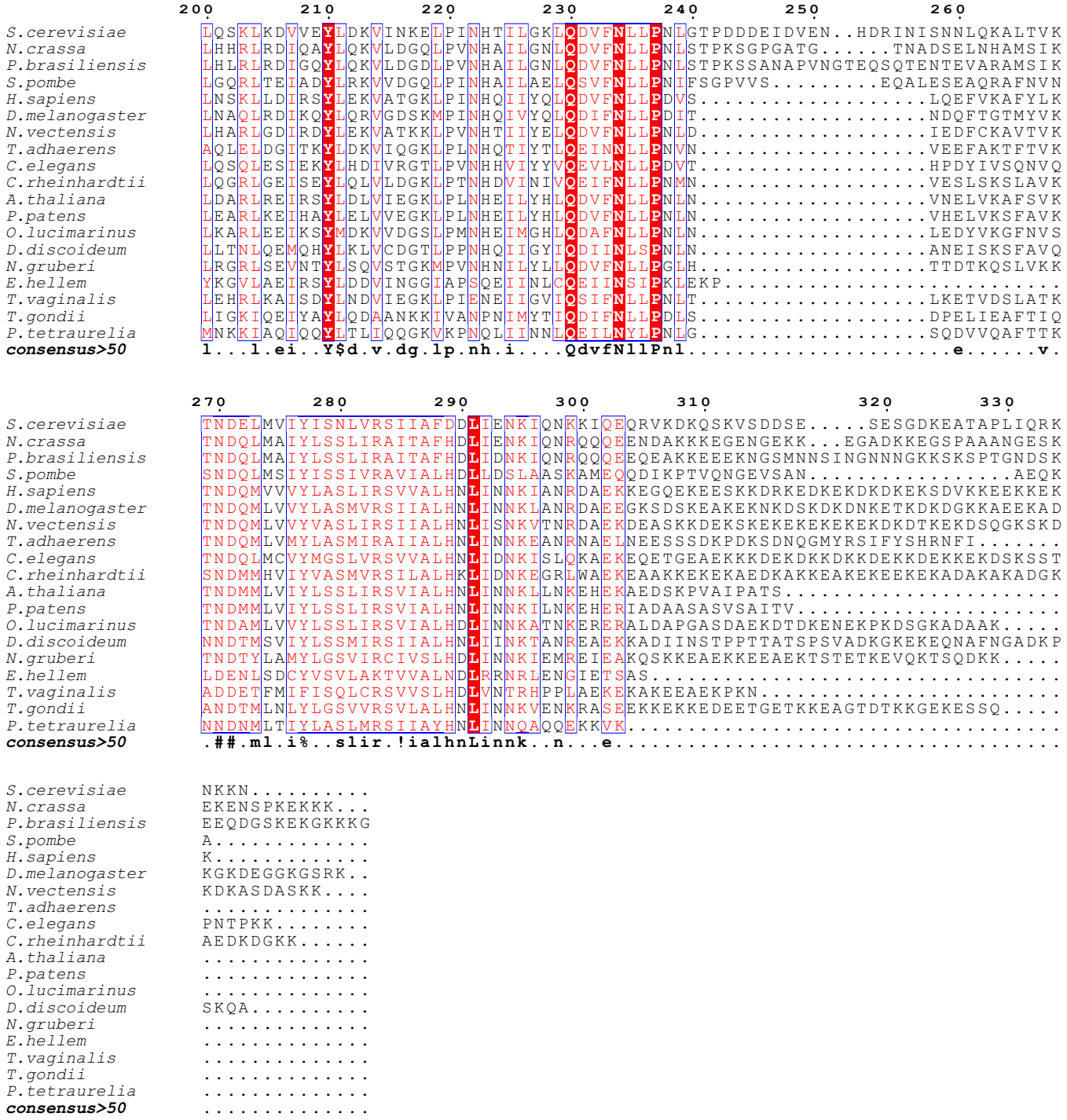

Fig. S3. (Continued)

B

Rpn11

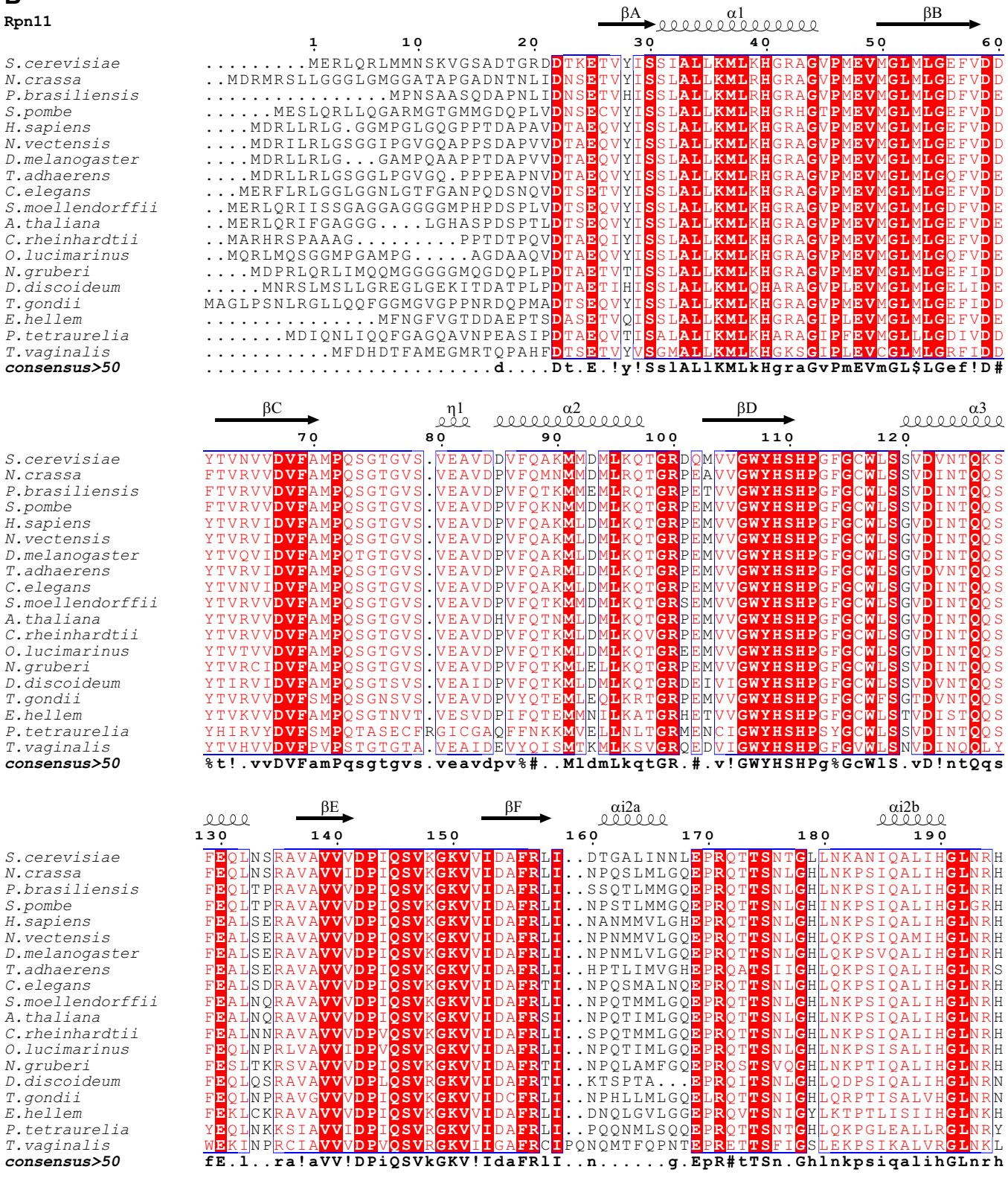

Fig. S3. (Continued)

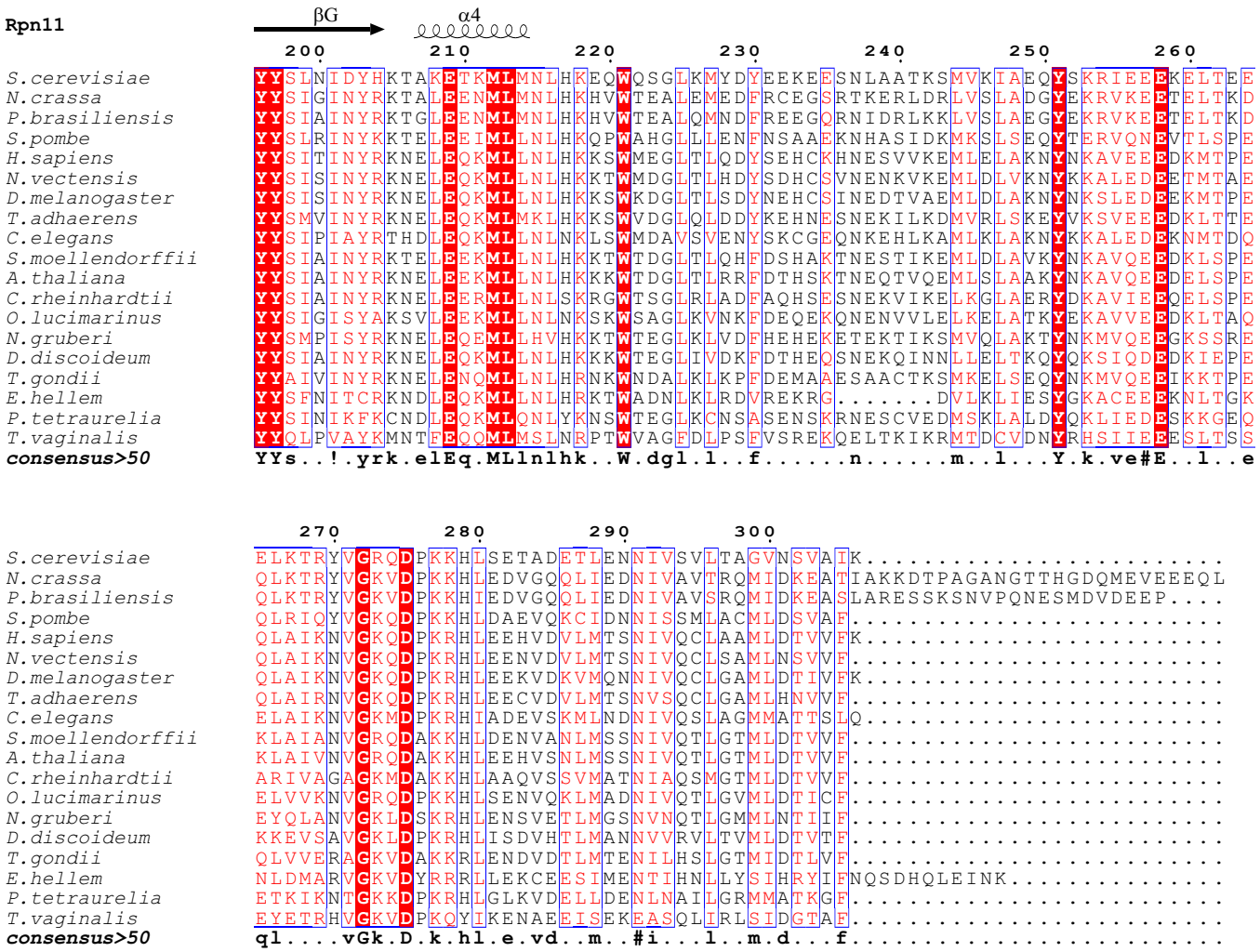

Fig. S3. Alignment of representative Rpn8 and Rpn11 sequences. (*A* and *B*) Amino acid sequences of selected Rpn8 and Rpn11 homologs were aligned using ClustalW. Secondary structure elements for the *S. cerevisiae* Rpn8 and Rpn11 are indicated above the sequences. Similar residues are shown in red, and identical residues are shown in white on red background. Blue frames indicate homologous regions. The consensus sequences are shown at the bottom. The Uniprot/TrEMBL accession codes for the Rpn8 sequences are as follows: 08723, *S. cerevisiae*; 8WZY4, *Neurospora crassa*; 1HB79, *Paracoccidioides brasiliensis*; 74440, *Schizosaccharomyces pombe*; 51665, *Homo sapiens*; 26270, *Drosophila melanogaster*; 7RRK5, *Nematostella vectensis*; 3RVP1, *Trichoplax adhaerens*; 61792, *Caenorhabditis elegans*; 8J8V5, *Chlamydomonas rheinhardtii*; 24412, *Arabidopsis thaliana*; 9TB60, *Physcomitrella patens*; 4RZB8, *Ostreococcus lucimarinus*; 54WI8, *Dictyostelium discoideum*; 2VRX4, *Naegleria gruberi*; 6UC02, *Encephalitozoon hellem*; 2EN06, *Trichomonas vaginalis*; 9PHD3, *Toxoplasma gondii*; 0EGJ8, *Paramecium tetraurelia*. The Uniprot/TrEMBL accession codes for the Rpn11 sequences are as follows: P43588, *S. cerevisiae*; Q7SEB1, *N. crassa*; C0S0C1, *P. brasiliensis*; P41878, *S. pombe*; O00487, *H. sapiens*; Q9V3H2, *D. melanogaster*; A7RQF7, *N. vectensis*; B3SA12, *T. adhaerens*; O76577, *C. elegans*; D8R1P1, *Selaginella moellendorffii*; Q9LT08, *A. thaliana*; A8HPA0, *C. rheinhardtii*; A4RZR1, *O. lucimarinus*; D2VEL9, *N. gruberi*; Q86IJ1, *D. discoideum*; B9PHM3, *T. gondii*; I6UPI3, *E. hellem*; A0DLR9, *P. tetraurelia*; A2FD84, *T. vaginalis*.

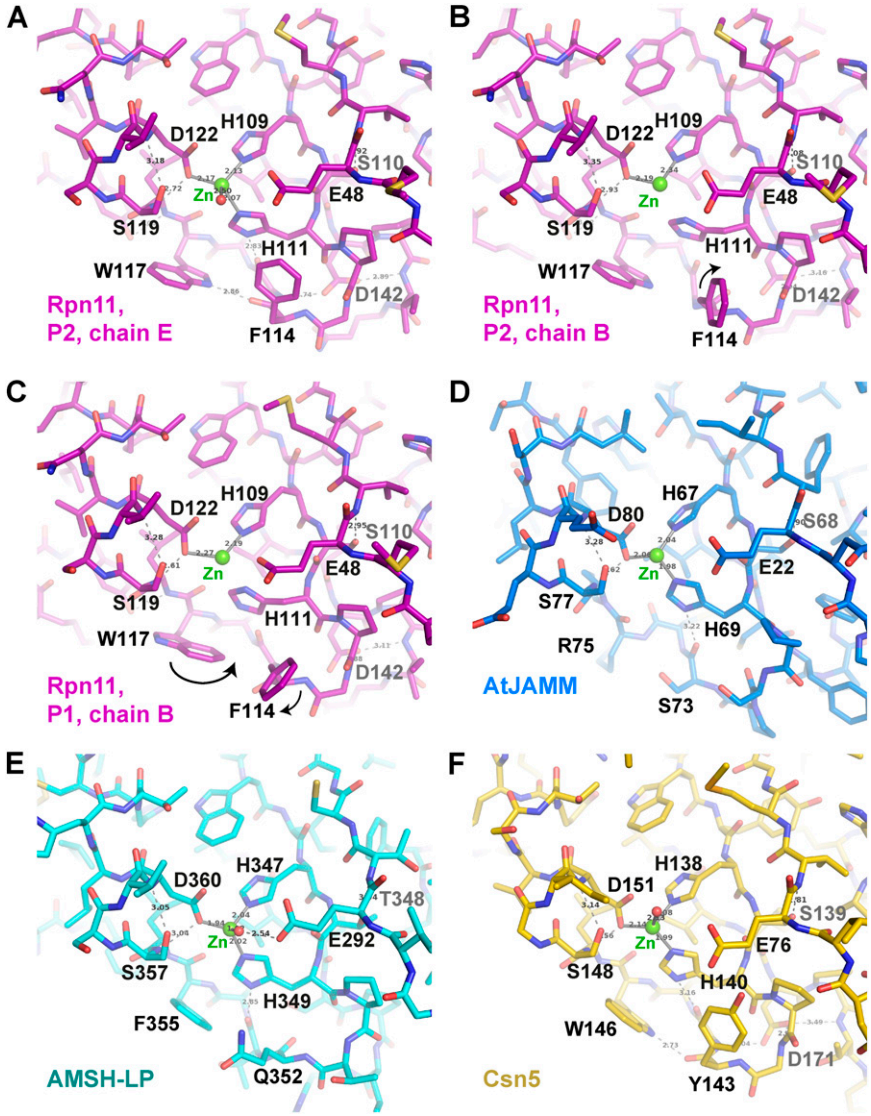

Fig. S4. Comparison of active sites from MPN domain metalloprotease structures. (*A–C*) Active site geometry and hydrogen bond networks in Rpn11 structures. The structures are shown in stick representation. Hydrogen bonds are represented by dotted lines. Insertion 1 has been omitted for clarity. The E chains in crystal forms Ia (P2) and Ib (P1) have almost identical active site geometry. (*D–F*) Active site structures of AfJAMM, AMSH-LP, and Csn5 (17-19). The respective protein structures are shown in blue, cyan, and gold (Refs). Orientation is the same as in *A–D*. Insertion-1 and insertion 2 have been omitted for clarity.

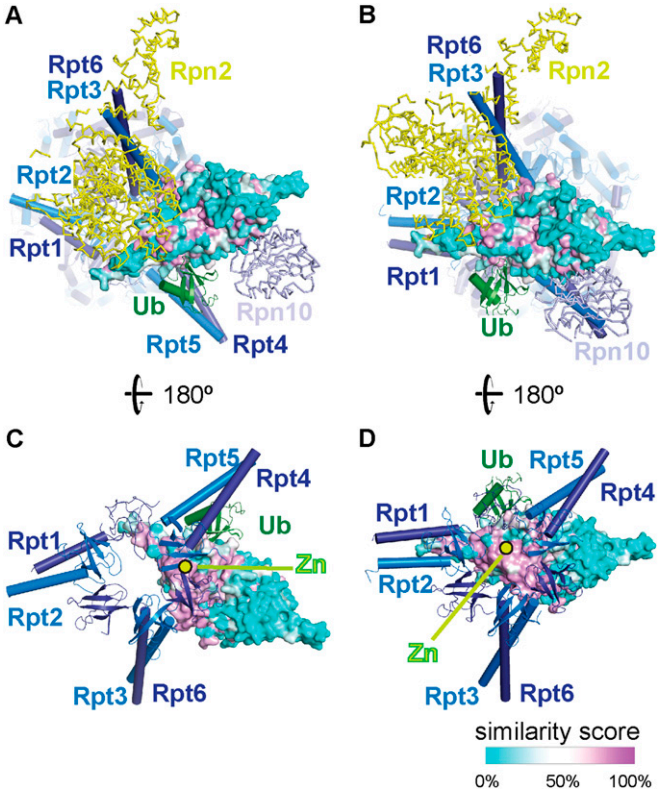

Fig. S5. Surface conservation of the Rpn8-Rpn11 deubiquitylation module. (*A* and *B*) Top views of Rpn8-Rpn11 in the substrate-accepting (*Left*) and -engaged (*Right*) states of the 26S proteasome. The Rpn8-Rpn11 MPN domain complex is shown in surface representation, with surface conservation indicated by a cyan-white-magenta color gradient. The interactors Rpn2 (yellow) and Rpn10 (violet) are shown as Cα traces. Other lid subunits were removed for clarity. The primary Ub in its putative binding orientation is indicated in green. (*C* and *D*) Bottom views of the docked crystal structure in the two proteasomal states, using the same representation. The active site zinc centers are indicated. For clarity, only the coiled coils and the OB ring of the AAA subunits are shown.

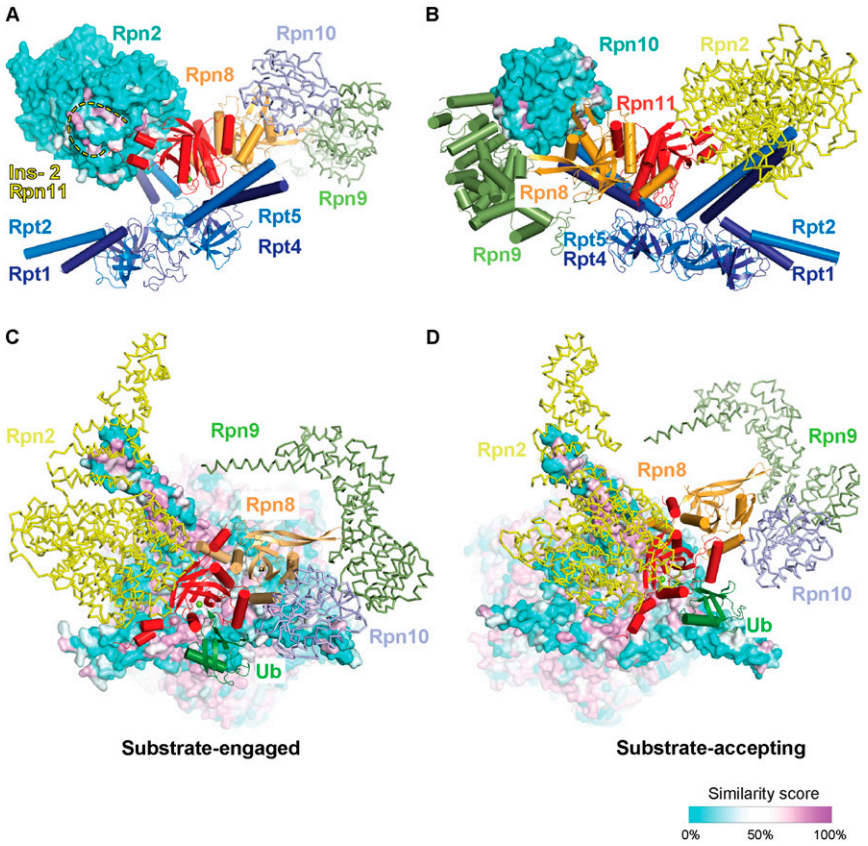

Fig. S6. Surface conservation of subunits surrounding the Rpn8-Rpn11 MPN domain complex. (*A*) Putative interaction site for the Rpn11 insertion 2 loop on Rpn2 (side view). A highly conserved surface cleft on Rpn2 is situated close to the ordered part of insertion 2 of Rpn11. A yellow dotted line indicates the putative path of the disordered tip of insertion 2. Rpn2 is shown in surface representation, with the similarity score indicated by a color gradient. (*B*) Surface conservation in Rpn10 (side view). Rpn10 is shown in surface representation. Conserved areas map to the contact areas with Rpn8 and Rpn9. (*C* and *D*) Surface conservation in the coiled-coil helices and the OB ring of the ATPase subunits. Shown are top views of the substrate-engaged and -accepting state models of the 26S complex. The orientation of the Rpn11 catalytic site toward the coiled-coil helices and the OB ring in the two proteasomal conformations is shown. In the substrate-engaged state, the catalytic machinery is in tight contact, and insertion 1 is removed from the coiled-coil protrusion of Rpt4-Rpt5. The primary Ub in its putative binding orientation is indicated in green.

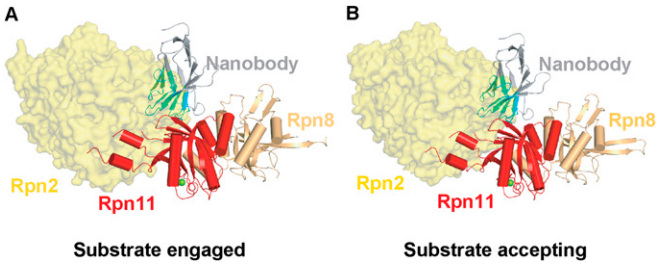

Fig. S7. Clash of nanobody with the Rpn2 subunit. Rpn8-Rpn11-nanobody complex docked into substrate-engaged (*A*) and -accepting (*B*) states of the 26S proteasome. The bound nanobody severely clashes with the Rpn2 subunit in both states (arrow). Overlapping regions in the nanobody are highlighted in cyan.

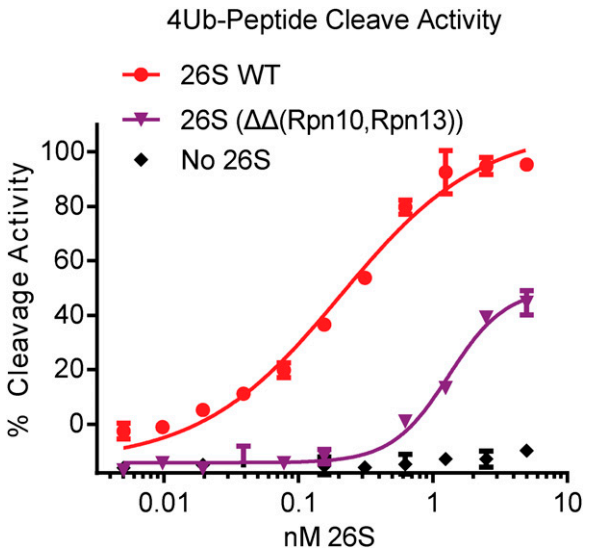

Fig. S8. Role of proteasomal Ub receptors in substrate deubiquitylation. Ub_4 cleavage activity of WT and ΔΔ(*rpn10Δ*, *rpn13Δ*) 26S proteasome was measured by fluorescence polarization at the indicated concentrations after 1 h of incubation at 37 °C.

Table S1. Data collection and refinement statistics

	Crystal form		
Variable	Ia	Ib	II
Beamline	SLS, X10SA	ESRF, ID23-1	ESRF, ID23-1
Wavelength, Å	1.03320	1.000	1.000
Space group	*P*1	*P*2	$P4_32_12$
Cell dimensions			
a, b, c, Å	45.26, 63.43, 100.11	63.40, 44.96, 199.99	80.04, 80.04, 386.21
α, β, γ, °	100.08, 92.75, 90.62	90, 98.41, 90	90, 90, 90
Resolution limits, Å*	48.98–2.4 (2.52–2.4)	44.97–2.0 (2.1–2.0)	48.83–2.25 (2.37–2.25)
R_{merge}*	0.081 (0.634)	0.078 (0.600)	0.058 (0.806)
I/sigma*	10.1 (2.4)	9.1 (1.9)	20.3 (2.2)
Multiplicity*	3.5 (3.4)	3.2 (3.2)	7.8 (8.0)
Completeness, %*	96.4 (90.4)	96.8 (88.0)	99.8 (99.2)
Refinement			
Resolution range	30–2.4	30–2.0	30–2.25
Reflections (test set)	39,520 (2,089)	70,928 (3,108)	57,894 (2,042)
R_{work}/R_{free}	0.1951/0.2522	0.2158/0.2623	0.2321/0.2811
Number of atoms	7,359	7,522	7,341
rmsd bonds, Å	0. 017	0.022	0.009
rmsd angles, °	1. 733	1.933	1. 178
Ramachandran plot†			
% in preferred regions	95.23	94.07	95.75
% in allowed regions	3.69	5.16	3.47

*Values in parentheses are for the outer shell.
†As defined in Coot (11).

Chapter 5: Discussion

Purifying protein complexes from native hosts often yields low amount of proteins which prevents a detailed structural and biochemical characterization of these proteins. Recombinant over-expression in suitable hosts is the preferred method of producing large amounts of proteins for structure determination. Using recombinant over-expression approach, all of the *D. melanogaster* 19S RP subunits could be cloned and expressed in *Rhodococcus erythropolis* as a heterologous expression system. Some of the RP subunits expressed formed insoluble inclusion bodies, possibly due to the lack of neighboring subunits stabilizing their structures and keeping them in soluble form. In addition to the *R. erythropolis* heterologous expression system, DNA sequences of *S. cerevisiae* RP subunits having a codon usage optimized for *E. coli* were also used for the expression of proteins, protein domains and protein subcomplexes in *E. coli.* These constructs were further used for the reconstitution of the lid sub complex.

Although most of the RP subunits from *D. melanogaster* were expressed in high yield *R. erythropolis* and *E. coli*, subunits like Rpn1, Rpn2, Rpn3, Rpn8 and Rpn11 were difficult to purify. This may be due to the formation of protein aggregates and protein precipitation during purification. The other *D. melanogaster* RP subunits Rpn6, Rpn7, Rpn5, Rpn9, and Rpn12, were purified to apparent homogeneity. Amongst these proteins, crystals could be grown from Rpn6 protein. Furthermore, crystals of sufficient quality to solve the structure were obtained after N-terminal truncation of the Rpn6 construct. Crystallization of the other subunits failed, probably owing to sample heterogeneity, aggregation and precipitation. Insoluble proteins or proteins aggregating after purification were expressed using different solubility-promoting fusion protein tags, such as GST, MBP, NusA, SUMO and SAMP. Expression and purification of full-length Rpn11 of *S. cerevisiae* was tedious due to its unstable nature. This protein could be expressed in soluble form using the small archaeal modifier protein (SAMP) fusion tag. The Rpn8-Rpn11 structure has been discussed in detail in chapter 4.2.

Table1: Overview of the different stages accomplished in the structure determination of 19S RP subunits.

Protein/subcomplex	Cloning	Expression	Purification	Crystallization	Structure solution
Rpn1	→	→	→		
Rpn2	→	→	→	→	
Rpn3	→	→			
Rpn5	→	→	→	→	
Rpn6	→	→	→	→	→
Rpn7	→	→	→	→	
Rpn8	→	→	→	→	→
Rpn9	→	→	→	→	
Rpn10	→	→	→		
Rpn11	→	→	→	→	
Rpn12	→	→	→		
Rpn13	→	→	→		
Rpn15	→	→	→		
PCI + MPN domain protein subcomplex	→	→	→	→	
PCI domain protein subcomplex	→	→	→	→	
Rpn8-Rpn11	→	→	→	→	→
Rpn7-Rpn15	→	→	→		
Rpn6-Rpn7	→	→	→		
Rpn5-Rpn6-Rpn9-Rpn8-Rpn11	→	→	→	→	
Rpn5-Rpn9	→	→	→	→	

Length of the arrows implicates partial success of the experiments.

Structural studies on the Rpn6 subunit and its importance in elucidation of the molecular architecture of the RP

The structural and biochemical analyses of the Rpn6 subunit provides insights into its location within the 26S proteasome, which confirm its pivotal role in holding the regulatory particle and the 20S core particle together during substrate processing (82). It is noteworthy that the high-resolution structure of Rpn6 had an impact on evaluating and analyzing other PCI domain proteins. The Rpn6 structure provided a template for homology modeling of the other PCI domain containing proteins. The structure of Rpn6 contributed vitally to the

elucidation of the architecture of the RP. Because of its characteristic curved shape, the density for Rpn6 could be identified with high confidence in the 26S particle. The respective volume was in contact with the lid, the AAA ring and the beta ring of the core particle, substantiating the pivotal role of Rpn6 in holding the regulatory particle and the 20S core particle together.

In the lid density, Rpn6 forms part of a structure resembling a horseshoe from which appendages protrude radially. In the crystal, the *C*-terminal winged-helix domains of Rpn6 form a continuous spiral structure from which the helical solenoids project outwards, suggesting that the six-proteasomal PCI domain proteins might interact with each other in a similar way. Mutation studies of the putative PCI domain interfaces in Rpn6 and pull-down experiments with other PCI domain subunits confirmed this hypothesis. Based on the size of the PCI domain subunits and crosslinking data, the subunit order Rpn9-Rpn5-Rpn6-Rpn7-Rpn3-Rpn12 was found (Fig 6).

Sakata, et al. (83) localized the ubiquitin receptors Rpn10 and Rpn13 in the 26S complex by comparison with the structures of complexes isolated from Rpn10 and Rpn13 deletion strains. Combining the above information with crosslinking data and computational models of the individual subunits led to a complete model of the 19S RP complex (84). Independently, Andreas Martin and coworkers (36) came up with a closely similar model. They reconstituted the lid by recombinant expression of the subunits in *E. coli*, using fusion protein tags for determining the position of individual subunits. A third assignment was published somewhat later by Edward Morris and coworkers (85). Today distinct conformational states of the 26S proteasome determined by single-particle reconstruction of cryo-EM data are known to sub-nm resolution (41). To understand mechanistic details, however, further high-resolution structures of individual subunits are needed.

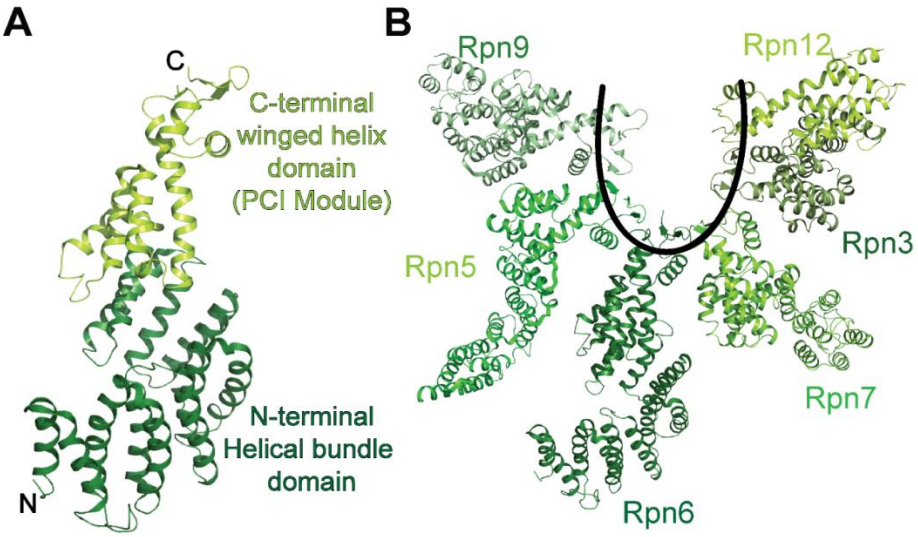

Fig 6. PCI domain subunits.

(A) Crystal structure of the PCI domain protein Rpn6 (PDB: 3TXN)(86), a representative model for all the PCI domain proteins. The C-terminal winged-helix domain is represented in yellow-green and the N-terminal helical bundle domain in forest green.

(B) All the PCI domain containing subunits coming together through their C-terminal winged helix domains and forming a horseshoe (U-shape) like structure with their N-terminal domains flanking away (PDB: 4B4T)(41). All the six subunits are colored in different shades of green for clarity.

Crystal structures and atomic models of RP subunits

As discussed above, the high-resolution structures of proteins in the RP would help to understand the detailed mechanism of substrate processing. During the course of this work a crystal structure of another PCI domain protein Rpn12 was solved (39). Rpn6 being used as a template to model other PCI domain proteins, the structure of Rpn12 provided an additional confirmation for the models of other PCI domain subunits.

Subcomplexes of different proteins were cloned using the information available from MS analysis and of complexes formed during RP assembly. A major subcomplex composed of six

PCI domain proteins and two MPN domain proteins was cloned, expressed and purified. Attempts to obtain the high-resolution maps of this complex did not provide any new details. Other subcomplex of subunits Rpn5, Rpn9, Rpn6, Rpn8, and Rpn11 also didn't yield high-resolution structural details.

In addition to the PCI-MPN subcomplex, structural studies on the two largest subunits of the 19S regulatory particle Rpn1 and Rpn2 were carried out independently. Surprisingly these subunits show low sequence identity but display a similar architecture. A crystal structure of *S. cerevisiae* Rpn2 solved by He J. et.al., becoming available in the course of this work provides a detailed structural characterization of PC subunits (87). Rpn2 has a characteristic tobacco-pipe-shaped structure with N-terminal helices forming a stem and the C-terminally located PC domain forming the bowl (Fig 7). The C-terminal helices form 11 proteasome/cyclosome (PC) repeats consisting of 36 to 42 amino acid residues. The C-terminal 20 residue-long unstructured part of Rpn2 provides a binding site for Rpn13 (88). The PC domain protein Rpn2 also represents a structural model template for Rpn1. Both these proteins bind at least one ubiquitin receptor and one deubiquitinating enzyme. Negative-stain EM analysis of purified Rpn1 indicates that it shares a similar architecture with a slight difference in the rod domain orientation.

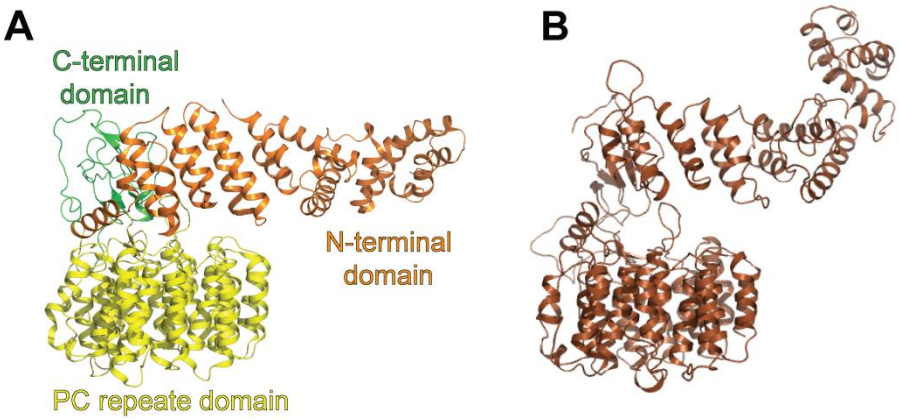

Fig 7. Crystal structure of Rpn2 and modeled structure of Rpn1

(A) Crystal structure of Rpn2. The N-terminal domain is represented in orange, the PC repeats are colored in yellow and the C-terminal domain is colored in green (PDB: 4ADY)(87) .

(B) Homology model of Rpn1 derived from the crystal structure of Rpn2.

The crystal structure of Rpn2 could be fitted into the assigned densities on cryo EM maps with high confidence and hence no further structure solution was necessary. In the case of Rpn1 the newly derived high-resolution cryo EM maps of the 26S complex provide discrete densities for Rpn1 making it easier to model this protein structure (Fig. 7).

With the availability of crystal structures of some of the important subunits and homology models of other protein subunits the efforts of Beck et.al. (41), who modeled all of the subunits into the high-resolution cryo EM maps, provided details of the structure of the 26S proteasome at pseudo-atomic resolution. However, the C-terminal helical bundle formed by the PCI and MPN domain subunit was ambiguously fitted into previously modeled structures, which was later resolved and confirmed by mutational and computational analysis by Matyskiela et.al. (Fig. 8)(89).

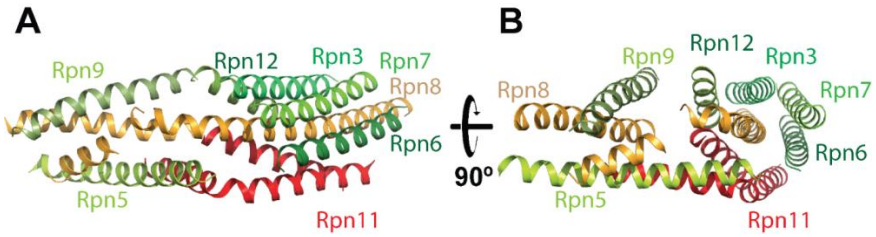

Fig 8. C-terminal helical bundle

(A) The C-terminal helices of the PCI domain proteins and the MPN domain proteins form a helical bundle (PDB: 3J47)(90). The C-terminal helices from different subunits are represented in different colors.

(B) 90° rotation of the helical bundle in A.

The availability of crystal structures of the 20S proteasome, Rpn6, Rpn2, Rpn12, and the structure of AAA ATPases of PAN revealed the complete architecture of the 26S proteasome. Thereafter we sought to gain deeper insights into the catalytic mechanism of proteasome. The proteasomal iso-peptidase Rpn11 is still structurally not well-characterized. The

structure of the substrate-engaged proteasome revealed its position right above the ATPase pore presumably allowing deubiquitination of substrates just prior to translocation. The structure further indicated that Rpn11 forms a heterodimer with Rpn8, which explains the problems in obtaining stable Rpn11 protein (Fig. 9). Therefore, the crystal structure of the core complex consisting of the MPN domains of Rpn8 and Rpn11 was determined. The mechanism underlying substrate processing remains elusive, but the crystal structure of the Rpn8-Rpn11 complex provides a platform for understanding the mechanism of deubiquitination.

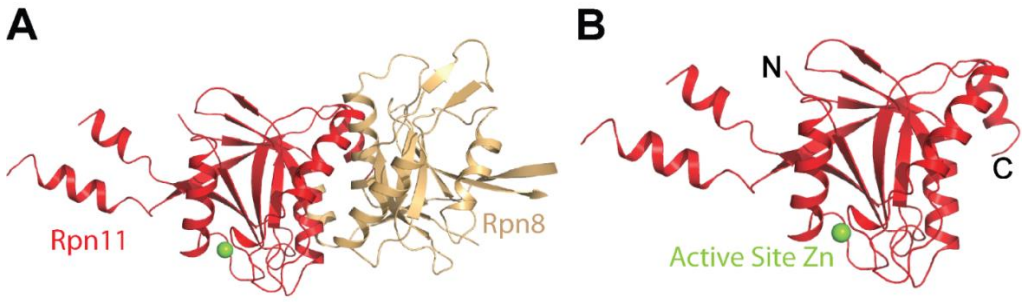

Fig 9. MPN domain proteins.

(A) Crystal structure of the heterodimer (PDB: 4OCL, 4OCM, 4OCM)(91) of the two MPN domain containing proteins Rpn8 and Rpn11 shown in sandy brown and red respectively.

(B) The MPN domain of the active site containing subunit Rpn11. Active-site zinc is represented in green.

Mechanistic details of substrate deubiquitination at the Rpn11 active site

The MPN domain of Rpn11 is located above the mouth of OB domain ring of the AAA-ATPase, placing the zinc ion coordinated catalytic site on the pore of the AAA ATPase in substrate-engaged confirmations. The substrate-engaged state is considered to be the active confirmation of Rpn11 whereas, in the substrate-accepting state, the active site of Rpn11 moves 18° (89) towards the OB domain of Rpt4. This rotation presumably blocks the access

of ubiquitinated substrate to the active site of Rpn11, rendering it an inactive conformer. The whole process of deubiquitination is coupled to ATP hydrolysis.

The crystal structure of the fused Rpn8-Rpn11 heterodimer helped us to formulate potential mechanisms of preventing premature initiation of the isopeptidase activity of Rpn11. The low affinity of the proximal Ub to its docking site on Rpn11 might prevent premature deubiquitination of substrates. The Establishment of the correct active site geometry might be required to promote the proper rearrangement of Rpn11 (and its insertion-1 loop) that allows access of the proximal Ub C-terminus to the catalytic site. We believe that only a crystal structure of a poly-ubiquitinated substrate bound to Rpn11 in context with a stalled proteasome will reveal the molecular mechanism of deubiquitination in full detail.

As discussed previously, the potential of Rpn11 as a drug target will provide more versatility in developing drugs for different diseases including cancer, for which there are already other drugs inhibiting the proteasome by targeting mainly the CP.

Proposed Model for substrate processing by the RP subcomplex

Substrates are targeted for proteasomal degradation by tagging with polyubiquitin chains. The ubiquitin receptors Rpn10 and Rpn13 recognize polyubiquitin-tagged substrates. Thereafter the substrate will be deubiquitinated and is threaded into the pore of the AAA ATPase ring, which commences pulling at the substrate, triggering further unfolding.

In the beginning of this project, partial information about the AAA ATPase subunits was available but information on the localization and functional characterization of the non-regulatory particle subunits was lacking. The data available was insufficient to put forward a reliable model of substrate processing. By crystal structure determination and by localization of different subunits in the 19S RP we were able to put forward a detailed mechanistic model for substrate processing by the 19S RP subcomplex.

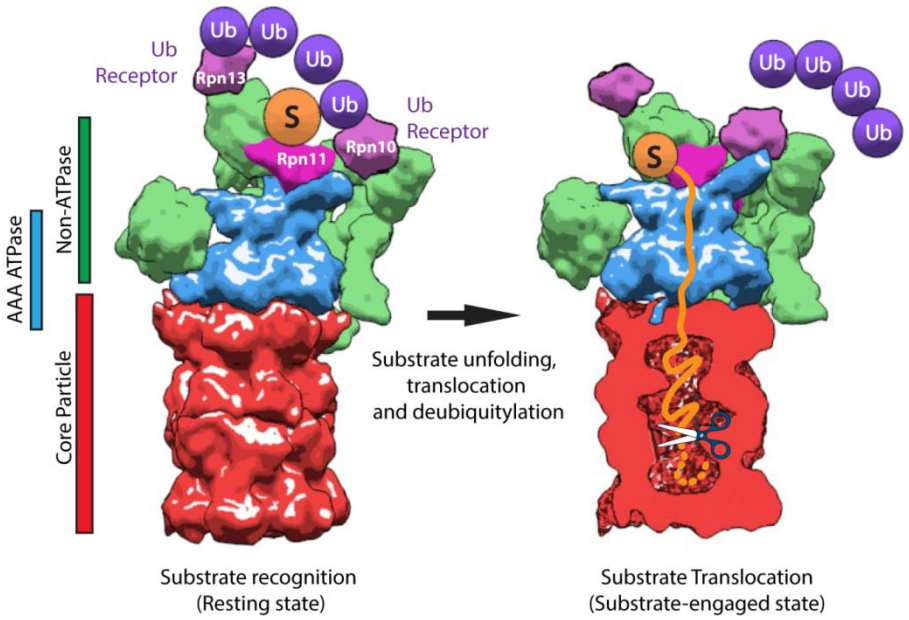

Fig 10. Model for substrate processing

The ubiquitin receptors Rpn10 and Rpn13 (in purple) receive the tetra-ubiquitinated substrate and place it close to the AAA ATPase (in blue). While the AAA ATPase pulls the substrate the iso-peptide bond is placed at the active site of Rpn11 where it is cleaved (magenta). The Rpn11 subunit, which is the internal DUB of the 26S proteasome, is located above the AAA ATPase ring and monitors the removal of ubiquitin. The substrate is translocated further into the 20S core particle (red) where it's degraded into peptides of 6-14 amino acids.

In the course of our project we found that the affinity of the Rpn11 subunit for ubiquitin must be only modest. This explains the need for ubiquitin recognition by other subunits in the RP which select ubiquitinated substrates and process them. The close proximity of the Rpn10 UIM motif to Rpn11 on one side and the presence of Rpn13 on the other side would allow efficient substrate binding. When a poly-ubiquitinated substrate comes into the vicinity of the 26S proteasome, the ubiquitin receptors Rpn10 and Rpn13 will act like antennas sensing a degradation signal (Resting state/substrate accepting state). At this point, an unfolded end of the substrate protein is pulled into the pore of the AAA ATPase ring. During this process a polyubiquitinated lysine residue reaching the mouth of the AAA ring might stall further process. Now the proximal ubiquitin is placed adjacent to Rpn11,

triggering binding, displacement of the insertion-1 segment, and ultimately isopeptide bond cleavage. The AAA ATPase will pull the substrate with the aid of ATP hydrolysis which causes a conformational change of the 19S RP. This allows further translocation of the substrate towards the catalytic chamber of the CP through the ring of AAA ATPases (Fig. 10).

New features of the Rpn11 enzyme, the only deubiquitinating enzyme present in the 19S RP has low affinity towards ubiquitin. To date the active sites of the 20S proteasomes have been the principal drug targets. However, with the advance in the knowledge of the mechanism of the 19S RP and with the advent of high-resolution crystal structures, new potential drug targets have become available. Probably crystal structures of subcomplexes like ubiquitin bound to ubiquitin receptors, poly-ubiquitinated substrate and deubiquitinating enzyme-complex would allow insights into the complete mechanism from ubiquitin tagging to substrate degradation into small peptides.

Chapter 6: Abbreviations used

UPS- ubiquitin-proteasome system

CP core particle

RP-Regulatory particle

Rpn- Regulatory Particle Non-ATPase

Rpt- Regulatory Particle ATPase

PCI- proteasome, COP9 signalosome and eukaryotic translation initiation factor (eIF3)

eIF3-Eukaryotic translation initiation factor 3

MPN- MPR1, PAD1 N-terminal

AAA ATPase domain - *ATPase's* associated with diverse cellular Activities

CSN -COP9 signalosome

CTD-C-terminal domain

LRR's - Leucine rich repeats

UIM- Ubiquitin Interacting Motifs

JAMM- Jab1/MPN domain-associated metalloisopeptidase

AfJAMM- *Archaeoglobus fulgidus* JAB1/MPN/Mov34 metalloenzyme

AMSH-LP - associated molecule with the SH3 domain of STAM- like protein

HbYX - hydrophobic-tyrosine-any amino acid-C-terminus

OB- oligosaccharide/oligonucleotide binding domain

PAN - Proteasome Activating Nucleotidase

ARC- ATPases forming ring-shaped complexes

PRU- pleckstrin-like receptor for ubiquitin

vWA- von Willebrand factor type A domain

MDa- Mega Dalton

KDa- Kilo Dalton

DDW-Double-distilled water

DTT-dithiothreitol

LC-Liquid chromatography

MS/MS- Tandem mass spectometry

MW-Molecular weight

PBS-Phosphate-buffered saline

TCA-trichloroacetic acid

WT-Wild-type

Chapter 7: References

1. Matthews W, Driscoll J, Tanaka K, Ichihara A, & Goldberg AL (1989) Involvement of the proteasome in various degradative processes in mammalian cells. *Proceedings of the National Academy of Sciences of the United States of America* 86(8):2597-2601.
2. Goldberg AL (2003) Protein degradation and protection against misfolded or damaged proteins. *Nature* 426(6968):895-899.
3. Hershko A, Ciechanover A, & Varshavsky A (2000) Basic Medical Research Award. The ubiquitin system. *Nature medicine* 6(10):1073-1081.
4. Voges D, Zwickl P, & Baumeister W (1999) The 26S proteasome: a molecular machine designed for controlled proteolysis. *Annual review of biochemistry* 68:1015-1068.
5. Hershko A & Ciechanover A (1986) The ubiquitin pathway for the degradation of intracellular proteins. *Progress in nucleic acid research and molecular biology* 33:19-56, 301.
6. Ciechanover A, Finley D, & Varshavsky A (1984) The ubiquitin-mediated proteolytic pathway and mechanisms of energy-dependent intracellular protein degradation. *Journal of cellular biochemistry* 24(1):27-53.
7. Hershko A & Ciechanover A (1982) Mechanisms of intracellular protein breakdown. *Annual review of biochemistry* 51:335-364.
8. Meusser B, Hirsch C, Jarosch E, & Sommer T (2005) ERAD: the long road to destruction. *Nature cell biology* 7(8):766-772.
9. Brooks P*, et al.* (2000) Subcellular localization of proteasomes and their regulatory complexes in mammalian cells. *The Biochemical journal* 346 Pt 1:155-161.
10. Kniepert A & Groettrup M (2014) The unique functions of tissue-specific proteasomes. *Trends in biochemical sciences* 39(1):17-24.
11. Goldberg AL, Akopian TN, Kisselev AF, Lee DH, & Rohrwild M (1997) New insights into the mechanisms and importance of the proteasome in intracellular protein degradation. *Biological chemistry* 378(3-4):131-140.
12. Kisselev AF, van der Linden WA, & Overkleeft HS (2012) Proteasome inhibitors: an expanding army attacking a unique target. *Chemistry & biology* 19(1):99-115.
13. Tanaka K (2009) The proteasome: overview of structure and functions. *Proceedings of the Japan Academy. Series B, Physical and biological sciences* 85(1):12-36.
14. Forster F, Unverdorben P, Sledz P, & Baumeister W (2013) Unveiling the long-held secrets of the 26S proteasome. *Structure* 21(9):1551-1562.
15. Baumeister W, Walz J, Zuhl F, & Seemuller E (1998) The proteasome: paradigm of a self-compartmentalizing protease. *Cell* 92(3):367-380.
16. Peters JM, Cejka Z, Harris JR, Kleinschmidt JA, & Baumeister W (1993) Structural features of the 26 S proteasome complex. *Journal of molecular biology* 234(4):932-937.
17. Yoshimura T*, et al.* (1993) Molecular characterization of the "26S" proteasome complex from rat liver. *Journal of structural biology* 111(3):200-211.
18. Nandi D, Tahiliani P, Kumar A, & Chandu D (2006) The ubiquitin-proteasome system. *Journal of biosciences* 31(1):137-155.
19. Lowe J*, et al.* (1995) Crystal structure of the 20S proteasome from the archaeon T. acidophilum at 3.4 A resolution. *Science* 268(5210):533-539.
20. De Mot R, Nagy I, & Baumeister W (1998) A self-compartmentalizing protease in Rhodococcus: the 20S proteasome. *Antonie van Leeuwenhoek* 74(1-3):83-87.
21. Glickman MH*, et al.* (1998) A subcomplex of the proteasome regulatory particle required for ubiquitin-conjugate degradation and related to the COP9-signalosome and eIF3. *Cell* 94(5):615-623.
22. Groll M*, et al.* (1997) Structure of 20S proteasome from yeast at 2.4 A resolution. *Nature* 386(6624):463-471.

23. Chu-Ping M, Vu JH, Proske RJ, Slaughter CA, & DeMartino GN (1994) Identification, purification, and characterization of a high molecular weight, ATP-dependent activator (PA700) of the 20 S proteasome. *The Journal of biological chemistry* 269(5):3539-3547.
24. DeMartino GN & Slaughter CA (1993) Regulatory proteins of the proteasome. *Enzyme & protein* 47(4-6):314-324.
25. Eleuteri AM*, et al.* (2000) Isolation and characterization of bovine thymus multicatalytic proteinase complex. *Protein expression and purification* 18(2):160-168.
26. Griffin TA*, et al.* (1998) Immunoproteasome assembly: cooperative incorporation of interferon gamma (IFN-gamma)-inducible subunits. *The Journal of experimental medicine* 187(1):97-104.
27. Tanaka K (1994) Role of proteasomes modified by interferon-gamma in antigen processing. *Journal of leukocyte biology* 56(5):571-575.
28. Takahama Y, Takada K, Murata S, & Tanaka K (2012) β5t-containing thymoproteasome: specific expression in thymic cortical epithelial cells and role in positive selection of CD8+ T cells. *Current opinion in immunology* 24(1):92-98.
29. Murata S*, et al.* (2007) Regulation of CD8+ T cell development by thymus-specific proteasomes. *Science* 316(5829):1349-1353.
30. Etlinger JD & Goldberg AL (1977) A soluble ATP-dependent proteolytic system responsible for the degradation of abnormal proteins in reticulocytes. *Proceedings of the National Academy of Sciences of the United States of America* 74(1):54-58.
31. Ciehanover A, Hod Y, & Hershko A (1978) A heat-stable polypeptide component of an ATP-dependent proteolytic system from reticulocytes. *Biochemical and biophysical research communications* 81(4):1100-1105.
32. Hershko A, Ciechanover A, & Rose IA (1979) Resolution of the ATP-dependent proteolytic system from reticulocytes: a component that interacts with ATP. *Proceedings of the National Academy of Sciences of the United States of America* 76(7):3107-3110.
33. Enenkel C, Lehmann A, & Kloetzel PM (1998) Subcellular distribution of proteasomes implicates a major location of protein degradation in the nuclear envelope-ER network in yeast. *The EMBO journal* 17(21):6144-6154.
34. Pamnani V*, et al.* (1997) Cloning, sequencing and expression of VAT, a CDC48/p97 ATPase homologue from the archaeon Thermoplasma acidophilum. *FEBS letters* 404(2-3):263-268.
35. Yao T & Cohen RE (2002) A cryptic protease couples deubiquitination and degradation by the proteasome. *Nature* 419(6905):403-407.
36. Lander GC*, et al.* (2012) Complete subunit architecture of the proteasome regulatory particle. *Nature* 482(7384):186-191.
37. Finley D (2009) Recognition and processing of ubiquitin-protein conjugates by the proteasome. *Annual review of biochemistry* 78:477-513.
38. Schreiner P*, et al.* (2008) Ubiquitin docking at the proteasome through a novel pleckstrin-homology domain interaction. *Nature* 453(7194):548-552.
39. Boehringer J*, et al.* (2012) Structural and functional characterization of Rpn12 identifies residues required for Rpn10 proteasome incorporation. *The Biochemical journal* 448(1):55-65.
40. Riedinger C*, et al.* (2010) Structure of Rpn10 and its interactions with polyubiquitin chains and the proteasome subunit Rpn12. *The Journal of biological chemistry* 285(44):33992-34003.
41. Beck F*, et al.* (2012) Near-atomic resolution structural model of the yeast 26S proteasome. *Proceedings of the National Academy of Sciences of the United States of America* 109(37):14870-14875.
42. Scheel H & Hofmann K (2005) Prediction of a common structural scaffold for proteasome lid, COP9-signalosome and eIF3 complexes. *BMC bioinformatics* 6:71.
43. Kim T, Hofmann K, von Arnim AG, & Chamovitz DA (2001) PCI complexes: pretty complex interactions in diverse signaling pathways. *Trends in plant science* 6(8):379-386.

44. Djuranovic S*, et al.* (2009) Structure and activity of the N-terminal substrate recognition domains in proteasomal ATPases. *Molecular cell* 34(5):580-590.
45. Zhang F*, et al.* (2009) Structural insights into the regulatory particle of the proteasome from Methanocaldococcus jannaschii. *Molecular cell* 34(4):473-484.
46. Smith DM*, et al.* (2007) Docking of the proteasomal ATPases' carboxyl termini in the 20S proteasome's alpha ring opens the gate for substrate entry. *Molecular cell* 27(5):731-744.
47. Rabl J*, et al.* (2008) Mechanism of gate opening in the 20S proteasome by the proteasomal ATPases. *Molecular cell* 30(3):360-368.
48. Agrawal V & Kishan KV (2003) OB-fold: growing bigger with functional consistency. *Current protein & peptide science* 4(3):195-206.
49. Religa TL, Sprangers R, & Kay LE (2010) Dynamic regulation of archaeal proteasome gate opening as studied by TROSY NMR. *Science* 328(5974):98-102.
50. Forster F, Lasker K, Nickell S, Sali A, & Baumeister W (2010) Toward an integrated structural model of the 26S proteasome. *Molecular & cellular proteomics : MCP* 9(8):1666-1677.
51. Kusmierczyk AR, Kunjappu MJ, Kim RY, & Hochstrasser M (2011) A conserved 20S proteasome assembly factor requires a C-terminal HbYX motif for proteasomal precursor binding. *Nature structural & molecular biology* 18(5):622-629.
52. Dessau M*, et al.* (2008) The Arabidopsis COP9 signalosome subunit 7 is a model PCI domain protein with subdomains involved in COP9 signalosome assembly. *The Plant cell* 20(10):2815-2834.
53. Kapelari B*, et al.* (2000) Electron microscopy and subunit-subunit interaction studies reveal a first architecture of COP9 signalosome. *Journal of molecular biology* 300(5):1169-1178.
54. Enchev RI, Schreiber A, Beuron F, & Morris EP (2010) Structural insights into the COP9 signalosome and its common architecture with the 26S proteasome lid and eIF3. *Structure* 18(4):518-527.
55. Faza MB*, et al.* (2009) Sem1 is a functional component of the nuclear pore complex-associated messenger RNA export machinery. *The Journal of cell biology* 184(6):833-846.
56. Jantti J, Lahdenranta J, Olkkonen VM, Soderlund H, & Keranen S (1999) SEM1, a homologue of the split hand/split foot malformation candidate gene Dss1, regulates exocytosis and pseudohyphal differentiation in yeast. *Proceedings of the National Academy of Sciences of the United States of America* 96(3):909-914.
57. Reinman M*, et al.* (2003) Functional inactivation of the conserved Sem1p in yeast by intrabodies. *Yeast (Chichester, England)* 20(12):1071-1084.
58. Sone T, Saeki Y, Toh-e A, & Yokosawa H (2004) Sem1p is a novel subunit of the 26 S proteasome from Saccharomyces cerevisiae. *The Journal of biological chemistry* 279(27):28807-28816.
59. Verma R*, et al.* (2002) Role of Rpn11 metalloprotease in deubiquitination and degradation by the 26S proteasome. *Science* 298(5593):611-615.
60. Ambroggio XI, Rees DC, & Deshaies RJ (2004) JAMM: a metalloprotease-like zinc site in the proteasome and signalosome. *PLoS biology* 2(1):E2.
61. Kikuchi K, Ishii N, Asao H, & Sugamura K (2003) Identification of AMSH-LP containing a Jab1/MPN domain metalloenzyme motif. *Biochemical and biophysical research communications* 306(3):637-643.
62. Reyes-Turcu FE, Ventii KH, & Wilkinson KD (2009) Regulation and cellular roles of ubiquitin-specific deubiquitinating enzymes. *Annual review of biochemistry* 78:363-397.
63. Sato Y*, et al.* (2008) Structural basis for specific cleavage of Lys 63-linked polyubiquitin chains. *Nature* 455(7211):358-362.
64. Rinaldi T*, et al.* (2008) Dissection of the carboxyl-terminal domain of the proteasomal subunit Rpn11 in maintenance of mitochondrial structure and function. *Molecular biology of the cell* 19(3):1022-1031.

65. Sanches M, Alves BS, Zanchin NI, & Guimaraes BG (2007) The crystal structure of the human Mov34 MPN domain reveals a metal-free dimer. *Journal of molecular biology* 370(5):846-855.
66. Kajava AV (2002) What curves alpha-solenoids? Evidence for an alpha-helical toroid structure of Rpn1 and Rpn2 proteins of the 26 S proteasome. *The Journal of biological chemistry* 277(51):49791-49798.
67. Kajava AV & Kobe B (2002) Assessment of the ability to model proteins with leucine-rich repeats in light of the latest structural information. *Protein science : a publication of the Protein Society* 11(5):1082-1090.
68. Elsasser S*, et al.* (2002) Proteasome subunit Rpn1 binds ubiquitin-like protein domains. *Nature cell biology* 4(9):725-730.
69. Rani N, Aichem A, Schmidtke G, Kreft SG, & Groettrup M (2012) FAT10 and NUB1L bind to the VWA domain of Rpn10 and Rpn1 to enable proteasome-mediated proteolysis. *Nature communications* 3:749.
70. Verma R, Oania R, Graumann J, & Deshaies RJ (2004) Multiubiquitin chain receptors define a layer of substrate selectivity in the ubiquitin-proteasome system. *Cell* 118(1):99-110.
71. Chandra A, Chen L, & Madura K (2010) Synthetic lethality of rpn11-1 rpn10Delta is linked to altered proteasome assembly and activity. *Current genetics* 56(6):543-557.
72. Hamazaki J*, et al.* (2007) Rpn10-mediated degradation of ubiquitinated proteins is essential for mouse development. *Molecular and cellular biology* 27(19):6629-6638.
73. Al-Shami A*, et al.* (2010) Regulators of the proteasome pathway, Uch37 and Rpn13, play distinct roles in mouse development. *PloS one* 5(10):e13654.
74. Chen X, Lee BH, Finley D, & Walters KJ (2010) Structure of proteasome ubiquitin receptor hRpn13 and its activation by the scaffolding protein hRpn2. *Molecular cell* 38(3):404-415.
75. Husnjak K*, et al.* (2008) Proteasome subunit Rpn13 is a novel ubiquitin receptor. *Nature* 453(7194):481-488.
76. Zhang N*, et al.* (2009) Structure of the s5a:k48-linked diubiquitin complex and its interactions with rpn13. *Molecular cell* 35(3):280-290.
77. Lenkinski RE, Chen DM, Glickson JD, & Goldstein G (1977) Nuclear magnetic resonance studies of the denaturation of ubiquitin. *Biochimica et biophysica acta* 494(1):126-130.
78. Turowski G, Zak Z, & Galka M (1977) The ubiquitin system as a balance between monomers and polymers in polypeptide structure. *Folia biologica* 25(4):429-433.
79. Reeks J*, et al.* (2013) Structure of the archaeal Cascade subunit Csa5: relating the small subunits of CRISPR effector complexes. *RNA biology* 10(5):762-769.
80. Humbard MA*, et al.* (2010) Ubiquitin-like small archaeal modifier proteins (SAMPs) in Haloferax volcanii. *Nature* 463(7277):54-60.
81. Vijay-Kumar S, Bugg CE, & Cook WJ (1987) Structure of ubiquitin refined at 1.8 A resolution. *Journal of molecular biology* 194(3):531-544.
82. Vilchez D*, et al.* (2012) RPN-6 determines C. elegans longevity under proteotoxic stress conditions. *Nature* 489(7415):263-268.
83. Sakata E*, et al.* (2012) Localization of the proteasomal ubiquitin receptors Rpn10 and Rpn13 by electron cryomicroscopy. *Proceedings of the National Academy of Sciences of the United States of America* 109(5):1479-1484.
84. Lasker K*, et al.* (2012) Molecular architecture of the 26S proteasome holocomplex determined by an integrative approach. *Proceedings of the National Academy of Sciences of the United States of America* 109(5):1380-1387.
85. da Fonseca PC, He J, & Morris EP (2012) Molecular model of the human 26S proteasome. *Molecular cell* 46(1):54-66.
86. Pathare GR*, et al.* (2012) The proteasomal subunit Rpn6 is a molecular clamp holding the core and regulatory subcomplexes together. *Proceedings of the National Academy of Sciences of the United States of America* 109(1):149-154.

87. He J*, et al.* (2012) The structure of the 26S proteasome subunit Rpn2 reveals its PC repeat domain as a closed toroid of two concentric alpha-helical rings. *Structure* 20(3):513-521.
88. Kish-Trier E & Hill CP (2013) Structural biology of the proteasome. *Annual review of biophysics* 42:29-49.
89. Matyskiela ME, Lander GC, & Martin A (2013) Conformational switching of the 26S proteasome enables substrate degradation. *Nature structural & molecular biology* 20(7):781-788.
90. Estrin E, Lopez-Blanco JR, Chacon P, & Martin A (2013) Formation of an intricate helical bundle dictates the assembly of the 26S proteasome lid. *Structure* 21(9):1624-1635.
91. Pathare GR*, et al.* (2014) Crystal structure of the proteasomal deubiquitylation module Rpn8-Rpn11. *Proceedings of the National Academy of Sciences of the United States of America* 111(8):2984-2989.

Chapter 8: Acknowledgements

I was nervous when I first stepped into the street “Am Klopferspitz 18”, the campus of Max-Planck Institute for Biochemistry, Martinsried. It took me 10 minutes to walk a distance of 100 m to the reception of the institute as being afraid of the new place, new people and new environment. But, later felt home when I was at the reception and my supervisor Dr. Istvan Nagy first received on behalf of Prof. Dr. Wolfgang Baumeister. I smiled, and it all started, and since then I had the most happy and productive time of my life at the Max-Planck Institute of Biochemistry.

This thesis represents not only my work on the bench but, it is a milestone in more than 48 months of my work at the MPI and specifically within Baumeister department. I have been provided with a favourable environment and opportunities which I could seize. During all this time I came across many nice people whom I would like to acknowledge.

First and foremost I wish to thank my Ph.D. advisor, **Prof. Dr. Wolfgang Baumeister**, director of the MPI for Biochemistry. He has been supportive since the day I began working on the project as Master’s thesis student. Ever since, Prof. Baumeister has supported me not only by providing me with the opportunity to work in his lab, but also academically to finish this thesis. Thanks to him I had the opportunity to build a strong research profile where I would be benefiting in future.

I owe a lot to **Istvan Nagy** as, without him it wouldn’t be the most beautiful time of my life. He was not just my major advisor for the work, but more like my parents who supported every move of mine and believed me. Be it academics, research or emotional, in all he was a reliable hand of blessing. Without him, I would never have ended up successfully.

Thank you to **Andreas Bracher** for being my one of the major advisors for taking it easy to teach me the structural biology. It wasn’t easy at all for me to learn the new and difficult things but you made it so easy that I started to believe in myself.

Special thanks to Jurgen Peters and Friedrich Foersters who provided valuable inputs into the projects time to time and also thoroughly corrected my thesis.

Roland Knispel, Marius Boicu, Agnes Hubert, Andreas Schwetizer and **Stephan Nickell** were the people around me whom I could ask help for every small thing where their contributions made a lot of difference during all this time. Special thanks to **Inga Wolf** who played a very major role in troubleshooting every computational difficulty which was in the way and the Magician, **Tim Laugkas** from the workshop who had solution to every problem with the instruments and could fix them with no loss of time. **Günter Pfeifer, Oana Mihalache** and **Florian Beck** were of immense help with cryo electron microscopy sample preparation and data procession. And finally I would thank all the people from the Baumeister department along with the people from Fredos group who were around for maintaining the smile on my face.

I also would like to thank the staff from the other departments and core facilities in the institute especially **Sabina Suppmann** and her colleagues from the Micro-chemistry core facility and **Jerome Basiquin** and **Karina Vale**r from the Crystallization facility, without their cooperative nature and timely help; I wouldn't have finished my projects in time.

My acknowledge list would remain incomplete if I fail to thank the Secretariat, **Birgit Book** along with **Sabina** and **Nathalie**. Last but not the least all my Indian friends especially **Vaibhav Janbandhu** who was like an elder brother during my time here guiding throughout the path.